Peptide Functionalisation and Characterisation of Gold (Nano) Surfaces

Lynsey A. Aitken

A thesis presented to the Department of Pure and Applied Chemistry, University of Strathclyde, in fulfilment of the requirements for the degree of Doctor of Philosophy.

2016

This thesis is the result of the author's original research. It has been composed by the author and has not been previously submitted for examination which has led to the award of a degree.

"...need I remind you that not a lot of scientific discoveries were made by people having a good time?"

Sheldon Cooper, Ph.D

Lorre, C. (Writer); Prady, B. (Writer); Cendrowski, M. (Director), 2011, The Agreement Disection, *The Big Bang Theory*, Warner Bros. Televison.

ACKNOWLEDGEMENTS

I would like to thank my supervisor Professor Rein V. Ulijn for his help and support throughout my PhD. His guidance over the last 4 (and a bit...) years has been invaluable. I thank Professor Duncan Graham for the opportunity to use the instruments in the Centre for Molecular Nanometrology.

I would also like to thank everyone who has contributed towards the work detailed in this thesis. In particular, I would like to thank Dr. Louise S. Birchall for the friendship and help during her time in Glasgow, Dr. David. J. Scurr for running the ToF-SIMS instrument, Emily F. Smith and Prof. Morgan R. Alexander for organising the XPS analysis and assisting with the interpretation of the data respectively. Thanks to Patricia Keating with the instrument set-up for the LDI-ToF MS work, Dr. Andrew J. Urquhart for the use of his CAG instrumentation and Dr. Dimitrios Lamprou for his advice regarding experimental set-up, Renishaw Diagnostics for providing Klarite samples, Dr. Kirsty F. Gibson for her help with the Witec analysis, , Dr. Iain A. Larmour for running SEM samples, Dr. Stacey Laing for repeatedly re-calibrating the Witec instrumentation and Hiran Vegad (Analytik Ltd.) for running samples on the CPS Disc Centrifuge instrument.

Thank you to the Ulijn group members (past and present) who have kept me motivated, gone on chocolate missions and listened to rap music with me in the hope it will improve experimental results... My twin Dr. Meghan Hughes, my most initialled friend Dr. Pim W. J. M. Frederix and my ninja buddy Lauren Bayne deserve special thanks for keeping me sane and reading drafts of my thesis in the final few months.

I would like to say a huge thank you to my Mum and Dad for all their support both financially and emotionally during the course of my university “career”, particularly during the latter stages of my PhD. I appreciate it more than I can say.

Finally, and most importantly, I would like to thank my husband, Callum. I honestly would not have submitted my PhD thesis without his constant encouragement, vastly superior Chemdraw skills and late night trips to Tesco for chocolate, printer paper and ink... Thank you.

ABSTRACT

This work describes the successful preparation and characterisation of peptide functionalised gold surfaces, with a focus towards developing enzyme response applications. The serine protease, elastase, was the primary focus of this work; however, all of the systems described herein have the utility to be modified for alternative proteolytic enzymes.

1.0 provides background and context to the work presented in this thesis and additionally describes the layout of the work to be presented.

2.0 reviews the literature on enzyme responsive nanomaterials (ERNMs), providing a brief overview of the design considerations, routes to functionalisation and characterisation techniques which must be taken into account when developing such materials.

3.0 describes the development of a method for the step-wise functionalisation of planar gold surfaces with short peptide derivatives, which contained elastase cleavable moieties. (±)-α-lipoic acid was utilised to provide an anchor to the gold surface and conventional Fmoc chemistry used to prepare the peptide sequences. The fluorenyl functional group provided a convenient marker for surface analysis, enabling the verification of each synthetic step by ToF-SIMS, XPS and LDI-ToF MS. Step-wise solid-phase synthesis on the gold surface is a facile means of preparing peptide-conjugates, providing a method whereby no additional purification or final "grafting-on" steps are required. The use of LDI-ToF MS and ToF-SIMS in tandem ensured confidence in the stepwise synthesis method. These techniques provided complimentary data to one another through the analysis of both the fully desorbed peptide derivative and molecular fragments respectively.

4.0 presents investigations into the use of SERS as a technique to follow the elastase responsive system developed in 3.0. The nanostructure surface of Klarite, a

commercially available SERS substrate, was functionalised using the same methodology and proof-of-concept work towards a SERS-active system was detailed.

5.0 discusses the development of the first elastase detection system found on gold nanoparticles, progressing on from the work on flat surfaces presented in 3.0 and 4.0. The remainder of the work presented in the chapter focuses on the development of a potentially more robust system, with several target molecules successfully synthesised; however, none of these molecules provided an elastase responsive system.

6.0 then provides conclusions of the work carried out, followed by a description of potential future investigations that could be carried out. Finally, 7.0 provides a detailed description of the experimental methodology followed, providing evidence for the findings and conclusions presented in 3.0-6.0.

ABBREVIATIONS

A	Alanine
AFM	Atomic Force Microscopy
Boc	*tert*-Butyloxycarbonyl
BSA	Bovine Serum Albumin
CA	Contact Angle
CAG	Contact Angle Goniometer
CPS	CPS Instruments Europe Ltd.
DIPEA	*N*,*N*-Diisopropylethylamine
DTT	Dithiothreitol
DNA	Deoxyribonucleic acid
DLS	Dynamic Light Scattering
EDC·HCl	*N*-(3-Dimethylaminopropyl)-*N*′-ethylcarbodiimide hydrochloride
eq.	Equivalents
ERNM	Enzyme Responsive Nanomaterial
ESI	Electrospray Ionisation
FAT	Fixed Analyser Transmission
Fmoc	9-*H* Fluorenylmethyloxycarbonyl
FRET	Förster Resonance Energy Transfer
GABA	γ-Aminobutyric acid
HBTU	*N*,*N*,*N*′,*N*′-Tetramethyl-*O*-(1*H*-benzotriazol-1-yl)uronium hexafluorophosphate
HCTU	*O*-(6-Chlorobenzotriazol-1-yl)-*N*,*N*,*N*′,*N*′-tetramethyluronium hexafluorophosphate
HPLC	High Performance Liquid Chromatography
IUPAC	International Union of Pure And Applied Chemistry

LDI-ToF MS	Direct Laser Desorption/Ionisation Time-of-Flight Mass Spectrometry
Ltd.	Limited
MALDI MS	Matrix Assisted Laser Desorption/Ionisation Mass Spectrometry
ME	Mercaptoethanol
MERS	Middle East Respiratory Syndrome
MMP	Matrix metalloproteinases
MRI	Magnetic Resonance Imaging
MRSA	*Methicillin-resistant Staphylococcus aureus*
MS	Mass Spectrometry
m/z	Mass to Charge Ratio
n-ACT PSA	α_1-Antichymotrypsin Prostate Specific Antigen
NIRF	Near Infrared Fluorescence
NHS	*N*-Hydroxysuccinimide
NMM	*N*-Methylmorpholine
NMR	Nucleic Magnetic Resonance
PBS	Phosphate Buffered Saline
PEG	Poly(ethylene glycol)
PEGA	Poly(ethyleneglycol acrylamide) Co-polymer
PLpro	Papin-like Proteases
ppb	Parts per Billion
ppm	Parts per Million
r.p.m.	Revolutions Per Minute
RSC	Royal Society of Chemistry
SAM	Self-assembled Monolayer
SAMDI MS	Self-assembled Monolayers with Matrix Assisted Laser Desorption/Ionisation Mass Spectrometry
SARS	Severe Acute Respiratory Syndrome

SEM	Scanning Electron Microscopy
SERS	Surface Enhanced Raman Spectroscopy
SERRS	Surface Enhanced Resonance Raman Spectroscopy
SH2	Src Homology 2
SPPS	Solid Phase Peptide Synthesis
SPR	Surface Plasmon Resonance
T2	Relaxation Time
ToF-SIMS	Time of Flight Secondary Ion Mass Spectrometry
U.K.	United Kingdom
UV	Ultra-Violet
UV-Vis	Ultra-Violet & Visible Spectrophotometry
WCA	Water Contact Angle
XPS	X-ray Photoelectron Spectroscopy

UNITS

°	Degrees
°C	Degrees Celsius
cm^{-1}	Wavenumbers
D	Dalton
eV	Electron Volts
g	Gram
h	Hours
Hz	Hertz
m	Metre
kV	Kilovolts ($\times 10^{3}$ V)
L	Litre
M	Molar
mg	Milligram ($\times 10^{-3}$ g)
mg mL^{-1}	Milligram per Millilitre
min(s)	Minute(s)
min^{-1}	Per Minute
mL	Millilitre ($\times 10^{-3}$ L)
mm	Millimetre ($\times 10^{-3}$ m)
mM	Millimolar ($\times 10^{-3}$ M)
mmol	Millimoles ($\times 10^{-3}$ moles)
mW	Milliwatts ($\times 10^{-3}$ W)
nm	Nanometre ($\times 10^{-9}$ m)
nmol	Nanomoles ($\times 10^{-9}$ moles)
µg	Microgram ($\times 10^{-6}$ g)
µg mL^{-1}	Microgram per Millilitre
µL	Microlitre ($\times 10^{-6}$ L)
v:v	Volume:volume ratio

W	Watts
w:v	Weight:volume ratio
zg	Zeptogram ($\times 10^{-21}$ g)
zg mL^{-1}	Zeptogram per Millilitre

CONTENTS

CHAPTER ONE - INTRODUCTION
1.1 Introduction to Thesis 1
1.2 Motivation of Project 2
1.3 Layout of Thesis 2
CHAPTER TWO - ENZYME RESPONSIVE NANOMATERIALS
2.1 Abstract 6
2.2 Introduction 6
2.3 System Design 6
2.3.1 Enzymes as Stimuli 7
2.3.1.1 Enzymatic Action 10
2.3.2 Selection of Nanostructured Component 13
2.3.2.1 Metallic Nanoparticles 13
2.3.2.2 Non-metallic Nanoparticles 19
2.3.2.3 Non-Particulate Nanostructures 20
2.4 Conclusions 21
CHAPTER THREE - PEPTIDE FUNCTIONALISATION OF PLANAR GOLD SURFACES
3.1 Abstract 22
3.2 Introduction 22
3.2.1 Solution-Phase Synthesis of Peptides 23
3.2.2 Solid-Phase Peptide Synthesis 25
3.3 Project Aim 29
3.4 Results and Discussion 30
3.4.1 Surface Analysis 32
3.4.2 Time-of-Flight Secondary-Ion Mass Spectrometry (ToF SIMS) 33
3.4.3 X-ray Photoelectron Spectroscopy (XPS) 41
3.4.4 Direct Laser Desorption/Ionisation Time-of-Flight Mass Spectrometry (LDI-ToF MS) 47

3.4.5 Contact Angle Goniometry 52
3.4.6 Surface Coverage Analysis 53
3.4.7 Thiol Displacement Studies 54
3.5 Conclusions 54
CHAPTER FOUR - PEPTIDE FUNCTIONALISATION OF NANOSTRUCTURED GOLD SURFACES
4.1 Abstract 56
4.2 Introduction 56
4.2.1 Background 56
4.2.2 Project Aim 57
4.3 Results and Discussion 58
4.3.1 Direct Laser Desorption/Ionisation Time-of-Flight Mass Spectrometry (LDI-ToF MS) 58
4.3.2 SERS Response for Fmoc Functionalised Surfaces 62
4.3.3 Selection of Raman Reporter 63
4.3.4 Proof of Concept 65
4.3.5 Optimisation of a SERS Biosensor for Elastase 67
4.4 Conclusions 71
CHAPTER FIVE - DESIGN AND PREPARATION OF A COLORIMETRIC ELASTASE SENSOR
5.1 Abstract 72
5.2 Introduction 72
5.2.1 Background 73
5.3 Project Aim 73
5.4 Results and Discussion 74
5.4.1 Proof of Concept Work 74
5.4.2 Stepwise Solid-Phase Peptide Synthesis on Gold Nanoparticles 84
5.4.3 Solution-Phase Synthesis of an Elastase Cleavable Peptide Sequence 89
5.4.4 Solid-Phase Peptide Synthesis of an Elastase Cleavable Peptide Sequence 93
5.4.5 Elastase Detection 95

5.5 Conclusions 100
CHAPTER SIX - CONCLUSIONS
6.1 Conclusions 102
6.2 Future Work 103
CHAPTER SEVEN - MATERIALS AND METHODS
7.1 General Methods 106
7.2 Peptide Functionalisation of Planar Gold Surfaces (Chapter 3.0) 107
7.2.1 Peptide Synthesis on Gold-coated Cover Slips 107
7.2.2 Enzyme Treatment of Gold-coated Cover Slips 108
7.2.3 Time-of-Flight Secondary-Ion Mass Spectrometry (ToF-SIMS) 108
7.2.4 X-ray Photoelectron Spectroscopy (XPS) 109
7.2.5 Direct Laser Desorption/Ionisation Time-of-Flight Mass Spectrometry (LDI-ToF MS) 109
7.2.6 Contact Angle Geniometry (CAG) 110
7.2.7 Surface Coverage Analysis[2] 110
7.2.8 Thiol Displacement 110
7.3 Peptide Functionalisation of Nanostructured Gold Surfaces (Chapter 4.0) 111
7.3.1 Peptide Synthesis on Klarite, Nanohole and Nanorod Array Substrates 111
7.3.2 Direct Laser Desorption/Ionisation Time-of-Flight Mass Spectrometry (LDI-ToF MS) 111
7.3.3 Addition of Raman Reporter Molecules 112
7.3.4 Preparation of Klarite Surfaces with Mixed Monolayers 112
7.3.5 Raman Mapping 112
7.4 Design and Preparation of a Colorimetric Elastase Sensor (Chapter 5.0) 113
7.4.1 Solid Phase Peptide Synthesis for Proof of Concept Work 113
Preparation of (9*H*-fluoren-9-yl)methyl(1-((1-((1-amino-3-mercapto-1-oxopropan-2-yl)amino)-1-oxopropan-2-yl)amino)-1-oxopropan-2-yl)carbamate (5.2) 113
7.4.2 Stabilisation of Colloidal Gold Nanoparticles[9] 115
7.4.3 Synthesis of Colloidal Gold Nanoparticles 115

7.4.4 Stepwise SPPS on Gold Nanoparticles 116
7.4.5 Preparation of Peptide-Nanoparticle Conjugates[10] 117
7.4.6 Enzymatic Hydrolysis of Peptide-Nanoparticle Conjugates[10] 117
7.4.7 Synthesis of an Elastase Specific Peptide Sequence 117
Preparation of 2,5-dioxopyrrolidin-1-yl 5-(1,2-dithiolan-3-yl)pentanoate (5.6)[5], Scheme 5.2 117
Preparation of (9*H*-fluoren-9-yl)methyl (4-(5-(1,2-dithiolan-3-yl)pentanamido)-butyl)carbamate (5.7)[6-7], Scheme 5.2 118
Preparation of *N*-(4-aminobutyl)-5-(1,2-dithiolan-3-yl)pentanamide (5.4), Scheme 5.2 119
Preparation of (9*H*-fluoren-9-yl)methyl (1-((1-((4-(5-(1,2-dithiolan-3-yl)pentanamido)butyl)amino)-1-oxopropan-2-yl)amino)-1-oxopropan-2-yl)carbamate (5.3), Scheme 5.2 120
Preparation of *N*-(4-aminobutyl)-5-(1,2-dithiolan-3-yl)pentanamide (5.4), Scheme 5.3 120
Preparation of 5-(1,2-dithiolan-3-yl)-N-(4-hydroxybutyl)pentanamide (5.9), Scheme 5.4 121
Preparation of (9H-fluoren-9-yl)methyl (1-((1-((1,6-diamino-1-oxohexan-2-yl)amino)-1-oxopropan-2-yl)amino)-1-oxopropan-2-yl)carbamate (5.10) ... 122
Preparation of (9H-fluoren-9-yl)methyl (1-((1-((6-(5-(1,2-dithiolan-3-yl)pentanamido)-1-amino-1-oxohexan-2-yl)amino)-1-oxopropan-2-yl)amino)-1-oxopropan-2-yl)carbamate (5.11) 123
Preparation of (9*H*-fluoren-9-yl)methyl (1-((1-((4-((2-amino-2-oxoethyl)amino)-4-oxobutyl)amino)-1-oxopropan-2-yl)amino)-1-oxopropan-2-yl)carbamate (5.12), Scheme 5.5 124
Preparation of (9*H*-fluoren-9-yl)methyl (1-((1-((4-((aminomethyl)amino)-4-oxobutyl)amino)-1-oxopropan-2-yl)amino)-1-oxopropan-2-yl)carbamate (5.14), Scheme 5.5 126
Preparation of Diethyl 2-(Hex-5-enyl)malonate (5.16)[8], Scheme 5.6 126
Preparation of 2-(Hex-5-enyl)propane-1,3-diol (5.17)[8], Scheme 5.6 127
Preparation of 2-(Hex-5-en-1-yl)propane-1,3-diyl dimethanesulfonate (5.18)[8], Scheme 5.6 128

Preparation of 7-((methylsulfonyl)oxy)-6-(((methylsulfonyl)oxy)methyl)heptanoic acid (5.19) [8], Scheme 5.6 129

Preparation of Isolipoic Acid (5.20), Scheme 5.6 129

Preparation of 2,5-dioxopyrrolidin-1-yl 5-(1,2-dithiolan-4-yl)pentanoate (5.21) 130

Preparation of (9H-fluoren-9-yl)methyl (1-((1-((6-(5-(1,2-dithiolan-4-yl)pentanamido)-1-amino-1-oxohexan-2-yl)amino)-1-oxopropan-2-yl)amino)-1-oxopropan-2-yl)carbamate (5.22) 131

CHAPTER EIGHT - REFERENCES

8.1 Chapter 0ne References 132

8.2 Chapter Two References 132

8.3 Chapter Three References 135

8.4 Chapter Four References 138

8.5 Chapter Five References 139

8.6 Chapter Six References 140

8.7 Chapter Seven References 140

CHAPTER NINE - APPENDIX

9.1 Mass Spectra of Synthesised Compounds 142

CHAPTER ONE – INTRODUCTION

1.1 Introduction to Thesis

Since the completion of the Human Genome Project in 2003, scientists have been privy to intimate knowledge of the arrangement and ordering of the chemical base pairs present in each and every gene. Approximately 500 of the 30, 000 genes composing the genome are estimated to code for the class of enzymes known as the proteases.[1] As deregulation of protease expression has been shown to play a role in diseases, including but not limited to, rheumatoid arthritis, bacterial and viral infections, cancer and Alzheimer's disease,[2] these enzymes are of diagnostic importance.

Amongst the top-ten challenges for the chemical sciences, as identified by the Royal Society of Chemistry (RSC),[3] are diagnostics for human heath *i.e.* improving current methods of monitoring disease. Research in this area is concerned with the development of sensitive point-of-care devices to aid diagnosis without the need for expensive specialised equipment or invasive procedures. Designing a system whereby subtle changes, such as the expression of specific proteases, can be monitored may provide a means of detecting disease.

Metallic nanoparticles are of particular interest to the fields of diagnostics and sensing, as they display novel physical properties that are unlike either small molecular species or bulk material due to their size, shape and inter-particle distances. Gold nanoparticles have unusually high molecular extinct coefficients, and as a result are highly coloured ruby-red species. This red colouring is due to surface plasmon resonance (SPR) which absorbs at ~520 nm in the visible region.[4] Nanoparticle aggregation causes broadening and red-shifting of the SPR by up to 250 nm. This triggers a colorimetric change from red through purple to blue which

can be monitored using UV-Vis spectrophotometry and is a useful property for commercial applications such as biochemical assays.

1.2 Motivation of Project

The motivation of this research was to develop a colorimetric elastase sensor utilising peptide functionalised gold nanoparticles. Proof-of-concept research was undertaken upon a series of elastase responsive gold surfaces. Each surface type displayed an increasing degree of complexity from planar gold surfaces to nanostructured and then ultimately to colloidal gold nanoparticles. These sequential increases in complexity allowed full characterisation of the surfaces, and consequently indicate the surface interactions which will be present in the final particulate sensor. In the future systems such as these may serve a role in disease detection.

1.3 Layout of Thesis

This thesis begins with an extensive literature review (2.0) covering enzyme responsive nanomaterials. It is then split into separate experimental chapters; each with an introduction, results and conclusion sections with the intention that each may be consulted independently.

The first experimental chapter (3.0) detailed an investigation into the peptide functionalisation of planar gold surfaces. Peptide synthesis was carried out in a stepwise manner (figure 1.1) to enable full characterisation of the gold surfaces after each synthetic step and the final enzymatic digestion by elastase.

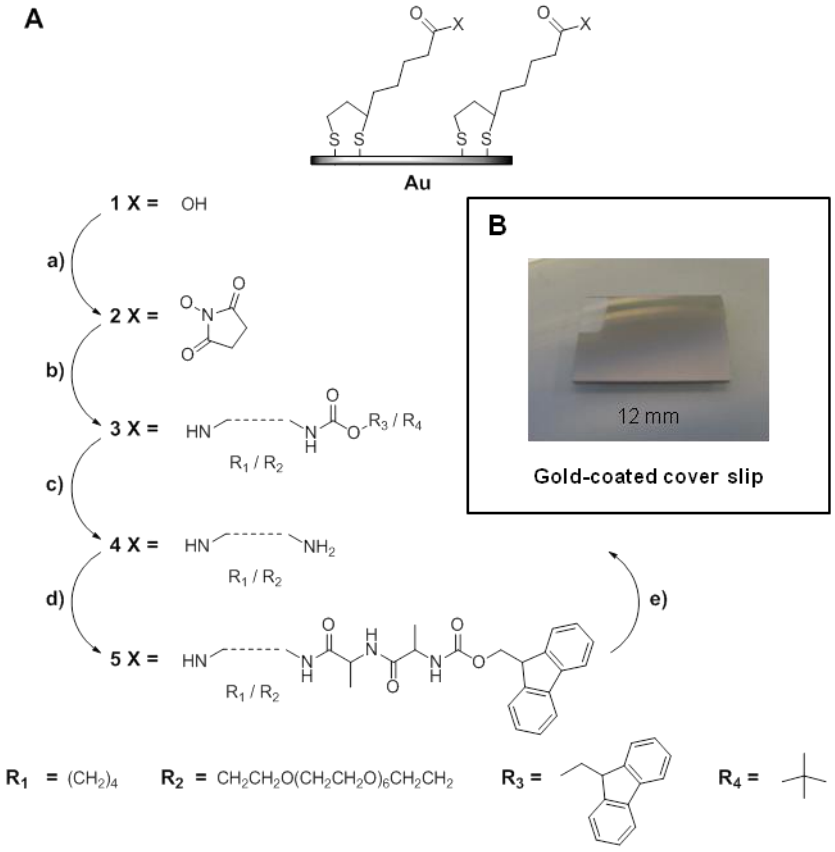

Figure 1.1
(A) Strategy for stepwise synthesis upon a (B) gold-coated cover slip.

The second experimental chapter (4.0) explored stepwise peptide synthesis on nano-structured gold surfaces. Surface enhanced raman spectroscopy (SERS) (figure 1.2) was utilised to determine the extent to which enzymatic digestion occurred.

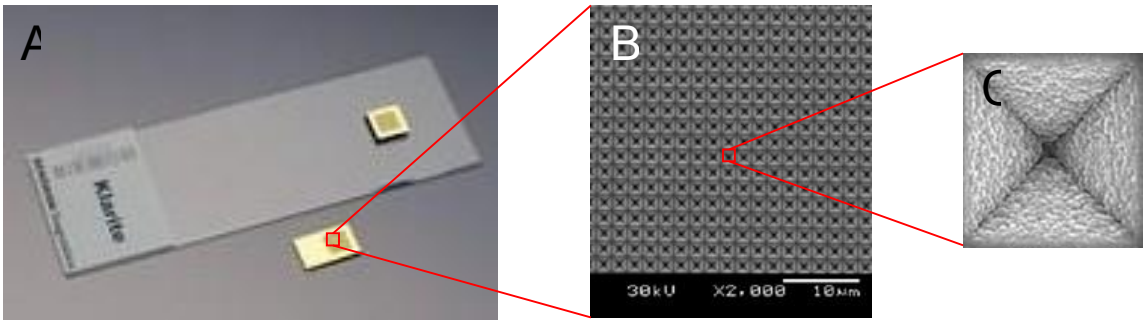

Figure 1.2

Klarite SERS substrate

The final experimental chapter (5.0) covered the development of a colorimetric sensor which utilises peptide-nanoparticle conjugates to elicit a response upon the introduction of a specific serine protease, elastase (figure 1.3). Preliminary work towards the optimisation of sensor sensitivity was detailed within the chapter.

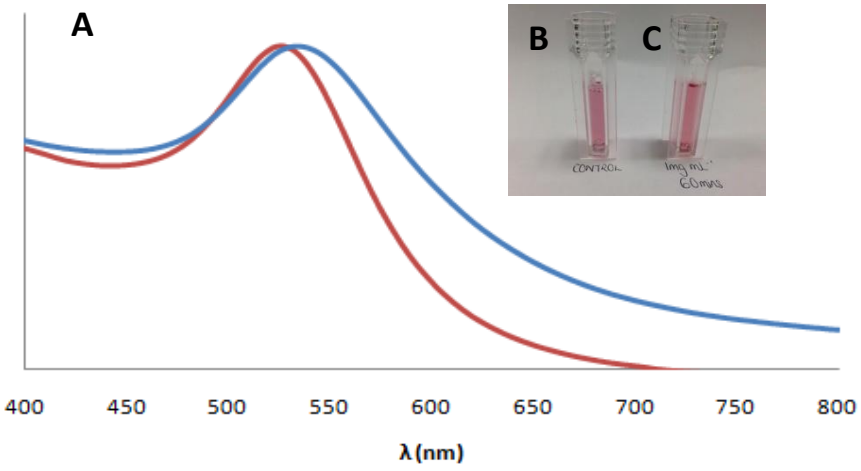

Figure 1.3

(A) UV-Vis spectra showing the difference in SPR position for (B) a control population of peptide functionalised gold nanoparticles *versus* (C) nanoparticles treated with elastase.

The experimental chapters are followed by an overall conclusion (6.0) detailing the research highlights of this work, and the thesis is brought to a close with a final chapter (7.0) detailing the materials and methods for the work contained herein.

CHAPTER TWO – ENZYME RESPONSIVE NANOMATERIALS

2.1 Abstract

Enzyme responsive nanomaterials (ERNMs) are a class of bio-responsive material i.e. materials which properties change upon application of an external biological stimuli. This literature review provides an overview of the design considerations, routes to functionalisation and characterisation techniques which must be taken into account when developing such materials.

2.2 Introduction

As the term enzyme responsive nanomaterial (ERNM) can be applied to a number of different nanoscale assemblies it is pertinent to clearly define the scope of material under review. In the context of this thesis, an ERNM is considered to be a system whereby an enzyme-sensitive substrate is immobilised on a nanoparticle, or similar nanoscale structure, in order to cause a reporting event i.e. the translation of a molecular change into a detectable, often macroscopic, transition. For brevity this chapter will not cover scholarly articles which detail the direct immobilisation of enzymes on/in the nanomaterial e.g. the work of Feringa on glucose oxidase/catalase propelled nanotubes.[1] Interested readers are directed to the review by Ansari and Husain which covers this topic in more depth.[2]

2.3 System Design

Ulijn *et al.*[3] identified three key features of an enzyme responsive material; (i) the inclusion of an enzymatically labile group or sequence, (ii) translation of the enzymatic response to the bulk of the material and (iii) a change in material properties as a result of (i) and (ii). This section will cover the rationale by which

enzymes and structural materials are selected to design such species on the nanoscale.

2.3.1 Enzymes as Stimuli

The field of biomaterials has embraced the use of enzymes as stimuli for a number of reasons; firstly, the intrinsic biocompatibility of enzymes is an attractive attribute for applications of a biological nature, and enables the use of mild reaction conditions when utilising ERNM systems. Furthermore, as a consequence of directing biochemical reactions, enzymes demonstrate a high level of substrate specificity including chemoselectivity, regioselectivity and enantioselectivity. As an ERNM exhibits a change in physical or chemical property (i.e. a reporting event occurs) upon the catalytic action of a particular enzyme, the high level of substrate selectivity ensures such systems are sensitive to only the enzyme of interest and may also lead to a high level of sensitivity e.g. if used in a sensing or diagnostic context.

Enzymes are also exploited for signal amplification purposes, as each individual enzyme molecule is capable of turning over many substrate molecules in a short space of time. For entirely solubilised systems the typical turnover rate is 10^6 min^{-1}, however, the use of Michealis-Menten kinetics is not appropriate in the context of ERNMs as the substrate is bound to a nanoscale structure which may have consequences in terms of reaction kinetics and steric effects,[4] described by a combination of the Langmuir and Michealis-Menton concepts.[5] Nevertheless, the use of enzymes in ERNM systems enables the conversion of large numbers of immobilised substrate molecules to elicit a detectable response.

As interest regarding ERNMs has increased in recent years, so too has the number of enzymes employed in such systems.[4] Table 2.1 provides a curated selection of ERNM systems in order to give the reader an idea of the breadth of enzyme classifications which can and have been utilised.

Table 2.1
A selection of ERNM systems, covering a range of enzyme classifications and nanostructured components

Enzyme	Role in Nature	Nanostructured Component	Reporting Event	Refs.
α-Amylase	Produced by mammalian and bacterial species; degradation of starch molecules	Mesoporous silica nanoparticles	Release of dye	6
α_1-Antichymotrypsin Prostate Specific Antigen	Produced by human prostatic epithelium; release increased in prostatic cancers	Gold nanoparticles	Colour change	7
α-Chymotrypsin	Produced by mammalian pancreas; digestion of protein	Quantum dot conjugates	Fluorescence Resonance Energy Transfer (FRET)	8
Elastase	Produced by mammals; elevated levels associated with chronic wounds	Gold nanoparticles	Colour change	Refer to 5.0
Glucose Oxidase	Produced by fungi; catalyses the degradation of glucose	Morphologically tailored gold nanoparticles	Shift of Surface Plasmon Resonance (SPR)	9
Kinase	Located within	Gold	Colour change	10

	cell membrane; activation of signal transducers & transcription factors	nanoparticles Quantum dot conjugates	FRET	11
Matrix Metalloproteinases (MMPs)	Produced by most eukaryotic species; interaction with cell receptors	Magnetic nanoparticles	Shortening of relaxation times by MRI	12
		Gold nanoparticles	Release of fluorescent dye molecule	13
Phosphatase	Produced by mammalian and plant species; regulation of signal transduction	Polyoxazoline nanostructures	Size change observed by Dynamic Light Scattering (DLS)	14
Thermolysin	Produced by bacterial, fungal and prokaryotic species; degradation of extracellular peptides & proteins	Gold nanoparticles	Colour change	7
Trypsin	Produced by mammals; elevated levels associated with pancreatic conditions	Gold nanoparticles	Colour change	15

2.3.1.1 Enzymatic Action

The catalytic targets of many enzymes are peptidic, thus it is unsurprising that many ERNMs utilise short chain amino acid sequences as substrates. Additionally, as peptides direct events within biological systems, the enzymes which interact with these sequences are of particular interest to researchers working in the field of sensing and diagnostics. ERNMs utilising alternative substrates including oligonucleotides, polysaccharides and phenolic esters are also detailed in the literature.[16-18]

Bond Cleavage

Proteases belong to the classification of enzymes known as hydrolases which catalyse the hydrolysis of various bond types. In particular, proteases break one or more peptide bonds in a protein or peptide, illustrated in figure 2.1.

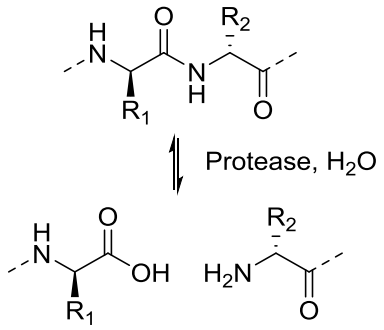

Figure 2.1
Schematic showing the hydrolysis of a peptide bond catalysed by a protease enzyme.

Proteolytic enzymes occur in every living organism, and are involved in a multitude of physiological processes; ranging from the simple degradation of proteins during the digestive process to highly regulated blood coagulation cascades and embryonic development.[19] Due to their central biological role; analysis of the human genome reveals the existence of ~ 500 different proteases.[20] These

enzymes are intrinsically linked to the pathological processes of degradation and disease, making them valuable targets for therapeutic applications.

Proteases are commonly utilised to hydrolyse, or cleave, functional groups prior to self-assembly of nanostructure components[21] i.e. this translation of enzyme action into a material response forms the basis of many ERNM systems. Endonucleases including esterases and phosphatases are further examples of hydrolase enzymes which have been employed by ERNM systems.[22]

Bond Formation

Kinases, part of the phosphotransferase family, can be used to phosphorylate a particular peptidic sequence resulting in a change in the ERNM properties. Bhatia *et al*. developed an ERNM system whereby two populations of magnetic nanoparticle conjugates were prepared, figure 2.2.[23] One population contained peptide substrates which could be phosphorylated or dephosphorylated by a kinase or phosphotase enzyme respectively, while the other population was modified with Src Homology 2 (SH2) domains which could bind phosphorylated sequences.

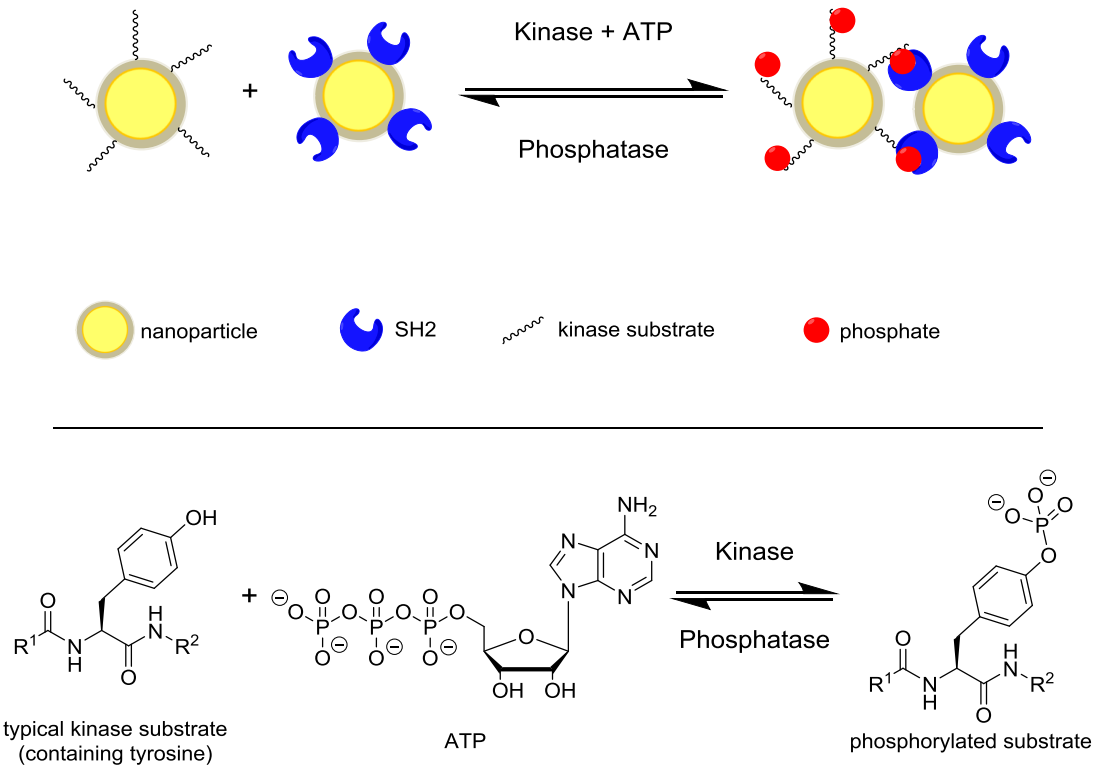

Figure 2.2
Schematic illustrating the reversible nature of the kinase/phosphatase ERNM system designed by Bhatia *et al*.[23]

The kinase directed assembly enabled coordination of the magnetic dipoles within the nanoparticles, which could be followed using MRI and T2 relaxation outputs. The addition of phosphatase into the system, causing dispersion of the nanoparticle assemblies can be followed in the same manner. This sensor was one of the first examples of ERNMs able to process antagonistic enzyme inputs.

Equally, those enzymes which enable the condensation of functional moieties to form chemical bonds could potentially be utilised in ERNM systems as they are in macro-scale applications.[24] This includes the use of proteases or transglutaminases to form covalent bonds between pairs of amino acids or amine and acyl groups respectively. When utilising proteases in this manner, care must be taken to ensure

an appropriate environment is provided to thermodynamically favour the reverse reaction.

2.3.2 Selection of Nanostructured Component

It is critical that an ERNM is able to operate under conditions which allow and maintain enzyme activity; most typically aqueous environments at neutral pH. A wealth of synthetic materials, such as polymers and inorganic particles can tolerate such conditions; readers are referred to the review by Ulijn *et al*. for a comprehensive list of materials used in the design of enzyme responsive applications.[4] Thus, careful consideration on the part of the researcher is required, as the chemical composition of the nanostructured component determines, and limits, the responses which can be generated by a particular ERNM.

2.3.2.1 Metallic Nanoparticles

The IUPAC agreed definition of the term "nanoparticle" is a "particle of any shape with dimensions in the 1×10^{-9} and 1×10^{-7} m range."[25] Such materials are found to display physical properties that are unlike either small molecular species or bulk material due to their size, shape and interparticle distances.[26] As a result, nanoparticles functionalised with enzyme sensitive substrates have become key components in the field of materials science, in particular diagnostics. ERNMs which utilise metal nanoparticles as the nanostructured component will form the main focus of this review article due to the experimental content of this thesis.

Nanoparticles of predictable size, suitable monodispersity and relative stability can be prepared in the size range of 1-100 nm. This size range falls between the realms of individual atoms and aggregates that are large enough to be considered "bulk" material. The physical properties of these nanomaterials are not like those displayed by the bulk or of molecular compounds. Their properties are influenced by their composition, particle size, shape, inter-particle distance and the nature of surface adsorbate.

Gold Nanoparticles

Gold nanoparticles have unusually high molecular extinct coefficients, and as a result are a highly coloured ruby-red species.[26-28] This red colouring is due to the surface plasmon resonance (SPR) which absorbs at ~520 nm in the visible region; the precise wavelength of the band is dependent upon the nanoparticle size, the dielectric constant of the suspension medium and the temperature.[27, 28] The SPR is due to the collective oscillations of conduction electrons on the surface of the nanoparticle, resulting from excitation by the electromagnetic field of incoming light i.e. excitation of the conduction band through interaction with light, figure 2.3.

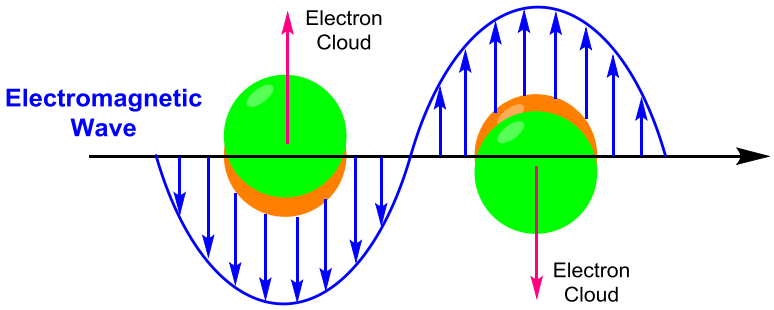

Figure 2.3
The interaction (not to scale) of nanoparticles with light and the propogation of the SPR.

Nanoparticle aggregation causes broadening and red-shifting of the SPR up to 250 nm.[27] This triggers a colorimetric change from red through purple to blue which can be monitored using UV-Visible spectroscopy and is a useful property for commercial applications such as biochemical assays (see section 2.6.1).[26, 29-30]

ERNM systems utilising the aggregation and/or dispersion of peptide-functionalised gold nanoparticles may have a number of interesting applications, including diagnostic testing. Scrimin *et al.* developed a simple assay which could be tailored to enable the detection of different proteases, notably thrombin & lethal factor.[31] The system involved incubating a enzymatically labile peptide sequence,

functionalised with two terminal cysteine residues, with the enzyme of interest. In the absence of enzyme, when the sequence was added to a solution of colloidal gold the thiol groups bound to the nanoparticles inducing aggregation and the resultant colour change to purple-blue. However, when the enzyme was present the cleaved peptides were unable to induce such a change and the nanoparticles remained disperse and burgundy-red in colour.

The Stevens group have developed a number of ERNMs and related enzyme inhibitor screening systems utilising nanoparticles.[7, 9-10] In particular, the group developed a method for protease detection by exploiting the dispersion state of gold nanoparticles, figure 2.4.

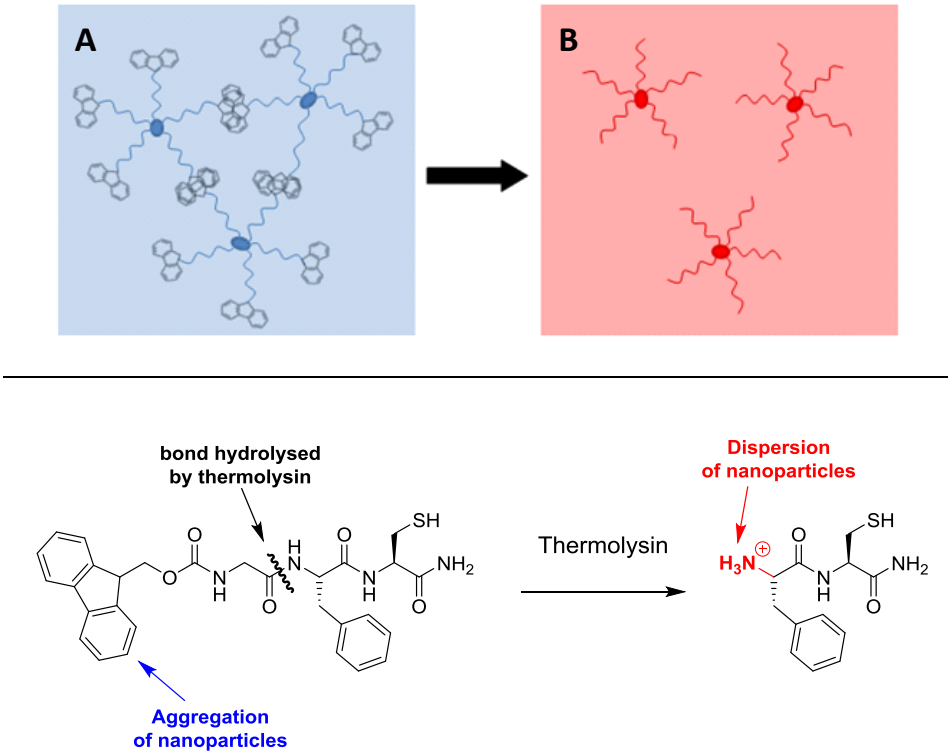

Figure 2.4
Schematic representation of the protease assay developed by Stevens *et al.*[7]

This assay consists of a homogeneous population of gold nanoparticles functionalised with an Fmoc-terminated thiolated peptide sequence. π-π

interactions between the fluorenyl groups causes the formation of nanoparticle assemblies. Proteolysis of the peptide sequence, by thermolysin, and upon system modification, α_1-antichymotrypsin prostate specific antigen (n-ACT PSA) results in particle dispersion and the associated colour change from purple-blue to burgundy-red, as indicated in figure 2.4.

Other notable examples of gold nanoparticle aggregation/dispersion type ERNM systems include; work by Bates *et al.* to form highly ordered assemblies of oligonucleotide functionalised nanoparticles by employing a system of DNA ligases and endonucleases,[32] the development of a kinase sensing system utilising biotinylated substrates by Brust *et al*.,[33] and Choi's work on phosphatase detection.[34] The recent review article by Hutter and Maysinger provides a helpful summary of the key published articles in this area.[35]

Such visual systems may overcome the need for expensive equipment and highly trained personnel for primary diagnosis of certain conditions. The inherent amplification of signal *versus* systems based upon antigen-antibody interactions also makes this an attractive concept. Whilst the methods outlined above can provide direct colorimetric signal output directly, the physical properties of gold nanoparticles lend themselves to near infrared fluorescence (NIRF) imaging,[36] nanoelectronics[37]and surface enhanced Raman spectroscopy (SERS) applications; although in many instances such sensors utilise a combination of gold/silver nanostructures (discussed further in silver nanoparticles sub-section).

Silver Nanoparticles

Raman scattering is an inherently weak process; at maximum efficiency, only one photon in every ten million undergoes Raman scattering. However, scattering efficiencies can be enhanced by the use of resonance Raman scattering (RRS), surface-enhanced Raman scattering (SERS), or a combination of both these techniques, surface-enhanced resonance Raman scattering (SERRS).

Colloidal silver nanoparticles are considerably less stable than gold and the synthesis of monodisperse solutions of a pre-determined size can be complex; consequently, silver nanoparticles have been utilised in fewer sensing applications.[38] Despite these limitations, silver nanoparticles are known to display superior catalytic and SER(R)S enhancement properties *versus* their gold counterparts.[31]

Graham *et al.* demonstrated that silver nanoparticles could be used to illustrate the differing activities of proteolytic enzymes by SERRS. A tri-component system; containing a (i) benzotriazole-dye as SERRS active species, joined to (ii) an enzyme recognition site *via* (iii) an enzymatically cleavable linker to an amino acid sequence was prepared and complexed to the surface of silver nanoparticles. Upon introduction of a protease, hydrolysis of the bond between the benzotriazole and the enzyme recognition site would occur to form a SERRS active compound (shown in figure 2.5). The strength of SERRS signal observed was proportional to the extent of hydrolysis, and thus could be used to discriminate between protease classifications, including pepsin & chymotrypsin.[39]

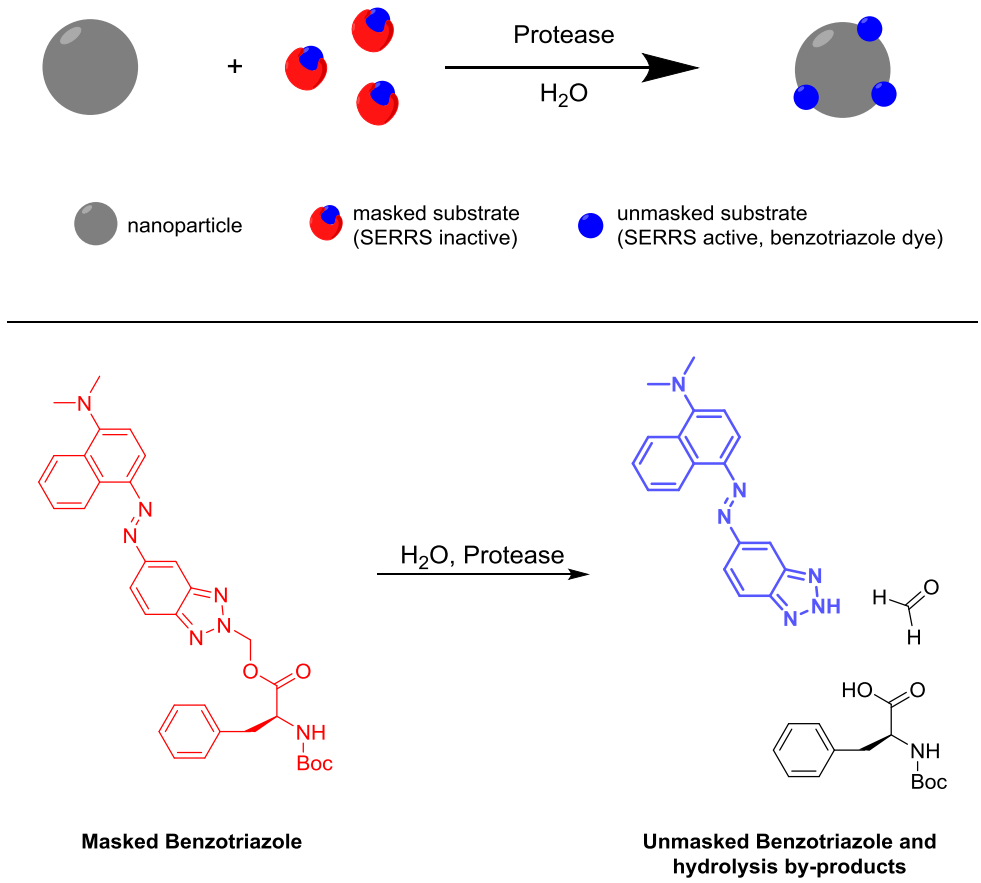

Figure 2.5
Schematic representation of the protease assay developed by Graham *et al.*.[39]

Previous work by Graham *et al.* entailed the use of a similar benzotriazole-containing system to monitor lipase activity over time by measuring peak intensity of the SERRS signal.[40] The extent of enzymatic activity observed was in-line with the enzyme reactivity towards the substrate, and this system was the first published example of using SERRS to measure enzymatic activity.[41]

In addition to Raman spectroscopy, silver nanoparticles have been utilised in alternative forms of spectrophotometric enzyme detection, such as UV-Vis. While most colorimetric assays for enzyme detection focus use gold nanoparticles due to the distinctive colorimetric shifts observed when the extent of dispersion is altered; a small number of colorimetric assays which utilise silver nanoparticles have been

developed. Wang *et. al*. describe preliminary work which utilises the colour differences between disperse and aggregated silver nanoparticle species to indicate whether or not enzymes related to phosphorylation were present.[42] Finally, silver nanoparticles are known to have antibacterial and antimicrobial properties. As pathogenic "super bugs" e.g. *Methicillin-resistant Staphylococcus aureus* (MRSA) continue to develop broad spectrum resistance to antibiotic drugs, the intrinsic therapeutic properties of such materials have been exploited to enable the development of silver impregnated medical devices such as surgical masks and creams/gels for chronic wound treatment.[43]

2.3.2.2 Non-metallic Nanoparticles

Although composed of metallic elements, it is pertinent to note that the physical properties of quantum dots and magnetic nanoparticles are often the result of their chemical composition. Thus, for the purpose of this review these nanostructures are being classified as non-metallic i.e. the particles of this type are typically heterogeneous species.

Quantum Dots

Quantum dots are nanoparticles composed of semiconducting material which display size dependent fluorescence. As these species have dimensions on the nanoscale they are able to exhibit quantum mechanical properties and display electronic behaviours which are intermediate between bulk semiconductors and discrete molecules.[44] The majority of quantum dots used for ERNM applications are core-shell structures composed of a CdSe core surrounded by a ZnS shell which is typically coated with an organic material to enable surface functionalisation.[45] The outer semiconductor shell functions as a protective layer against oxidation and it also enhances the quantum yield of the quantum dot.[47, 48] An additional coating of polymer or ligands allows for solubilisation of quantum dots in either organic or aqueous environments.[48]

ERNM systems which utilise quantum dots as the nanostructured component include Förster/fluorescence resonance energy transfer (FRET) or bioluminescence resonance energy transfer (BRET) systems. In such RET applications, quantum dots are proven to be superior fluorophores than fluorescent proteins as a consequence of their large Stokes shift.[45]

2.3.2.3 Non-Particulate Nanostructures

It is pertinent to note that in the wider context of ERNMs, i.e. outside the strict constraints of this literature review, not all enzyme responsive systems on the nanoscale utilise particulate materials as the nanostructured component.

Klarite and Nanostructured Surfaces

For the purposes of completeness, surfaces with localised regions of nanostructure should also be included within this section. Such materials include the commercially available SERS substrate, Klarite which has been used extensively for the detection of dye-labelled oligonucleotides.[47] A discussion of enzyme responsive

nanostructured surfaces, and the use of Klarite for enzymatic detection, is provided in Chapter 4.0.

2.4 Conclusions

This chapter was intended to provide a brief overview of ERNMs in order to highlight the sheer scope and breadth of materials which fall under this classification. Despite constraining the materials discussed to enzyme-sensitive substrates immobilised on nanoparticles or similar nanoscale structures, the examples included within this chapter illustrate the variety and versatility of ERNMs available.

The reader was directed through each of the design considerations required for the development of an ERNM; from enzyme choice to the selection of a nanostructured component.

CHAPTER THREE – PEPTIDE FUNCTIONALISATION OF PLANAR GOLD SURFACES

3.1 Abstract

A method for the step-wise functionalisation of planar gold surfaces with short peptide derivatives is reported. (±)-α-lipoic acid was utilised to provide an anchor to the gold surface and conventional Fmoc chemistry used to prepare the peptide sequences. The fluorenyl functional group provided a convenient marker for surface analysis, enabling the verification of each synthetic step by ToF-SIMS, XPS and LDI-ToF MS. Step-wise solid-phase synthesis on the gold surface is a facile means of preparing peptide-conjugates, providing a method whereby no additional purification or final "grafting-on" steps are required. The use of LDI-ToF MS and ToF-SIMS in tandem ensured confidence in the stepwise synthesis method. These techniques provided complimentary data to one another through the analysis of both the fully desorbed peptide derivative and molecular fragments respectively.

3.2 Introduction

Functionalising surfaces with biomolecules may enable the development of materials able to bridge the gap between man-made and biological matter.[1] Peptides in particular provide an extremely rich and versatile chemical toolbox; which combined with the inherent biocompatibility of such molecules, suggests that peptide functionalised surfaces are ideally suited to act as interfaces between biological and synthetic materials.[1-4] Such surfaces have been utilised extensively in biomaterials science,[5] as surface properties such as wettability, molecular architecture or topology can be tailored to the needs of specific applications.[6-8]

Two-dimensional gold surfaces have been widely used as model systems e.g. cell culture experiments and the design of "switchable" surfaces.[9-10] Furthermore, gold nanoparticles are of particular interest due to the unusually high molar extinction coefficient they possess, which has proved to be attractive in the fields of diagnostics and sensing.[11-12] To date, research has largely focused on oligonucleotide functionalised nanoparticles,[13-17] however, as peptides provide the language to direct biological events, it is no surprise that the number of peptide-functionalised gold nanoparticle systems has increased dramatically over the last 5 years.[18-20] As such, robust methods for peptide functionalisation and analysis of gold surfaces are required.

3.2.1 Solution-Phase Synthesis of Peptides

The range of interesting chemical properties possessed by peptides makes the ability to synthesise these molecules an important tool for researchers.[8] Chemical synthesis of peptides allows structure confirmation of naturally occurring peptides (deduced from sequencing studies), analysis of the structure-activity relationships of biologically active peptides, preparation of relatively large amounts of rare peptides and also affords the ability to synthesise peptide analogues, for applications such as human health care and enzyme screening.[5]

Peptides can be manufactured chemically by either "classical" solution-phase synthesis or solid-phase peptide synthesis (SPPS), developed by Merrifield in 1963.[15]

Peptide synthesis is based upon the stepwise condensation of a series of amino acids, from the C to the N terminus,[5] resulting in the formation of a peptide chain. Mechanistically, this coupling process involves nucleophilic attack by the amino group of one residue at the electrophilic carbonyl carbon of another amino acid, which has typically been activated with an electron withdrawing group,[6] figure 1.6.

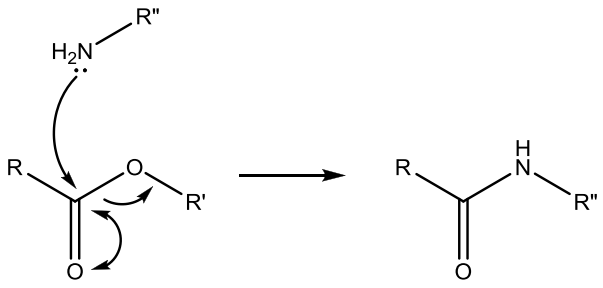

Figure 3.1
Peptide bond formation between an activated amino acid; R' is an electron-withdrawing group, and the α-amino group of an additional amino acid.

The first example of solution-phase peptide synthesis was the synthesis of the cyclic peptide, oxytocin, by du Vigneaud in 1953.[16] This work utilised mixed carbonic anhydrides to enable the coupling of individual amino acids; however, it is also possible to employ carbodiimides, N-carboxyanhydrides or coupling catalysts such as N-hydroxysuccinimide (NHS) and 1-hydroxybenzotriazole (HOBt) for this purpose.[17]

Although a useful means of preparing short peptide sequences, the solution-phase method is not ideally suited to the preparation of long peptide chains. The resultant peptide has to be purified and isolated after each coupling reaction; resulting in loss of yield, even if the coupling process was highly efficient.[8] In order to enable the synthesis of longer peptide sequences in a feasible manner, block synthesis and fragment condensation was utilised. This technique involves synthesising 5-10 residue "blocks" and then sequentially linking the blocks together to form the final product.[8]

In addition to the progressive decline in yield associated with this method, purification difficulties also arise as the number of amino acid residues increase; confirming solution-phase synthesis as a time, labour and skill intensive process. Consequently, solution-phase synthesis has been largely replaced by SPPS in most laboratories, unless large-scale quantities of peptide are required.[5]

3.2.2 Solid-Phase Peptide Synthesis

Solid Phase Peptide Synthesis (SPPS) was initially developed by Merrifield in 1963 as a rapid and automatic means of peptide synthesis, due to the labour intensive and repetitive nature of solution-phase synthesis.[15] Development and refinement of the technique ultimately culminated in the award of the 1984 Nobel prize in Chemistry to Merrifield for the development of a methodology for chemical synthesis on a solid matrix.[6]

The general procedure for SPPS involves attaching a suitably protected amino acid residue to an insoluble, functionalised solid support using a linker molecule resistant to all chemistries employed in the synthesis. This reaction proceeds from the C-terminus to the N-terminus, in the opposite manner to the biosynthesis of peptides, via deprotection of the first residue and successive introduction of additional amino acids. Once the desired chain length has been achieved, the amino acid side chains are deprotected and the sequence is cleaved from the solid support. The use of an insoluble, porous support enables excess reagents and by-products to be washed away while the growing peptide chain is covalently linked to the surface.[18]

The use of protecting groups is fundamental to the successful synthesis of peptides, as all reactive groups not required to participate in a synthetic step must be passivated to prevent reaction occurring.[8] Two common strategies exist in modern SPPS; the Boc/Bzl protection strategy and the Fmoc/^{t}Bu strategy whereby both methods involve a means of "temporarily" protecting the α-amino group of the amino acid, and a "permanent" means of protecting the amino acid side chains.[19]

The Boc/Bzl route, developed by McKay and Albertson,[20] was the method used by Merrifield in the original SPPS experimental design, figure 1.7.

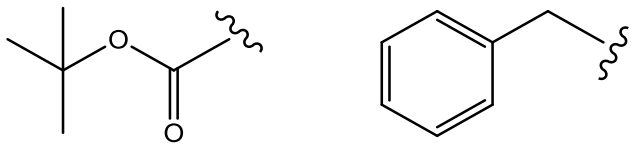

Figure 3.2
Structures of the Boc and Bzl protecting groups.

Tert-butoxycarbonyl (Boc) is used to temporarily protect the α-amino group, while benzyloxycarbonyl (Bzl) groups are used to permanently protect the side chain functionalities.[5, 8] This protection strategy cannot be termed orthogonal as acidolysis is used to remove both protecting groups; however, sufficient differences in acid lability afford selective removal of the α-amino protection. Thus this method can be deemed "quasi-orthogonal".[6, 19]

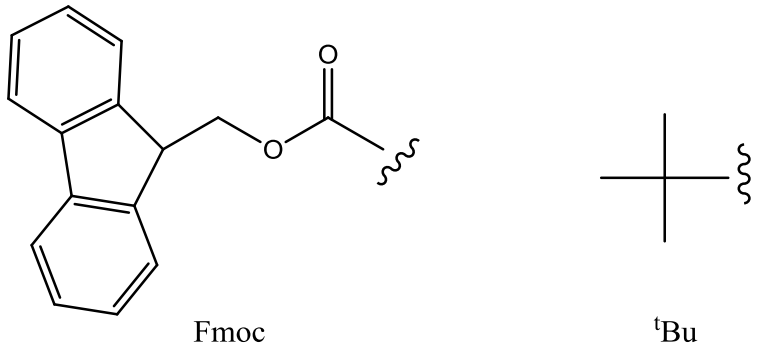

Figure 3.3
Structures of the Fmoc and ^{t}Bu protecting groups.

Fmoc/ ^{t}Bu protection, developed by Carpino,[21] is a truly orthogonal system; the 9-fluorenylmethoxycarbonyl (Fmoc) group used for temporary protection of the α-amino functionality is removed by the mild base piperidine, while the ^{t}Bu protecting groups on side chains are TFA labile. This system is more widely used than the Boc/Bzl route, as in addition to being orthogonal; the overall reaction conditions are milder and more user friendly, and the fluorogenic and chromogenic

nature of the Fmoc-group enables reactions to be monitored spectroscopically.[18] However, care must be taken when attempting to prepare peptides via this route, as Fmoc-protected amino acids are extremely hydrophobic which may reduce the solubility of derivatives and hamper deprotection.[6]

The basis of peptide bond formation is the conversion of the carboxylic acid function of one amino acid to a reactive derivative that is susceptible to nucleophilic attack by the amino group of another.[8] The most commonly used reagents are carbodiimides, such as diisopropylcarbodiimide (DIC) and dicyclohexylcarbodiimide (DCC),[22, 23] which react with the carboxylic acid of the reagent to form the highly reactive *O*-acylurea, which then reacts directly with the solid-supported amine to yield the desired amide and a urea by-product. However, *O*-acylurea can cause racemisation through oxazolone formation, a problem which has been overcome through the use of benzotriazole reagents such as 1-hydroxybenzotriazole (HOBt) and 1-hydroxy-7-azabenzotriazole (HOAt). Uronium salts based upon triazoles such as O-benzotriazole-N,N,N',N'-tetramethyl-uronium-hexafluoro- phosphate (HBTU) have also been introduced to ensure efficient catalysis of amide bond formation.[24]

Merrifield's original design used functionalised polystyrene beads as the solid support, due to the material's good swelling properties in organic solvents.[15] The solid support has been modified in modern techniques, whereby the most common matrix is a polystyrene copolymer crosslinked with 1 % divinylbenzene. This is ideal for peptide synthesis as the material is chemically inert under SPPS conditions and can be easily derivatised to enable facile surface attachment.[19] Another commonly used support are Wang resins, which utilise the 4-alkoxybenzyl alcohol linker to facilitate attachment of protected amino acids to the solid surface.[25] This support is ideal for synthesis via the Fmoc/^{t}Bu route, as the linkage is not affected by the basic conditions used to remove the Fmoc-group, yet is

sensitive to acid; enabling simultaneous deprotection of amino acid side chains and cleavage from the solid surface.[8]

Acidolytic cleavage of a peptide sequence from a solid support following SPPS yields a crude product containing the desired peptide and impurities such as truncated peptides, deletion products and by-products from the cleavage of protection groups. Purification is commonly undertaken by RP-HPLC using C_{18} modified silica and 0.1 % TFA as eluent. Elution of material is monitored spectroscopically using UV detection, enabling the fractions of pure peptide to be combined and lyophilised before use.[19]

Examples of researchers performing SPPS directly upon flat surfaces; including cellulose,[24] poly(ethyleneglycol acrylamide) co-polymer (PEGA),[25-26] glass,[27] gold[12, 28] and aminosilanised silicon oxide.[29-30] However, to the best of our knowledge, no comprehensive surface characterisation has been undertaken for peptide functionalised gold surfaces.

Peptide sequences for the functionalisation of gold conventionally contain a terminal cysteine residue or utilise alkane thiols to anchor the peptide, enabling surface attachment through standard gold-thiol chemistry. It is currently widely accepted that the covalent interaction at the gold–sulfur interface requires formation of gold–thiolate bond(s): that is, the sulfhydryl group is deprotonated, creating formally a thiyl radical (RS·), whereas the protonated SH group can interact with gold only by weaker coordination-type bonds through the sulfur lone-pair electrons. The thiolate–gold (RS–Au) bond has a strength close to that of the gold–gold bond, so it can significantly modify the gold–gold bonding at the gold–sulfur interface.

It has been demonstrated that thioctic acid, containing a disulfide linkage, can be utilised as a more robust anchor to the gold surface.[62] Stability testing confirmed such a linker molecule showed greatly enhanced stability over time, after treatment

with DTT at elevated temperatures, compared with traditional thiol approaches for the oligonucleotide systems under investigation.[81] Due to the potential stability benefits which may be afforded to peptide-nanoparticle conjugates, the predictable reactivity under typical peptide synthesis conditions and the low cost of starting material,[83, 84] thioctic acid was deemed an ideal ligand for nanoparticle functionalisation.

The functionalisation strategy discussed in this chapter contains three key elements: a 5-membered disulfide anchor to the gold surface, dialanine (AA) and a terminal Fmoc group. The serine protease elastase would be expected to selectively cleave between the two alanine residues (i.e. Fmoc-A↓A) liberating Fmoc-A;[32] with the fluorenyl group providing a convenient spectroscopic marker to facilitate reaction monitoring. Unlike approaches utilising similarly functionalised nanoparticles, where characterisation of the gold surface is a difficult task,[18] the two-dimensional nature of this system enables comprehensive analysis of the surface after each synthetic step and the enzymatic cleavage.

3.3 Project Aim

The aim of this research was to develop a robust strategy for the peptide functionalisation of gold. A model system is described whereby planar gold surfaces were functionalised with a peptide sequence in a stable, homogeneous and highly reproducible manner using stepwise SPPS; similar in approach to that used in studies by Flitsch.[12] A further intention of this work was to prepare enzyme sensitive surfaces which could be fully characterised using ToF-SIMS, XPS and LDI-ToF MS pre and post enzyme treatment. This would allow each synthetic step and the enzymatic cleavage to be monitored to confirm surface modification, and to allow any necessary steps for optimisation to be taken.

3.4 Results and Discussion

To enable SPPS, gold-coated glass cover slips were modified with (±)-α-lipoic acid (figure 3.1, surface 1). Once deposited on the gold surface, the terminal carboxylic acid was activated through formation of an *N*-hydroxysuccinimide ester (figure 3.1, surface 2), before treatment with either *N*-Fmoc-1,4-butanediamine·HBr (figure 3.1, surface 3 containing R_1 and R_3) or Boc-amino-PEG_6-amine (figure 3.1, surface 3 containing R_2 and R_4) and subsequent deprotection with 20:80 v:v piperidine: *N,N*-dimethylformamide or 50:50 v:v trifluoroacetic acid:dichloromethane respectively to expose the amine functionality (figure 3.1, surface 4). The surfaces then underwent repeated amino acid coupling and deprotection cycles using conventional Fmoc/piperidine chemistry to afford the target sequence (figure 3.1, surface 5). To confirm the surface modification was successful, the surfaces were characterised using ToF-SIMS, XPS, LDI-ToF MS and WCA after each stage of surface functionalisation.

As illustrated in Figure 3.4 spacer units R_1/R_2 were incorporated into the surfaces. The rationale for this was to provide a free amine moiety to enable coupling with the acid of Fmoc-protected amino acids, using standard Fmoc peptide chemistry (discussed in section 3.2.2).

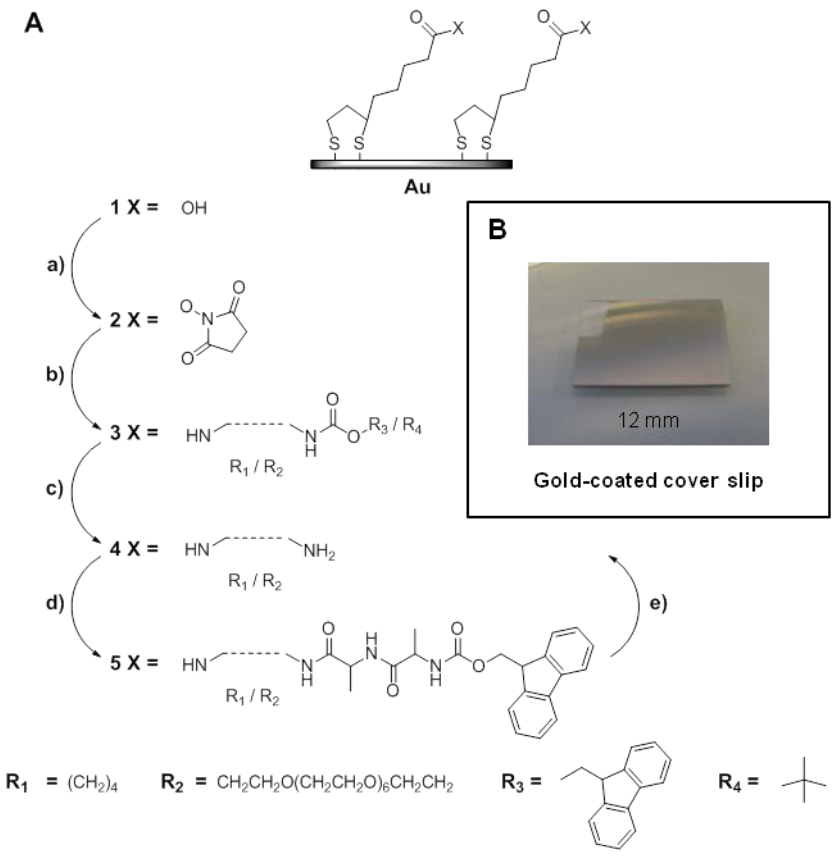

Figure 3.4

(A) Strategy for stepwise synthesis on (±)-α-lipoic acid coated gold surface. a) EDC·HCl, NHS, *N,N*-dimethylformamide, 2 h, room temperature; b) For 3a containing R_1 and R_3: *N*-Fmoc-1,4-butanediamine·HBr, *N,N*-dimethylformamide, overnight, room temperature; For 3b containing R_2 and R_4: Boc-amino-PEG_6-amine, *N,N*-dimethylformamide, overnight, room temperature; c) For 4a containing R_1: 20:80 v:v piperidine:*N,N*-dimethylformamide, 2 h, room temperature; For 4b containing R_2: 50:50 v:v trifluoroacetic acid:dichloromethane, 2 h, room temperature; d) i. Fmoc-A-OH, HBTU, DIPEA, *N,N*-dimethylformamide, overnight, 37 °C; ii. 20:80 v:v piperidine:*N,N*-dimethylformamide, 2 h, room temperature; iii. *N*-Fmoc-L-A, HBTU, DIPEA, *N,N*-dimethylformamide, overnight, 37 °C; e) 1 mg mL^{-1} elastase (*Porcine Pancreas*) in phosphate buffer (pH 8, 100 mM). (B) Gold-coated cover slip; 12 mm diameter, 5 nm Ti base layer and 15 nm Au thickness.

3.4.1 Surface Analysis

Surface modification at the molecular level is a difficult process; contamination of samples is a serious concern, while the proximity of reactive moieties to a surface may hinder reactions reaching completion. Thus, surface analysis at each step was required to ensure the synthesis proceeded as expected. Flitsch *et al*.[12] have previously described gold surfaces presenting peptide arrays which were used for enzyme detection. Building upon this work, surfaces containing an AA dipeptide, a target sequence for the serine protease elastase, were prepared. The success of the synthesis and the enzymatic cleavage were determined using the complimentary techniques of ToF-SIMS, XPS and LDI-ToF MS.

Over one-third of the known proteolytic enzymes are serine proteases and they constitute the largest group of homologous proteases in the human genome.[33] The typical serine protease hydrolysis reaction is considered to be a three step kinetic mechanism; an enzyme-substrate complex is formed by the hydroxyl group on the active site serine acting as a nucleophile, and attacking the carbonyl moiety of the substrate peptide bond. Subsequently this hydroxyl group is acylated, and then the acyl enzyme intermediate is finally hydrolysed to afford polypeptide fragments.[34]

Although all serine proteases have the same catalytic triad, different enzymes show different substrate specificities due to differences in their binding site. Elastase acts by digesting elastin; a protein present in connective tissue, composed of simple aliphatic amino acids.[35] While naturally occurring within the human body, elevated levels of elastase are present in chronic wounds such as bed-sores and diabetic ulcers *i.e.* 99.5 μg mL^{-1} in chronic wounds *versus* < 1 μg mL^{-1} in acute.[36] In order to ensure specificity towards small hydrophobic residues, bulky valine (V_{216}) and threonine (T_{226}) residues are present within the active site, preventing access to sequences containing large side chains.[34]

3.4.2 Time-of-Flight Secondary-Ion Mass Spectrometry (ToF SIMS)

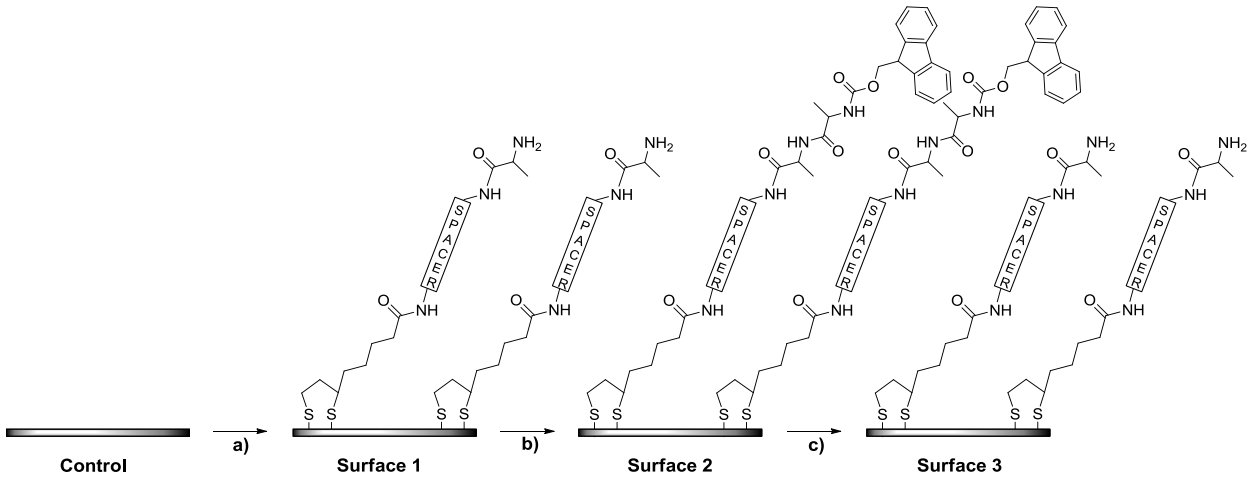

Figure 3.5
Schematic showing the surface functionality of the control and surfaces 1 - 3 analysed by ToF-SIMS and XPS in figures 3.3 and 3.4. The control sample was a clean, unmodified gold-coated glass cover slip. a) Treatment with (±)-α-lipoic acid followed by NHS activation, coupling of a protected diamino linker and subsequent deprotection of the linker; b) repeated amino acid coupling and deprotection cycles to afford target sequence; c) treatment with elastase. It should be noted that although surfaces 1 & 3 have the same structure, surface 3 is the result of enzymatic treatment i.e. surface 2 is treated with elastase to generate surface 3.

Time-of-Flight Secondary-Ion Mass Spectrometry (ToF-SIMS) is a surface analysis technique with an analysis depth of approximately 1 nm. Analysis involves a pulsed beam of primary ions being focused onto a sample surface to produce secondary ions in a sputtering process. Secondary ion mass spectrometry (SIMS) uses this effect to obtain information about the composition of the surface by analysing the fragments sputtered from the surface with a mass spectrometer.[37] The secondary ions drift through a field-free path prior to reaching a detector and as all ions have the same kinetic energy at the beginning of the path, the time taken is determined by the ion's mass. Since all ions have the same kinetic energy at the beginning of the path, the time it takes them to travel a fixed distance only depends

on their mass. Lighter ions reach the detector earlier than heavier fragments and can therefore be separated from each other. The main advantage of this method is that all ions of a given charge can be analysed at the same time.[37] Please refer to section 7.2.3 for experimental conditions.

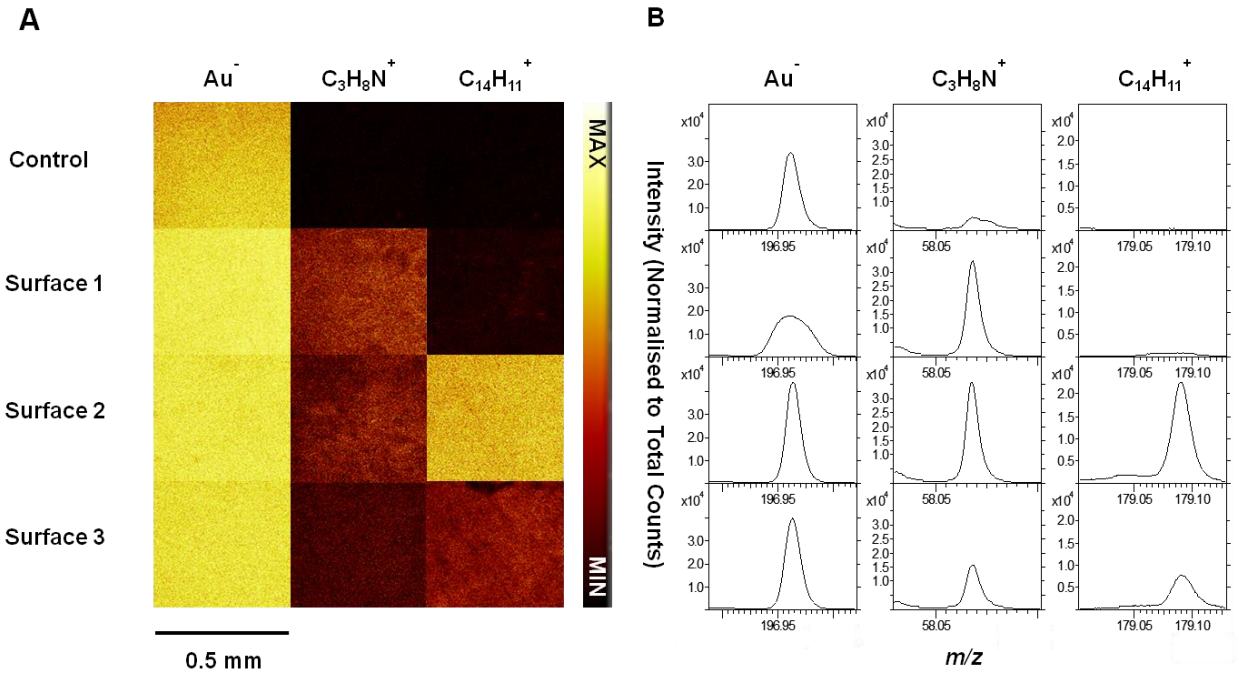

Figure 3.6
Surface modification strategy employing a $(CH_2)_4$ spacer. (A) SIMS ion intensity maps for each surface displayed for selected masses (Au^- = 196.953 D, $C_3H_8N^+$ = 58.054 D and $C_{14}H_{11}^+$ = 179.058 D). Images are scaled to the same maximum pixel value for each ion. (B) ToF-SIMS normalised intensity spectra for each of the surfaces obtained at selected *m/z* values.

The ToF-SIMS data (surface functionality shown in figure 3.5) are presented in figure 3.3 as ion intensity maps (figure 3.6 A) and normalised intensity spectra for each surface at selected masses (figure 3.6 B, scale = intensity (normalised total counts x 10^4)). The peak at *m/z* = 197 D represents gold, and is shown to provide a strong signal throughout the analysis process. The *m/z* = 58 D intensity maps follow the pattern predicted for the $C_3H_8N^+$ ion which represents the aliphatic

spacer unit present in the system (figure 3.3 A, surface 1). The *m/z* = 179 D peak is assigned to the $C_{14}H_{11}^{+}$ which is indicative of the Fmoc group. Full spectra are shown in figures 3.7 and 3.8.

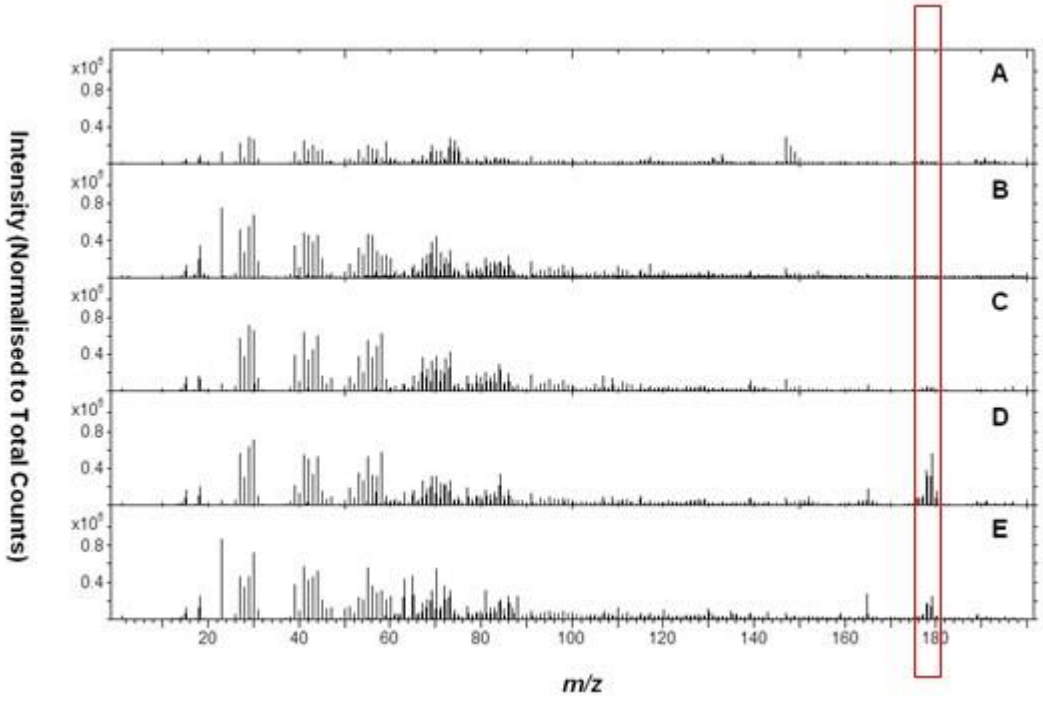

Figure 3.7
ToF-SIMS positive secondary ion spectra for surface modification strategy employing a $(CH_2)_4$ spacer. (A) Gold cover slip after piranha and plasma cleaning. (B) Gold cover slip treated with elastase (*Porcine Pancreas*, 1 mg mL^{-1} in phosphate buffer). (C) Gold cover slip after peptide functionalisation to surface 1. (D) Gold cover slip after peptide functionalisation to surface 2. (E) Gold cover slip after peptide functionalisation to surface 3.

Figure 3.7 shows the average positive secondary ion spectra generated for the gold surfaces prepared. Particular focus is paid to the region around 179.05 on surfaces 2 and 3 where the spectra have been highlighted. This region corresponds to the peaks shown in figure 3.6 B for the mass corresponding to $C_{14}H_{11}^{+}$ i.e. the fluorenyl fragment. As illustrated by the sections shown in red, it is clear that the spectra shown in figure 3.6 B are representative of the whole sample, not just an individual

region. Surface 2 shows the greatest intensity for the fluorenyl fragment as discussed previously.

Figure 3.8 shows the average negative ion spectra generated for the gold surfaces prepared. In this case the region around 196.95 has been highlighted to indicate that the signal for gold is observed throughout the analysis process, as illustrated in figure 3.6 B.

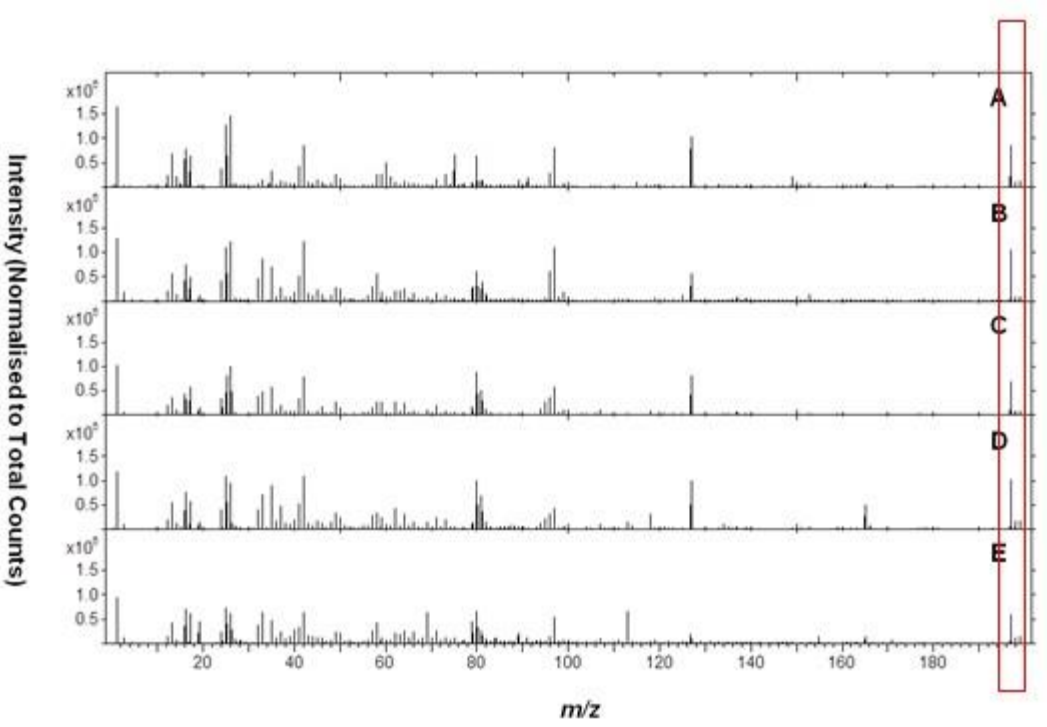

Figure 3.8
ToF-SIMS negative secondary ion spectra for surface modification strategy employing a $(CH_2)_4$ spacer. (A) Gold cover slip after piranha and plasma cleaning. (B) Gold cover slip treated with elastase (*Porcine Pancreas*, 1 mg mL^{-1} in phosphate buffer). (C) Gold cover slip after peptide functionalisation to surface 1. (D) Gold cover slip after peptide functionalisation to surface 2. (E) Gold cover slip after peptide functionalisation to surface 3.

It was anticipated that following the signals generated by the terminal fluorenyl group would allow the synthesis and digestion of the peptide derivative to be easily monitored. Through observation of the Fmoc fragment, it can be seen that the

introduction of Fmoc-L-A and the necessary coupling agents enabled the preparation of the peptide derivative structure (figure 3.5, surface 2). However, upon addition of elastase, although the predicted decrease in intensity for the $C_{14}H_{11}^+$ fragment is seen, a corresponding decrease is also observed for the $C_3H_8N^+$ ion. This was believed to be due to non-specific protein adsorption by elastase onto the gold surface; commonly observed when biocompatible materials are immersed in proteinaceous solutions.[37-39] This was confirmed by mapping the surface for $C_9H_8N^+$, a fragment specific for the amino acid tryptophan,[36] present in the amino acid sequence of elastase (figure 3.9 A).[37]

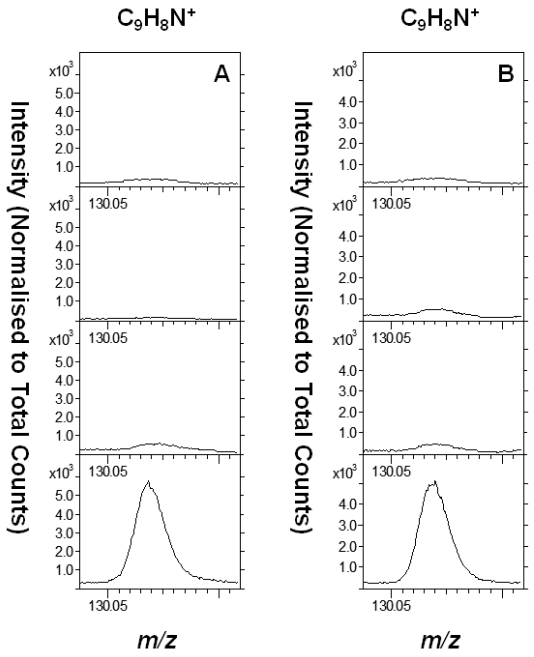

Figure 3.9
ToF-SIMS normalised intensity spectra for each of the surfaces at m/z 130.054, indicative of the amino acid tryptophan. (A) Surface modification strategy employing a $(CH_2)_4$ spacer. (B) Surface modification strategy employing a $CH_2CH_2O(CH_2CH_2O)_6CH_2CH_2$ spacer.

The capability of polyethylene glycol (PEG) to reduce non-specific protein binding has been reported extensively in the literature upon both two-dimensional[27, 42] and three-dimensional substrates.[43-44] Extensive research by Whiteside and Mrksich,

on SAMs has shown that the optimum chain length for protein resistance is six ethylene glycol units *i.e.* SAMs terminated with hexa(ethylene oxide) (PEG_6) prevent non-specific adsorption; regardless of protein size, charge or structure.[45-47] With this in mind, surfaces were prepared containing a $CH_2(C_2H_4O)_6CH_2$ spacer unit.

Figure 3.10 illustrates the ToF-SIMS data collected when the $(CH_2)_4$ spacer was replaced by a molecule containing a PEG_6 unit.

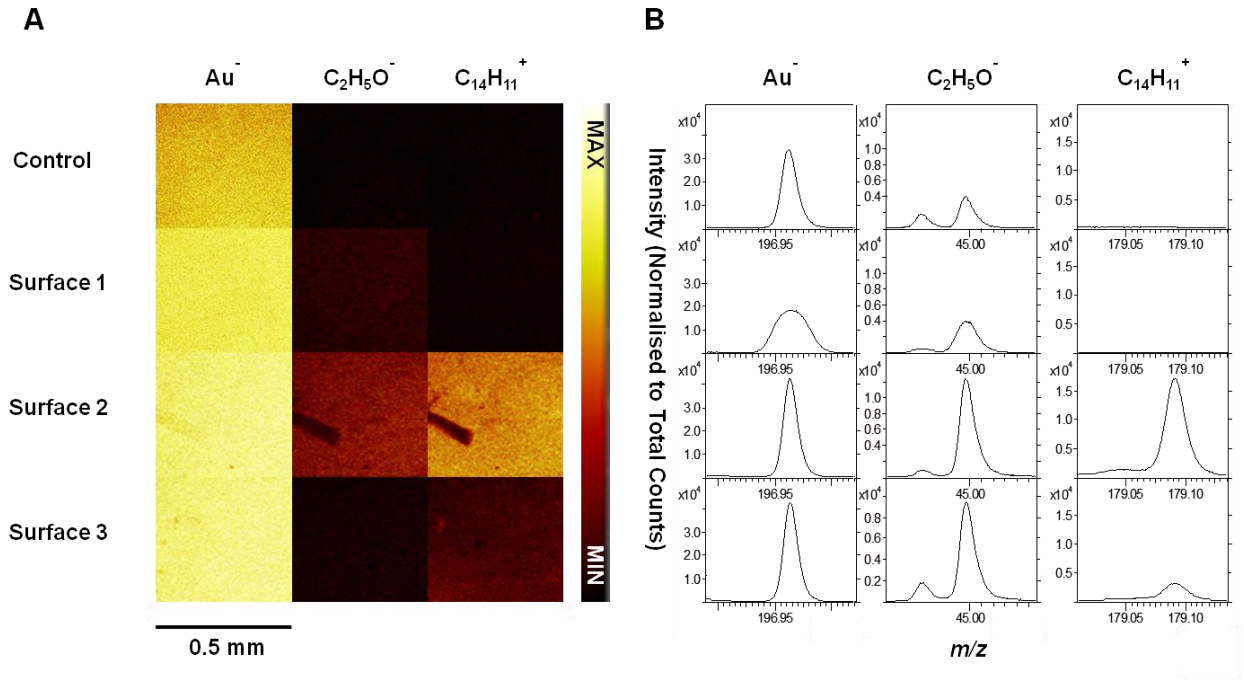

Figure 3.10
Surface modification strategy employing a $CH_2CH_2O(CH_2CH_2O)_6CH_2CH_2$ spacer. (A) SIMS ion intensity maps for each surface displayed for selected masses (Au^- = 196.953 D, $C_2H_5O^-$ = 45.001 D and $C_{14}H_{11}^+$ = 179.058 D). Images are scaled to the same maximum pixel value for each ion. (B) ToF-SIMS normalised intensity spectra for each of the surfaces obtained at selected *m/z* values.

The *m/z* intensity maps follow the signals generated by $C_2H_5O^-$ which is a fragment specific to polyethylene glycol containing molecules. Introduction of this species into the system significantly reduced the problem of non-specific protein

adsorption as a decrease in signal intensity was only observed for the fluorenyl specific fragment after elastase treatment (figure 3.7 B, surface 3). Upon further in-depth analysis, the $C_9H_8N^+$ fragment attributed to tryptophan was also detected (figure 3.9 B). ToF-SIMS is not an inherently quantitative technique, and has sensitivity down to ppm or ppb for certain species, so while this result clearly indicated a decrease in the abundance of tryptophan detected it is impossible to determine the exact amount adsorbed on the surface. Full spectra for the $CH_2CH_2O(CH_2CH_2O)_6CH_2CH_2$ spacer containing surface are shown in figures 3.11 and 3.12.

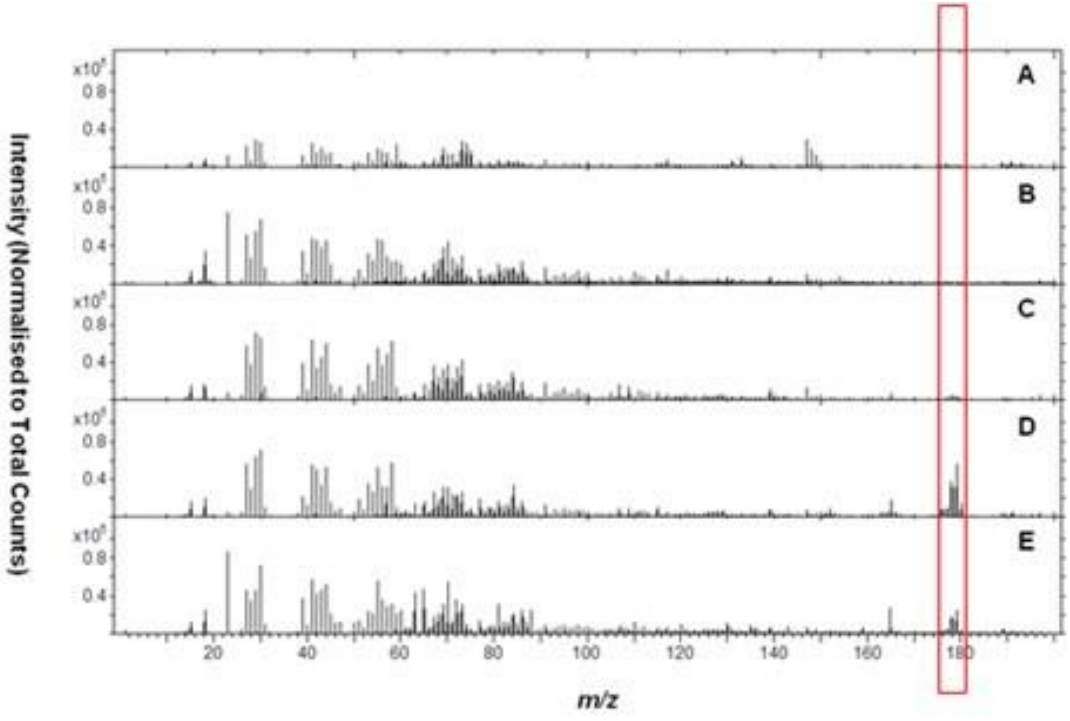

Figure 3.11
ToF-SIMS positive secondary ion spectra for surface modification strategy employing a $CH_2CH_2O(CH_2CH_2O)_6CH_2CH_2$ spacer. (A) Gold cover slip after piranha and plasma cleaning. (B) Gold cover slip treated with elastase (*Porcine Pancreas*, 1 mg mL^{-1} in phosphate buffer). (C) Gold cover slip after peptide functionalisation to surface 1. (D) Gold cover slip after peptide functionalisation to surface 2. (E) Gold cover slip after peptide functionalisation and treatment with elastase (surface 3).

Figure 3.11 shows the average positive secondary ion spectra generated for the gold surfaces prepared. Particular focus is paid to the region around 179.05 on surfaces 2 and 3 where the spectra have been highlighted. This region corresponds to the peaks shown in figure 3.10 B for the mass corresponding to $C_{14}H_{11}^{+}$ i.e. the fluorenyl fragment. As illustrated by the sections shown in red, it is clear that the spectra shown in figure 3.10 B are representative of the whole sample, not just an individual region. Surface 2 shows the greatest intensity for the fluorenyl fragment as discussed previously.

Figure 3.12 shows the average negative ion spectra generated for the gold surfaces prepared. In this case the region around 196.95 has been highlighted to indicate that the signal for gold is observed throughout the analysis process, as illustrated in figure 3.10 B.

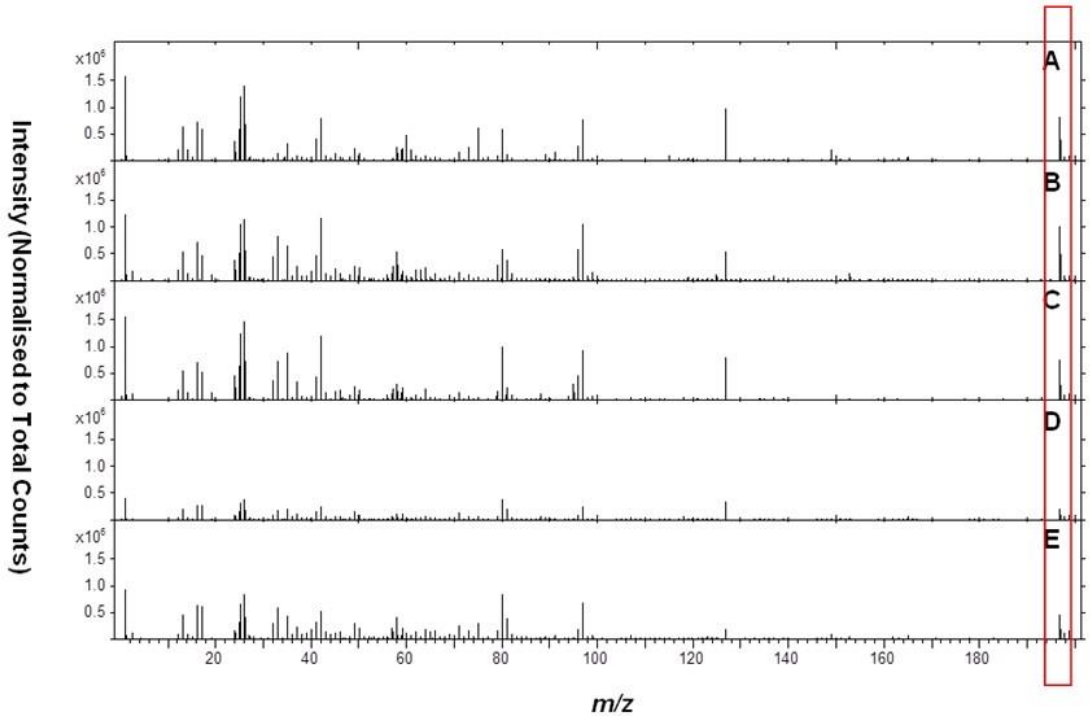

Figure 3.12
ToF-SIMS negative secondary ion spectra for surface modification strategy employing a $CH_2CH_2O(CH_2CH_2O)_6CH_2CH_2$ spacer. (A) Gold cover slip after piranha

and plasma cleaning. (B) Gold cover slip treated with elastase (*Porcine Pancreas*, 1 mg mL^{-1} in phosphate buffer). (C) Gold cover slip after peptide functionalisation to surface 1. (D) Gold cover slip after peptide functionalisation to surface 2. (E) Gold cover slip after peptide functionalisation and treatment with elastase (surface 3).

The introduction of a PEG_6 containing spacer unit would be expected to completely prevent non-specific protein adsorption, and this is not observed. However, this can be explained by examining the structure of the anchor to the gold surface; while the mono-thiol terminated SAMs used by Whitesides and Mrksich are able to pack together tightly and prevent non-specific protein adsorption,[9] the cyclic disulfide used in this system is too sterically crowded at the gold surface to pack together in this way and inevitably will allow some adsorption of elastase. This is in agreement with Mrksich *et al.* who postulated that monolayers prepared from disulfides contain a larger density of defect sites than monolayers prepared from thiols.[48] As future applications of this system are aimed at nanoparticle systems, the nanocurvature of the particle surface should play a role in preventing protein adsorption and the packing density of the disulfide anchored derivative is not expected to be prohibitive.

3.4.3 X-ray Photoelectron Spectroscopy (XPS)

X-ray Photoelectron Spectroscopy (XPS) is a surface analysis technique with an analysis depth of approximately 10 nm. Analysis involves irradiating a sample with an X-ray source to stimulate the emission of photoelectrons from the core-shell of surface atoms while simultaneously measuring the kinetic energy of the photoelectrons.

A sample irradiated with a monochromated X-ray source emits *photoelectrons* from the core shell of the surface atoms. To be able to stimulate the emission of a photoelectron, the energy of the X-rays has to be greater than the *binding energy* (*EB*) i.e. the energy difference between the ground state and the Fermi level of the electron. In addition, to separate the photoelectron from the bulk material, a small

and constant amount of energy is needed, which is referred to as *work function*. The remaining X-ray energy is transferred to the photoelectron as *kinetic energy* (*EK*) and can be measured.

Photoelectron emission occurs in all atoms in which core shell electrons have a binding energy that is lower than the X-ray energy. Since the binding energy is characteristic for each element, qualitative and quantitative analysis of the surface is possible. The binding energy not only depends on the nature of the element, but also on the chemical environment of the atom. While more electronegative binding partners increase the binding energy, more electropositive elements cause *EB* to decrease. This effect results in a *chemical shift* of the peak in the spectra that is characteristic for the elements bound to the atom in question. Thus, XPS can not only be used to confirm the presence of a certain element on the surface, but it can also be employed to gain information about its chemical state.[49] Please refer to section 7.2.4 for experimental conditions.

Using XPS analysis, the concentration of nitrogen species observed for surface 1 was shown to have increased with respect to the gold control. This was due to the introduction of nitrogen in the amide bonds of the $(CH_2)_4$ spacer unit and amino acid present in this peptide derivative. Upon further amino acid coupling (figure 3.5, surface 2), the N1s peak indicative of NH_2 (NH_3^+ at highest bond energy) functionality disappears, providing evidence that the coupling of the terminal Fmoc-A was successful. Additionally, there is an assignment denoting the carbamate moiety associated with the N1s peak, which appears on surface 2 which then decreases upon enzymatic digestion to surface 3 as would be expected. Peak fitting of the N1s spectra at each stage of production can be found in figure 3.13.

Upon introduction of the $CH_2CH_2O(CH_2CH_2O)_6CH_2CH_2$ spacer unit (figure 3.5, surface 1), the oxygen content of the samples observed by XPS increased due to the high proportion of this element associated with PEGylated molecules. As seen with the system containing the $(CH_2)_4$ spacer unit, additional amino acid coupling (figure

3.5, surface 2) results in the disappearance of the N1s signal representative of NH_2 functionality, providing clear evidence that the structure of interest was successfully prepared (figure 3.14). Finally, after enzymatic digestion of the derivative (figure 3.5, surface 3), no significant intensity was seen at the position of the carbamate functionality indicating removal of the Fmoc group (figure 3.15).

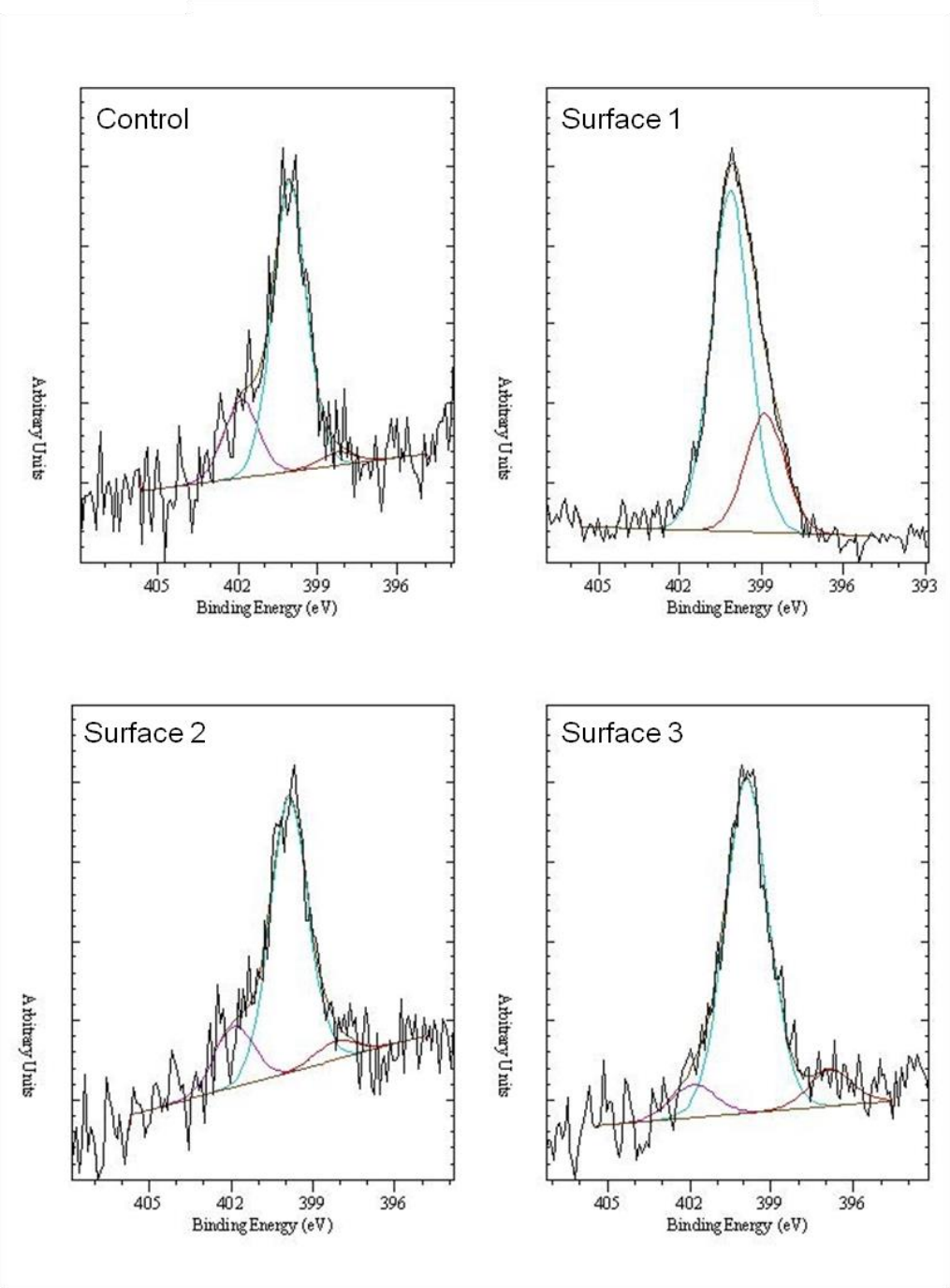

Figure 3.13
XPS N1s spectra for surface modification strategy employing a $(CH_2)_4$ spacer.

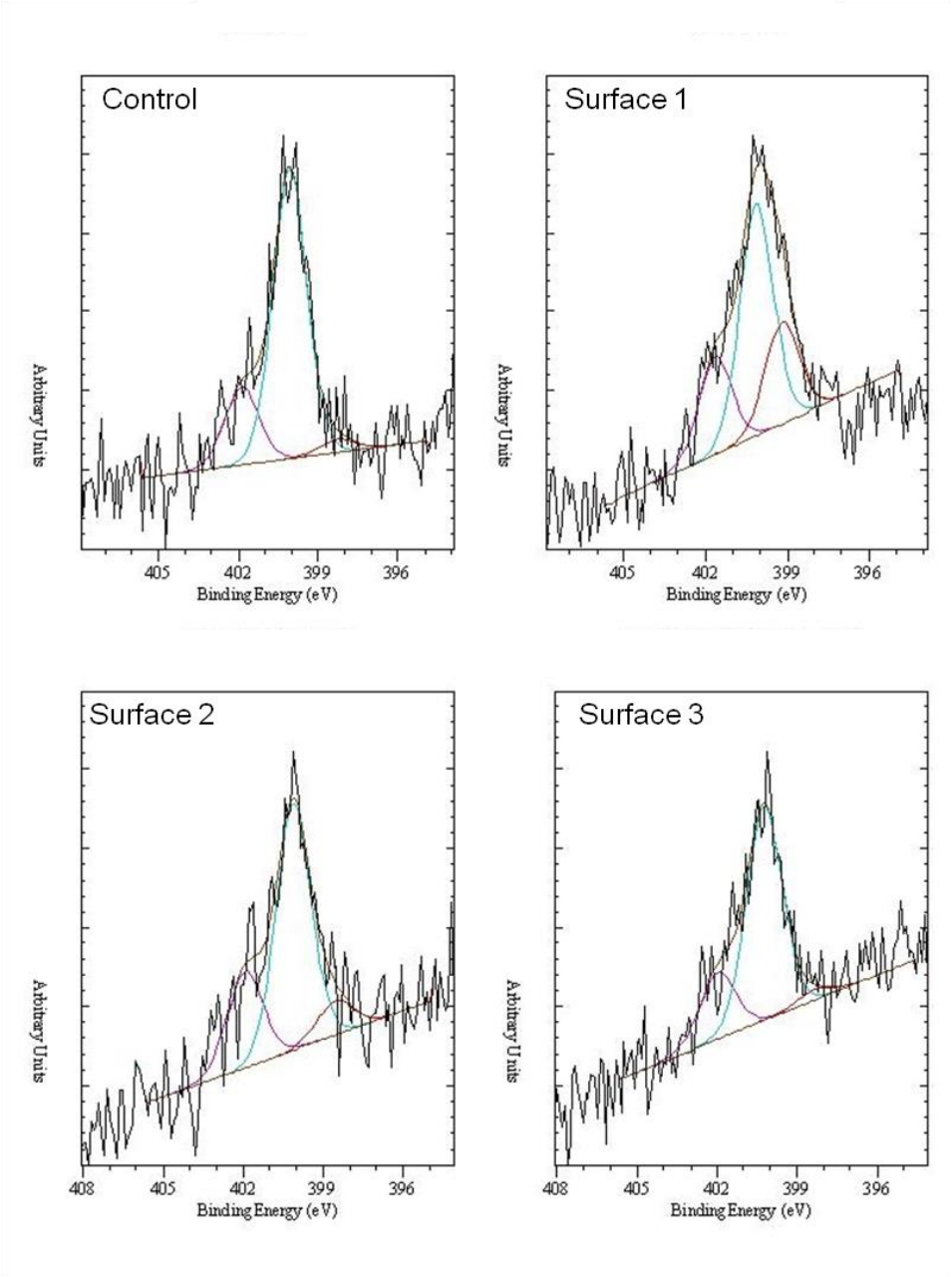

Figure 3.14
XPS N1s spectra for surface modification strategy employing a $CH_2CH_2O(CH_2CH_2O)_6CH_2CH_2$ spacer.

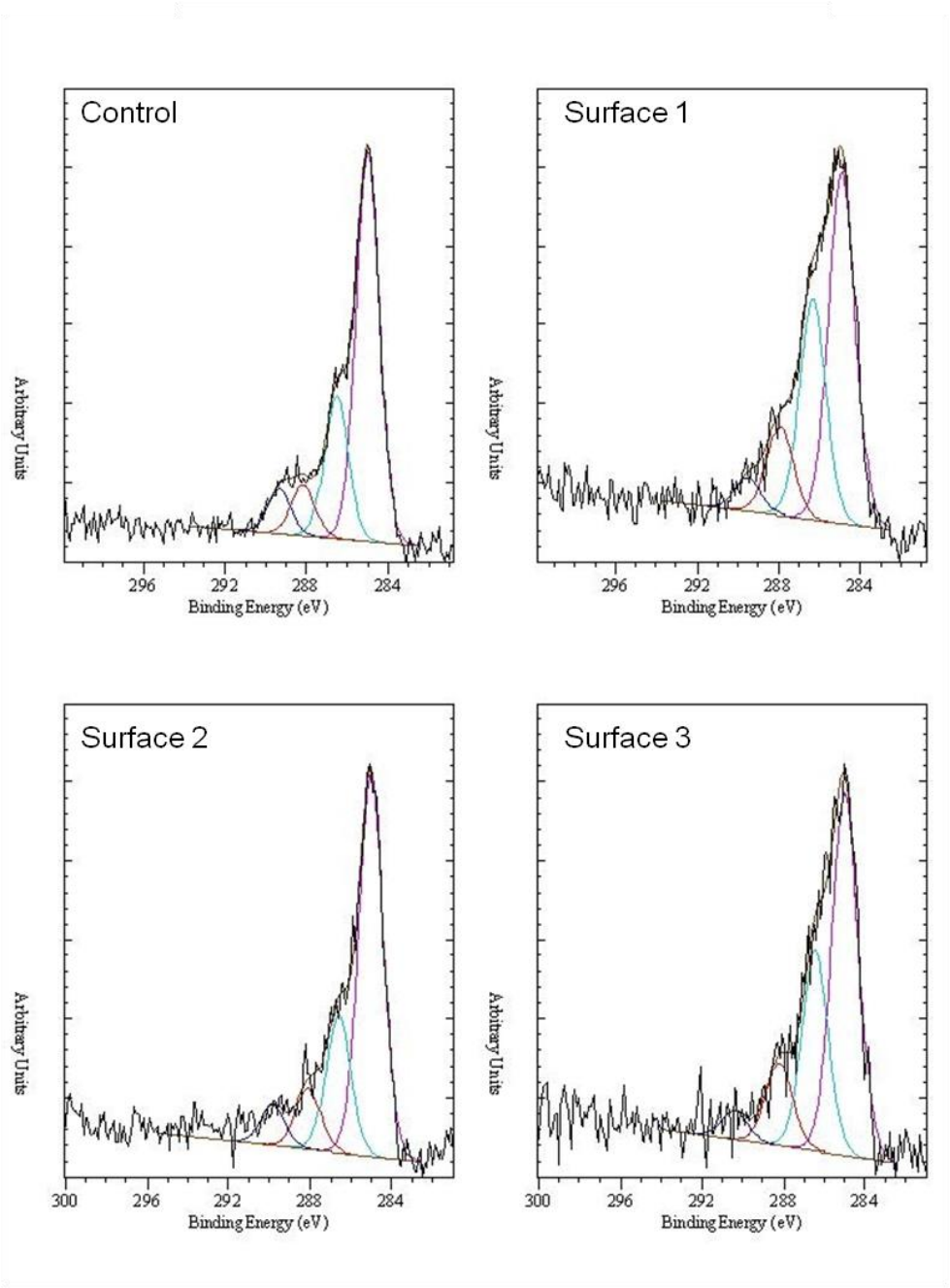

Figure 3.15
XPS C1s spectra for surface modification strategy employing a $CH_2CH_2O(CH_2CH_2O)_6CH_2CH_2$ spacer.

3.4.4 Direct Laser Desorption/Ionisation Time-of-Flight Mass Spectrometry (LDI-ToF MS)

Several mass spectrometry techniques are suitable for characterisation of planar surfaces. Mrksich *et al.* utilised a modified version of matrix-assisted laser desorption ionisation (MALDI) termed SAMDI to analyse materials prepared using self-assembled monolayers (SAMs),[48-51] while Flitsch *et al.* use MALDI to monitor the synthesis of peptide arrays on gold surfaces.[12] However, as MALDI is not well suited to the characterisation of molecules with masses below *m/z* 300 due to the intense background signals which arise from the matrix, analysis was undertaken using direct laser desorption/ionisation time-of-flight mass spectrometry (LDI-ToF MS).[52] This technique was utilised to follow the step-wise synthesis of the peptide derivatives on the gold surface, from the (±)-α-lipoic acid linker to the target molecule and subsequent digestion by elastase.

LDI-ToF MS is a modification of standard MALDI MS and involves the laser excitation of a sample. The work described within this thesis details the analysis of peptidic samples adsorbed to a gold surface, however, samples may be deposited onto the substrate surface rather than chemically adsorbed. Ablation and desorption of the sample is triggered by the laser treatment which results in subsequent ionisation of the sample. Similar to the technique of ToF-SIMS the analyte molecules are then accelerated into a mass spectrometer. Please refer to section 7.2.5 for details of instrumentation used.

A sequence of LDI-ToF MS spectra illustrating three discrete stages in the step-wise synthesis process are presented in figure 3.16. The peak visible at *m/z* 386 (figure 3.16 A, $[A + K]^+$) corresponds to the potassium adduct of the peptide derivative, while strong signals for both the sodium and potassium adducts of the Fmoc-terminated molecule are observed at *m/z* 663 and 679 respectively (figure 3.16 B, $[B + Na]^+$ and $[B + K]^+$). Upon treatment with elastase, a peak at *m/z* 370 (figure 3.16 C, $[C + Na]^+$) attributed to the sodium adduct of the digestion product is

observed. In addition to the digestion product, a signal is also detected at *m/z* 663 (figure 3.16 C, $[B + Na]^+$) which results from undigested peptide derivative on the gold surface. This residual material may be the result of elastase encountering access difficulties on the planar gold surface due to the dense packing of the terminal Fmoc group, which would in turn hinder the digestion process. Proof-of-concept work on electro-plated gold-coated MALDI plates (data not shown) supports this statement; enzymatic digestion consistently reached completion on plates which have a noticeably less even surface than the gold-coated cover-slips.

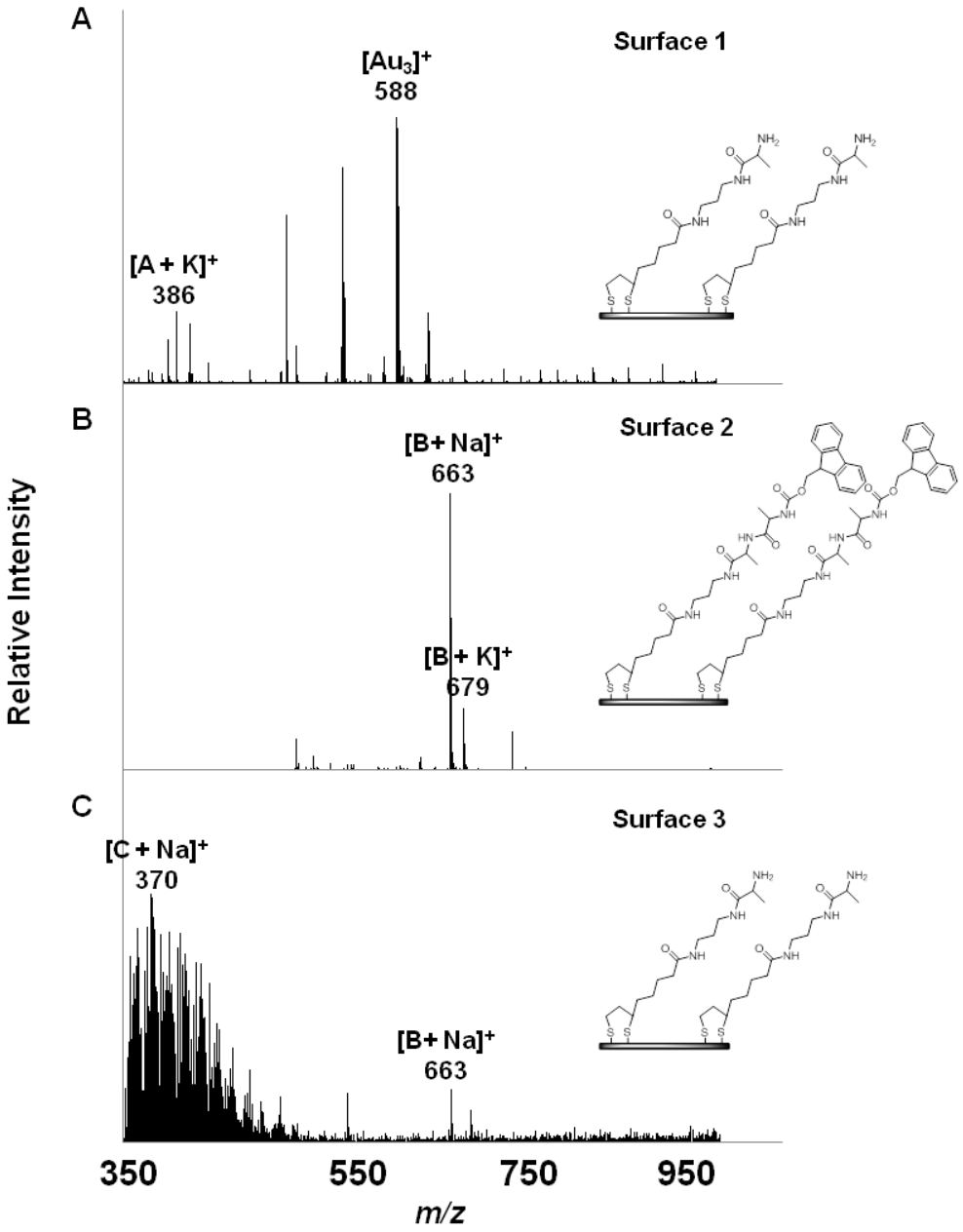

Figure 3.16

Step-wise peptide synthesis monitored directly by direct laser desorption/ionisation time-of-flight MS (A) LDI-ToF MS spectrum of surface 1 showing a peak at *m/z* 386, while a signal at *m/z* 588 is observed for the trimer of gold. (B) LDI-ToF MS spectrum of surface 2 showing peaks at *m/z* 663 and 679, indicative of target molecule. (C) LDI-ToF MS spectrum of surface 3 showing a peak at *m/z* 370 indicative of elastase digestion product.

In line with the samples analysed by ToF-SIMS, surfaces were also prepared containing a PEG_6 linker molecule. The signal observed at *m/z* 666 (figure 3. 17 A, $[A + K]^+$) is due to the potassium adduct of this peptide derivative; while upon amino acid coupling a peak corresponding to the full peptide derivative sequence was observed at *m/z* 960 (figure 3.17 B, $[B + K]^+$). After elastase treatment, a signal at *m/z* 627 (figure 3.17 C, $[C]^+$) was detected, corresponding to the expected mass of the digestion product. It is difficult to determine whether digestion of the peptide sequence is complete for the surfaces containing PEG_6 due to the high levels of background noise recorded in the spectra (figure 3.17 C). Signals produced by gold are also observed in the spectra, due to ionisation of the gold surface layer. These signals have been labelled for ease of figure interpretation.

For both the non-PEGylated and PEGylated systems, no comment can be made regarding the non-specific protein adsorption of elastase using LDI-ToF MS as the instrument was calibrated on the gold cover–slips between *m/z* 350 and *m/z* 1000. In order to determine whether or not elastase which has a molecular weight of approximately *m/z* 26, 000 was present, re-calibration of the whole experimental set-up would be required. However, as a decrease in non-specific adsorption is observed by ToF-SIMS (section 3.3.2), this was deemed unnecessary. The use of LDI-ToF MS and ToF-SIMS in tandem ensured confidence in the stepwise synthesis method. These techniques provided complimentary data through the analysis of both the full desorbed peptide derivative and the resulting molecular fragments respectively. Furthermore, these techniques have, to our knowledge, not been used in tandem before to comprehensively characterise peptide functionalized surfaces.

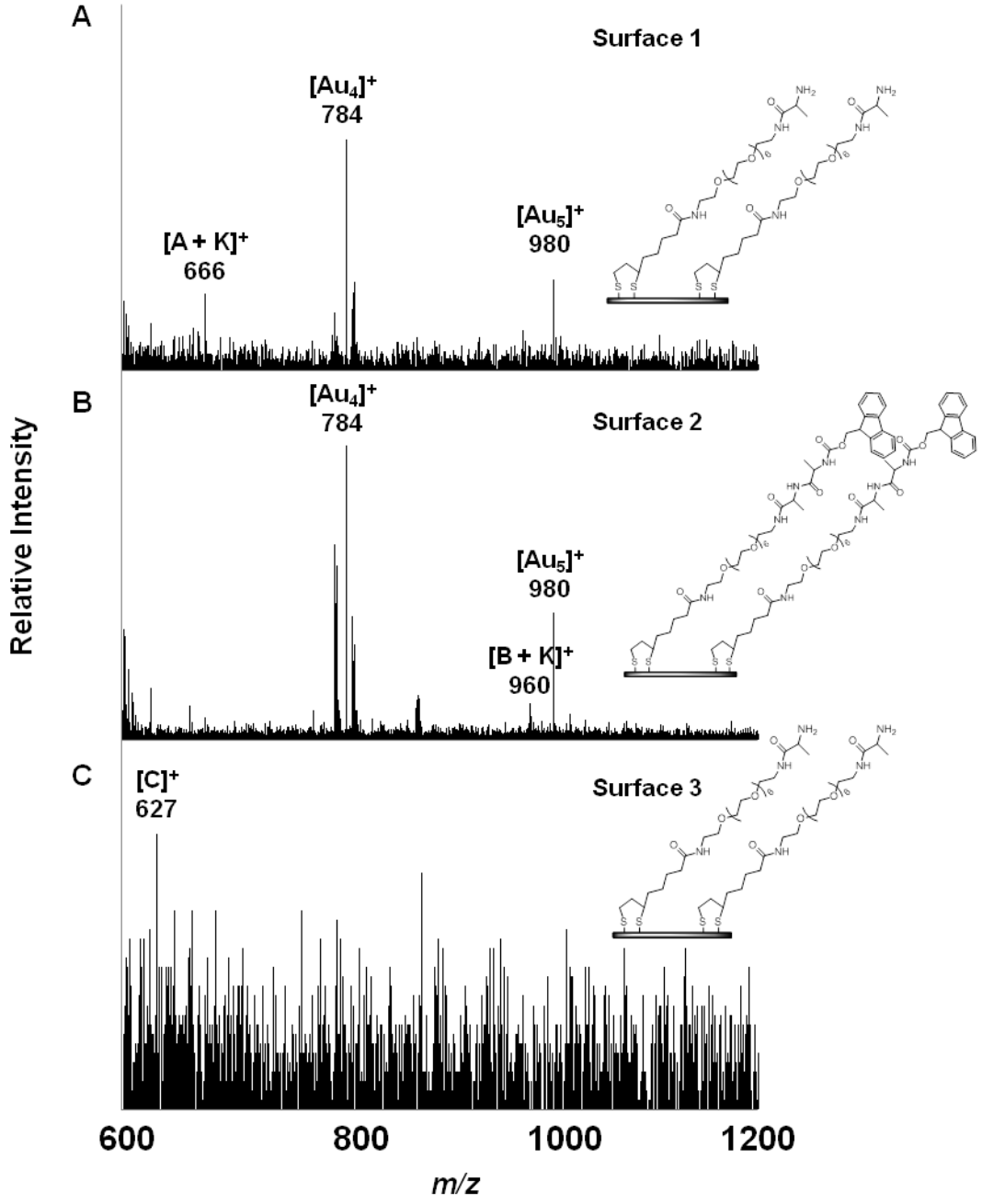

Figure 3.17

Step-wise peptide synthesis monitored directly by direct laser desorption/ionisation ToF MS (A) LDI-ToF MS spectrum of surface 1 showing a peak at *m/z* 666. Signals are also observed at *m/z* 784 and 980 for the tetramer and pentamer of gold. (B) LDI-ToF MS spectrum of surface 2 showing a peak at *m/z*

960. Signals are also observed at *m/z* 784 and 980 for the tetramer and pentamer of gold. (C) LDI-ToF MS spectrum of surface 3 showing a peak at *m/z* 627.

3.4.5 Contact Angle Goniometry

Contact angle goniometry (CAG) is a surface characterisation technique which provides information regarding the hydrophilic/ hydrophobic nature of a solid surface.[53] Contact angle (CA) is specific for a given system and determined by measuring the angle of intersection between a droplet of liquid, typically water, and the gas and solid interfaces. Water contact angle (WCA) is specific for a given system and determined by measuring the angle of intersection between a droplet of water with the gas and solid interfaces. Contact angle values < 90 ^{o} suggest the surface is hydrophilic, whereas contact angle values > 90 ^{o} indicate the surface is hydrophobic (figure 3.18.). Please refer to section 7.2.6 for experimental conditions.

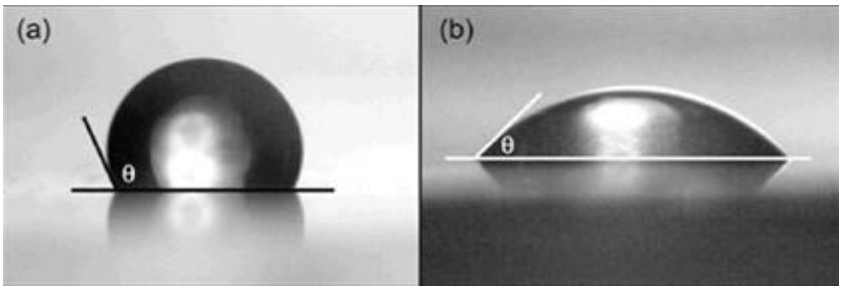

Figure 3.18.
Typical images of a hydrophobic surface (a) and a hydrophilic surface (b).[96]

The trends observed for WCA were in good agreement with those predicted for both the PEGylated and non-PEGylated systems (surface functionality illustrated by figure 3.1); an alternating pattern of increasing and decreasing contact angle was observed throughout the synthesis due to the addition and removal of hydrophobic groups through conventional Fmoc-chemistry. Final coupling of an Fmoc-protected amino acid to yield the target molecule gave a WCA of ~ 70 °, which is in agreement with previous work by Rawsterne and Frutos, indicating good coverage of the

surface with the Fmoc moiety.[54-56] Subsequent treatment with elastase showed an expected decrease in WCA; with the PEGylated surface showing evidence of non-specific protein adsorption resistance, as the contact angle observed for surface 3 is closer to that of surface 1 than for the system containing a $(CH_2)_4$ spacer (table 3.1).

Table 3.1
Comparison of water contact angle values, in degrees, between systems employing different spacer units.

Spacer Unit	Control	Surface 1	Surface 2	Surface 3
$(CH_2)_4$	84.4 °± 2.1	63.2 °± 5.9	67.5 °± 2.1	43.1 ° ± 9.8
$CH_2CH_2O(CH_2CH_2O)_6CH_2CH_2$	84.4 °± 2.1	62.1 °± 3.7	69.8 °± 3.9	55.3 °± 7.3

3.4.6 Surface Coverage Analysis

HPLC analysis following the method developed by Ulijn *et al.* was used to determine the efficiency of amino acid coupling.[57] This method utilises the deprotection of Fmoc as a means of measuring the extent to which amino-acid coupling has been successful. For all coupling steps, across both spacer systems, 0.57 ± 0.2 nmol was removed by piperidine treatment. Molecules were identified by comparison to *N*-Fmoc-L-A and quantified using calibration curves.

Using the same assumptions as Ulijn *et al.*;[57] the maximum number of Fmoc-peptide molecules that can be attached to the surface of a 12 mm diameter cover slip is estimated to be 3.25×10^{14} molecules (under monolayer conditions). This calculation is based on the approximate diameter of an Fmoc group (0.75 nm) acting as the limiting factor in the packing of molecules during coupling. The quantity of peptide attached to the surfaces, determined by HPLC (0.57 nmol), corresponds to approximately 3.42×10^{14} molecules. This estimate indicates that approximately a monolayer of peptides can be obtained on peptide functionalised gold surfaces.

HPLC analysis was also used to determine the efficiency of the enzyme reactions. Cleavage of Fmoc-A (i.e. Fmoc-A↓A) from the surface was 0.49 $\pm$ 0.06 nmol, corresponding to approximately 86 % of the total loading of the surface. Fmoc-A was the only peak observed by HPLC, confirming the highly specific nature of elastase.

3.4.7 Thiol Displacement Studies

Attempts were made to quantify solution-phase yields on the gold surface using dithiothreitol (DTT) displacement of the disulfide anchor. DTT and mercaptoethanol (ME) have both been utilised in literature to displace molecules bound to a surface through sulfur linkages, such as disulfides or thiols by promoting an exchange reaction.[58-59] Once displaced the approximate number of molecules is established using fluorescence; in this case, the fluorenyl group could be used as a spectroscopic marker. However, the anchor proved too stable to be removed in this way, even when a large excess of DTT was used. This echoes results shown by Graham *et al.*,[58] and corroborates our earlier statements regarding the robust nature of this anchoring molecule on gold.

3.5 Conclusions

A method was described which enables rapid and reproducible step-wise synthesis of peptide derivatives on planar gold surfaces in a homogeneous manner. The first example of using ToF-SIMS, XPS, LDI-ToF MS and WCA techniques in a complimentary fashion as a means of showing the successful stepwise synthesis of this derivative molecule, and when designed to contain an enzyme cleavable section, its subsequent digestion were described.

A fluorescence spectroscopy study was also undertaken to determine whether the presence of Fmoc could be observed before & after digestion by elastase, however,

the proximity of the fluorenyl group to the gold surface resulting in quenching of the signal.

In addition to comprehensive surface characterisation, this chapter also detailed the use of polyethylene glycol units to overcome non-specific protein adsorption in systems containing particularly hydrophobic sequences and enhance the degree to which enzymatic digestion occurred. This optimised system will be utilised in subsequent experimental chapters.

CHAPTER FOUR – PEPTIDE FUNCTIONALISATION OF NANOSTRUCTURED GOLD SURFACES

4.1 Abstract

This chapter presents investigations into the use of SERS as a technique to follow the elastase responsive system developed in 3.0. The nanostructure surface of Klarite, a commercially available SERS substrate, was functionalised using the same methodology and proof-of-concept work towards a SERS-active system was detailed.

4.2 Introduction

4.2.1 Background

When light interacts with a molecule, the molecule can absorb a photon which excites an electron to a higher energy level. The energy of the absorbed photon can be emitted *via* several mechanisms which ultimately result in the excited electron being relaxed to a lower energy level.

In addition to absorption, a second optical process can occur when light interacts with a molecule. The incident photon can cause distortion of the electron cloud surrounding the nucleus of the molecule resulting in scattering of the photon. If the scattered photon is different in energy to that of the incident photon, the scattering process is known as Raman scattering.

Enhancement of Raman scattering when a molecule is adsorbed onto a roughened metal surface was first observed by Fleischmann and co-workers in 1974.[1] The effect was denoted surface-enhanced Raman scattering (SERS) and it has been shown to enhance the Raman scattering up to 10^{14} under certain conditions.[4] The commercially available SERS substrate Klarite has been used extensively to greatly enhance the Raman signal of various analyte molecules. However, there are no published instances whereby stepwise SPPS and subsequent enzymatic digestion are monitored upon Klarite using SERS.

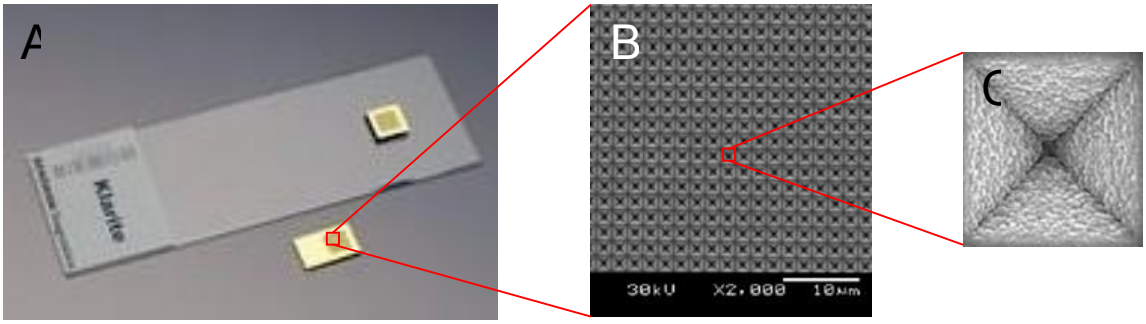

Figure 4.2

(A) Klarite SERS substrate. The active area for this substrate is the dark square in the golden rectangle; (B) SEM micrograph showing the surface structure (scale bar = 10 µm); (C) Close-up of pyramidal pit (diameter 1.4 µm). SEM images obtained from Renishaw Diagnostics.

4.2.2 Project Aim

Chapter 3.0 described a methodical investigation into the surface chemistry of peptide functionalised gold-coated glass cover slips. The aim of this chapter was to utilise the stepwise peptide synthesis method developed in 3.0 in order to prepare surface-enhanced Raman scattering (SERS) arrays for biosensing applications i.e. monitoring enzymatic digestion of a peptide sequence. Consultation with the literature indicates that such a system would be the first of its kind.

4.3 Results and Discussion

Prior to stepwise peptide synthesis, a gold-coated cover slip was analysed at 532 and 633 nm excitation to characterise the initial SERS signal of the substrate; ideally biosensing substrates should have little or no background signal. As expected, no SERS peaks were observed for the bare substrate at either excitation wavelength. This analysis was repeated after stepwise peptide synthesis had been performed, however, the spectra obtained were virtually identical to those of the bare substrate. This outcome was attributed to the use of vapour deposition while manufacturing of the gold cover slips which produced an extremely flat surface, which impeded surface plasmon generation and consequently no observable signal. The roughness of the metal surface is an important component in the development of SERS arrays; surface roughness features ranging from 20 - 100 nm are commonly utilised for laser wavelengths in the range of 532 - 780 nm.[5] Topography of the surface could be measured using AFM to analyse the surface topography of the gold-coated cover slip if development of a SERS responsive system on this particular substrate was desirable.

In order to introduce surface roughness, experimental work was continued upon Klarite, a commercially available surface-enhanced raman scattering (SERS) substrate. Klarite is a nanostructured surface prepared *via* photolithographic fabrication which comprises inverted square pyramidal pits (diameter 1.4 μm) arranged in a square lattice and coated with gold (figure 4.2). Such surfaces have been shown to give large Raman enhancements and produce highly reproducible SERS signals.[6]

4.3.1 Direct Laser Desorption/Ionisation Time-of-Flight Mass Spectrometry (LDI-ToF MS)

Employment of the surface analysis technique Direct Laser Desorption/Ionisation Time-of-Flight Mass Spectrometry (LDI-ToF MS) allowed facile comparison of the

surface chemistry of Klarite with that of the gold cover slips investigated in Chapter 3.0. LDI-ToF MS was utilised as described in section 3.3.4 to follow the step-wise synthesis of the peptide derivatives on the gold surface, from the (±)-α-lipoic acid linker to the target molecule and subsequent digestion by elastase.

LDI-ToF MS spectra illustrating three discrete stages in the step-wise synthesis process are presented in figures 4.2 and 4.3; figure 4.2 shows the spectra obtained for the system containing a $(CH_2)_4$ spacer, while figure 4.3 refers to the $CH_2CH_2O(CH_2CH_2O)_6CH_2CH_2$ spacer system. In results echoing those observed for the analysis of gold cover slips, the major peaks observed corresponded directly with the salt adducts of the anticipated surface tethered structures. For example, in figures 4.2 A & 4.3 A the free amines are observed at *m/z* 370 and 627 respectively.

Examination of figures 4.2 B and 4.3 B indicates that synthesis of the target molecule was achieved; *m/z* 663 and 960 respectively. Finally, evidence of enzymatic digestion was observed in figures 4.2 C and 4.3 C; *m/z* 370 and 650 respectively. It is pertinent to note that the surface of Klarite is divided into two areas; an active area with a distinct structural elemental (figure 4.1 B & C) which provides the SERS enhancement properties and the surrounding gold-coated handling area which has no inherent structure. Care was taken to ensure the LDI-ToF MS measurements were performed upon the flat handling regions of the Klarite substrate, thus ensuring the differing surface heights of the nanostructured region had no effect upon the *m/z* signals observed.

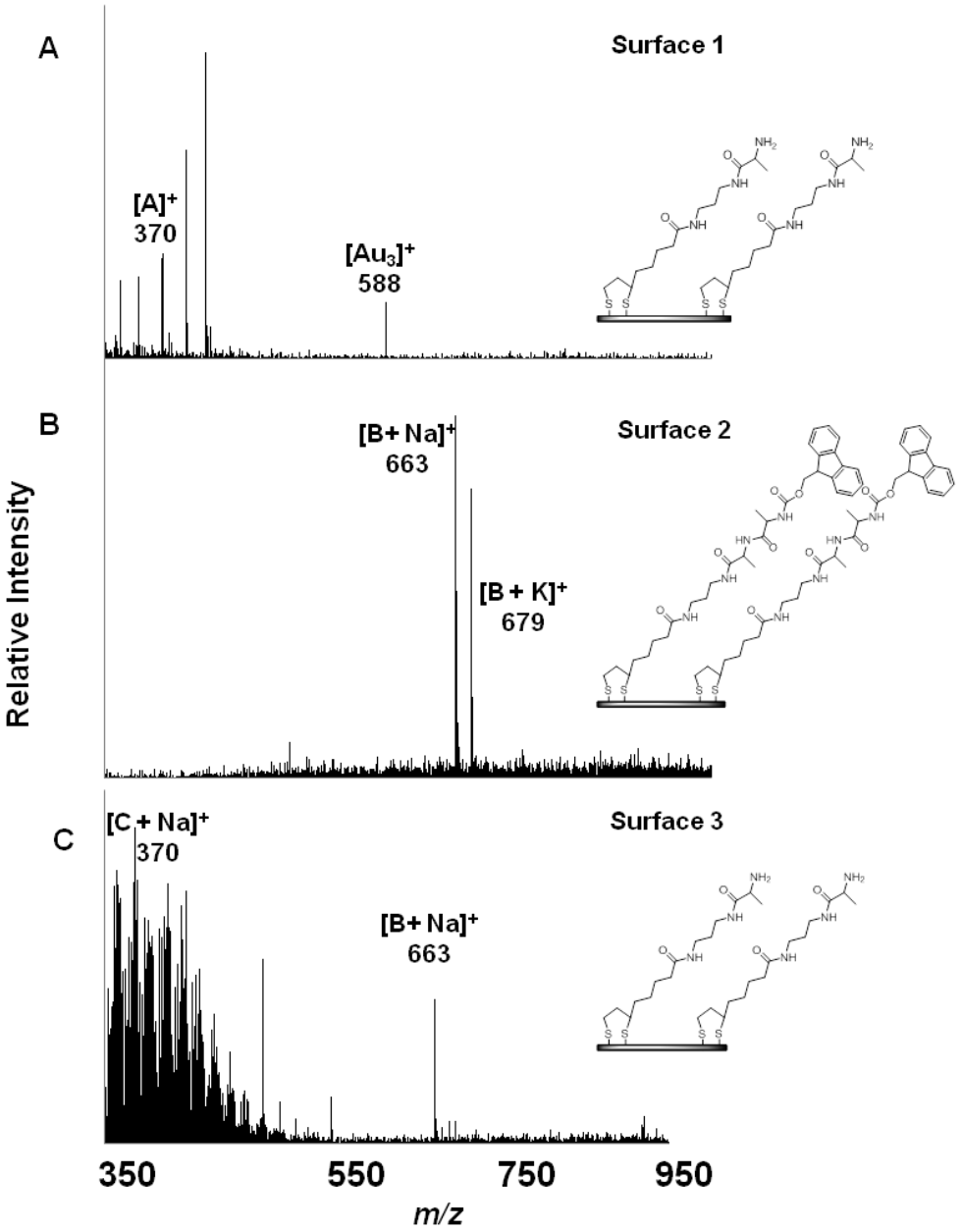

Figure 4.2

Step-wise peptide synthesis monitored directly by direct laser desorption/ionisation time-of-flight MS (A) LDI-ToF MS spectrum of surface 1 showing a peak at *m/z* 370, while a signal at *m/z* 588 is observed for the trimer of gold. (B) LDI-ToF MS spectrum of surface 2 showing peaks at *m/z* 663 and 679, indicative of target molecule. (C) LDI-ToF MS spectrum of surface 3 showing a peak at *m/z* 370 indicative of elastase digestion product.

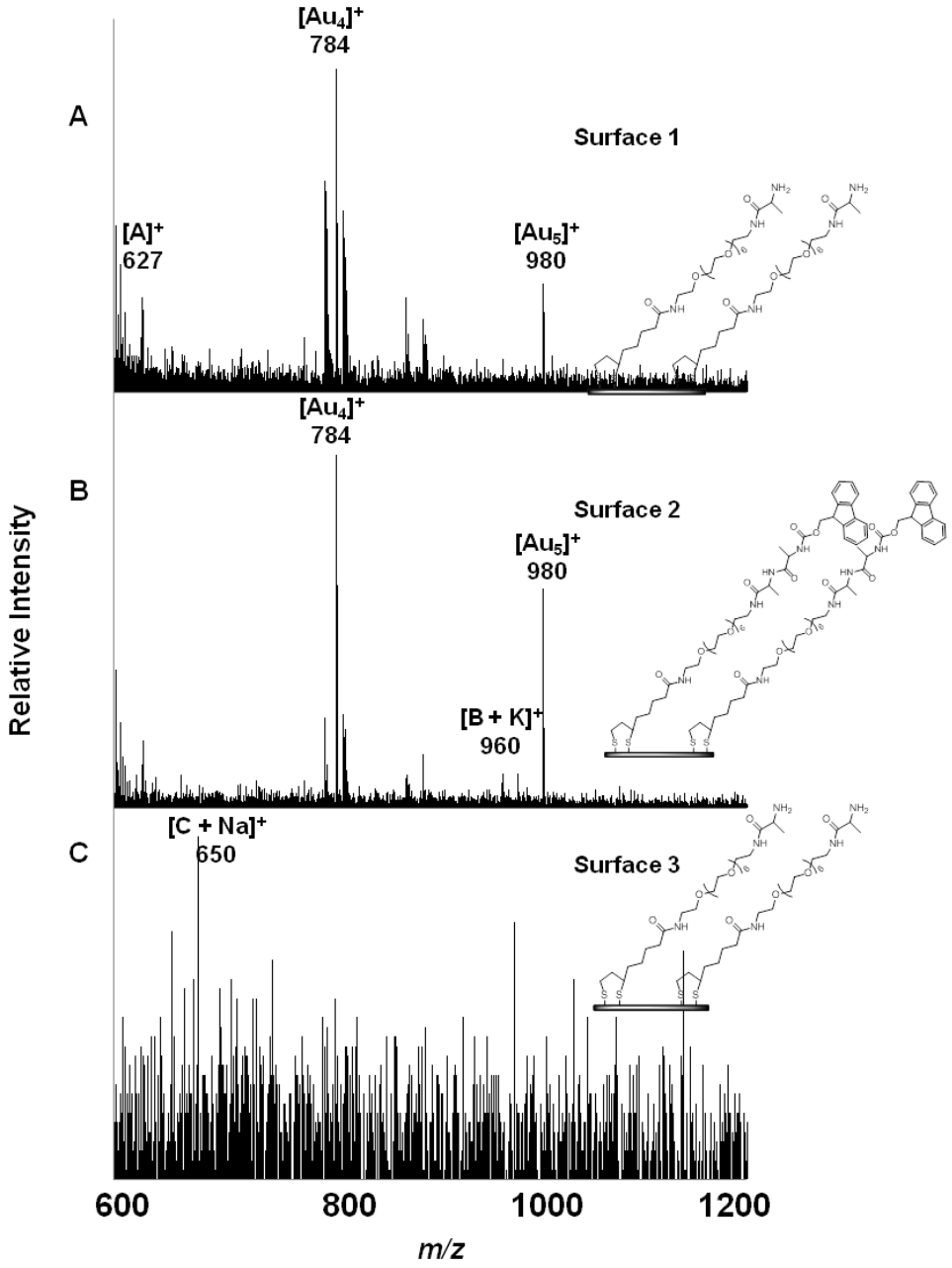

Figure 4.3

Step-wise peptide synthesis monitored directly by direct laser desorption/ionisation ToF MS (A) LDI-ToF MS spectrum of surface 1 showing a peak at *m/z* 627. Signals are also observed at *m/z* 784 and 980 for the tetramer and pentamer of gold. (B) LDI-ToF MS spectrum of surface 2 showing a peak at *m/z* 960. Signals are also observed at *m/z* 784 and 980 for the tetramer and pentamer of gold. (C) LDI-ToF MS spectrum of surface 3 showing a peak at *m/z* 650.

The spectra presented in figures 4.2 and 4.3 indicate that the method developed for stepwise solid-phase peptide synthesis (SPPS) in 3.0 was readily transferrable to Klarite surfaces and could be monitored using LDI-ToF MS. The remainder of this chapter will focus upon using stepwise peptide synthesis to prepare arrays for SERS biosensing applications.

4.3.2 SERS Response for Fmoc Functionalised Surfaces

Klarite is designed for use with Raman excitation parameters of 633 and 735 nm; figure 4.4 shows a representative spectrum for the blank Klarite analysed at 633 nm excitation. The spectrum shows that Klarite prior to surface functionalisation has almost no intrinsic Raman peaks.

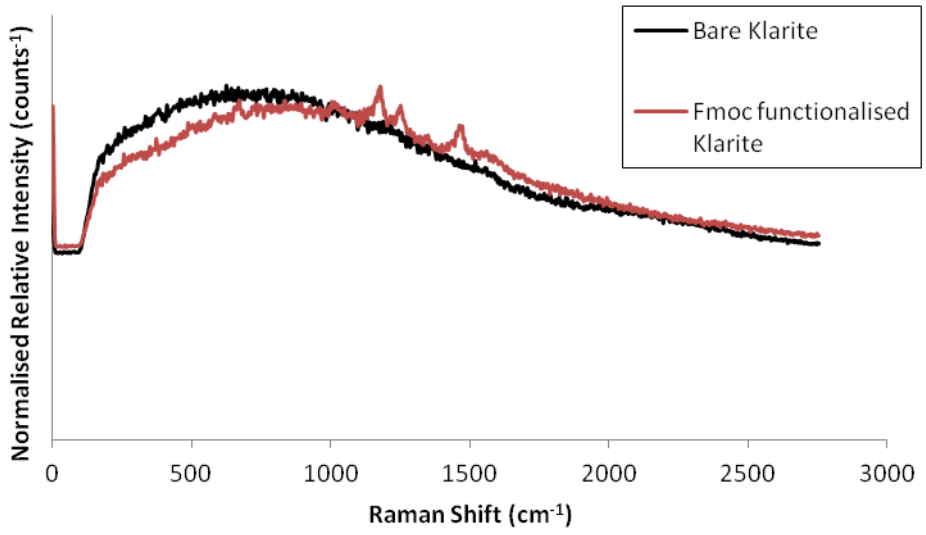

Figure 4.4
Normalised relative intensity of SERS spectra obtained from bare and Fmoc functionalised Klarite using 633 nm excitation.

As discussed in Chapter 3.0, Fmoc/piperidine chemistry is a convenient and popular means of preparing peptide sequences. Furthermore, the positions of Raman peaks for Fmoc are known (1615, 1487, 1297 and 1025 cm^{-1}).[7] Stepwise

SPPS to generate an Fmoc terminated peptide sequence was performed upon the Klarite SERS substrate, and the surface analysed at 633 nm excitation.

Equivalent spectra were obtained when the sequence containing a PEGylated spacer unit was tested. The low signal strength observed for the Fmoc functionalised sample is because the Fmoc absorption band (301 nm) is not excited by the 633 nm excitation laser necessary for use with Klarite, which results in a weak signal. It was postulated that the selection of a Raman reporter molecule with an absorbance peak closer to that of one of the excitation laser wavelengths would result in a resonance contribution to the Raman enhancement from the reporter. This in turn would lead to more intense signals, and allow ease of detection when used for biosensing applications such as enzyme detection.

4.3.3 Selection of Raman Reporter

The removal of an Fmoc protecting group to expose a terminal amino group is a facile process. Thus, in addition to the selection of a Raman reporter with an absorbance band closer to the laser excitation, a further selection criterion was that the reporter molecule had an acid moiety available to react with the free amine, thus labelling the surface tethered sequence. Rhodamine B (RB, figure 4.5) was selected as Raman reporter as it has an absorbance band at 554 nm, free acid functionality and is widely commercially available.

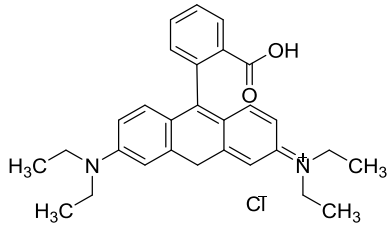

Figure 4.5
Structure of Rhodamine B.

Unmodified Klarite SERS substrates were immersed in a *N,N*-dimethylformamide solution of Rhodamine B (2 mM) before the samples were thoroughly washed, dried and analysed with the 633 nm laser. This work was designed to determine whether adsorption of Rhodamine B was observed on surfaces which do not possess free amine linkages to react with. No signals corresponding to the Raman shifts observed for Rhodamine B in the literature were observed.[8]

In order to fully confirm the suitability of Rhodamine B in this application, Klarite substrates were functionalised to surface 1 (structure shown as inset in figure 4.6 A) i.e. a surface presenting free amine functionality. Coupling of the Raman reporter molecule was then undertaken by immersing the Klarite overnight, at 37 ℃, in a *N,N*-dimethylformamide solution of Rhodamine B (2 mM), HBTU (2 mM) and DIPEA (2.6 mM).

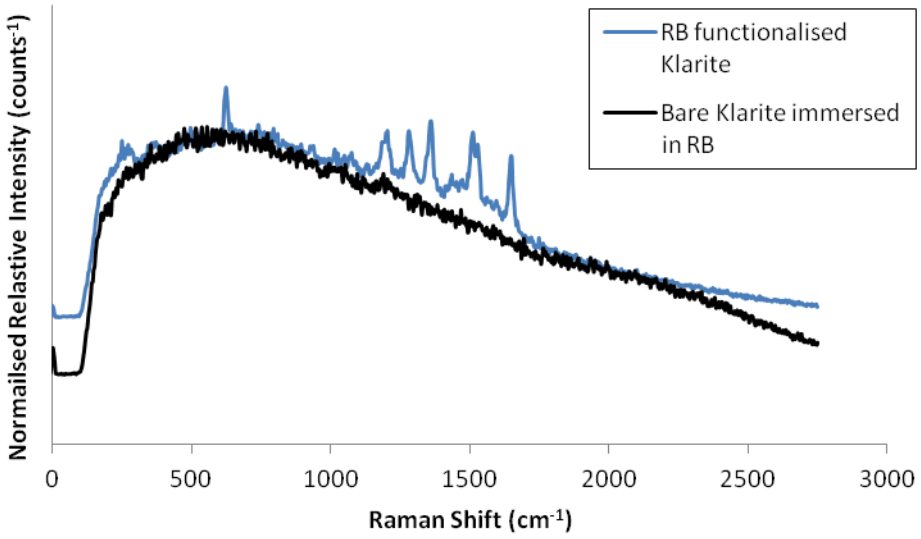

Figure 4.6
Normalised relative intensity of SERS spectra obtained from bare Klarite immersed in Rhodamine B and Klarite functionalised with Rhodamine B via an amide bond using 633 nm excitation.

Thus, it was decided that 633 nm excitation would be used to analyse Rhodamine B labelled peptide surfaces; as no background signal was exhibited by the bare Klarite and adsorption of dye onto the surface was not detected.

4.3.4 Proof of Concept

Rhodamine B provides a means by which the terminal amines on a peptidic sequence may be labelled.

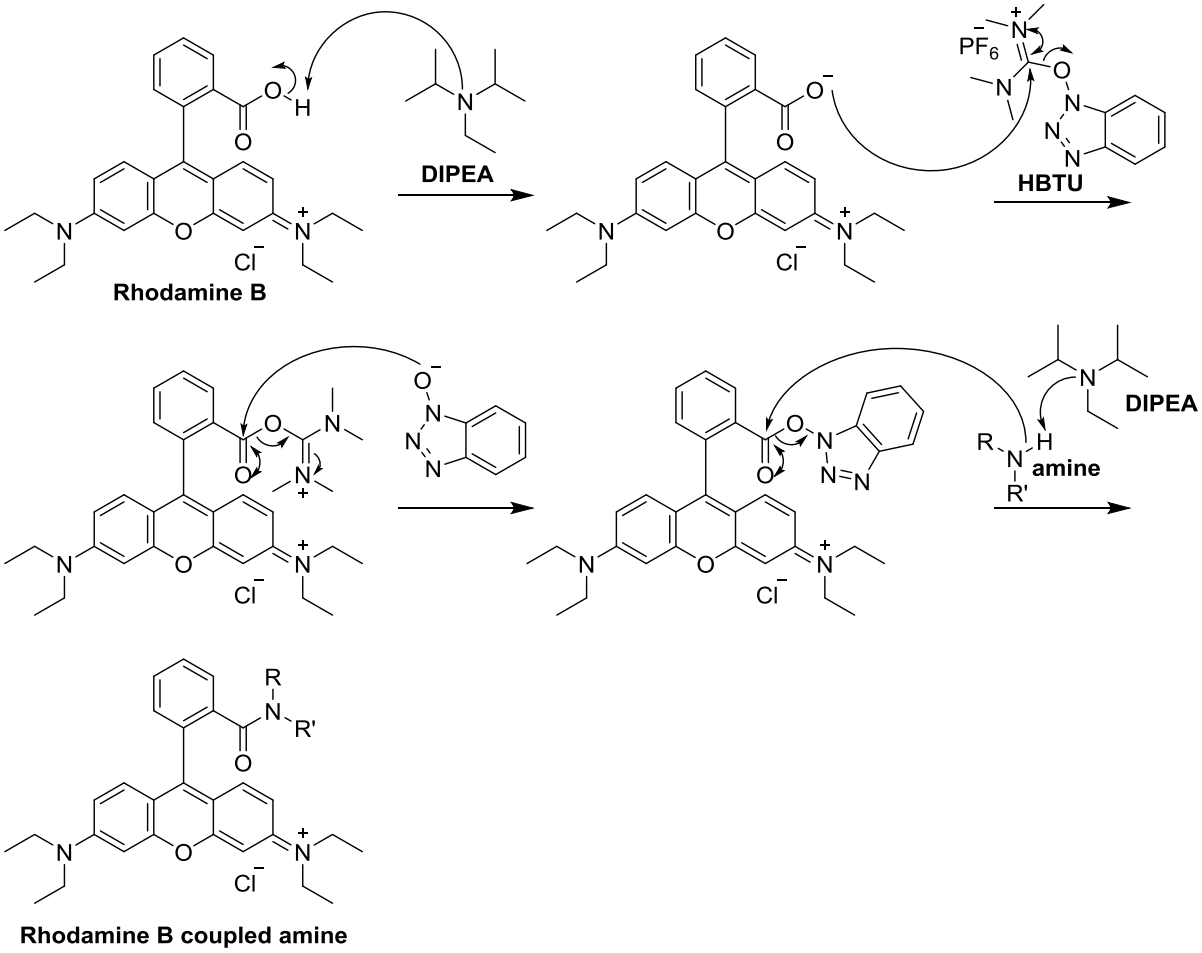

Schematic 4.1
Schematic of the labelling of an amine by Rhodamine B via HBTU coupling.

Using the stepwise SPPS methodology developed in 3.0, confirmed by LDI-ToF MS to transferrable to Klarite substrates, labelled peptide sequences could be prepared on a SERS substrate. Functionalisation in this manner would provide evidence that non-particulate SERS substrates could be used for enzyme detection purposes. To the best of our knowledge Klarite has never been used to monitor the enzymatic digestion of peptides.

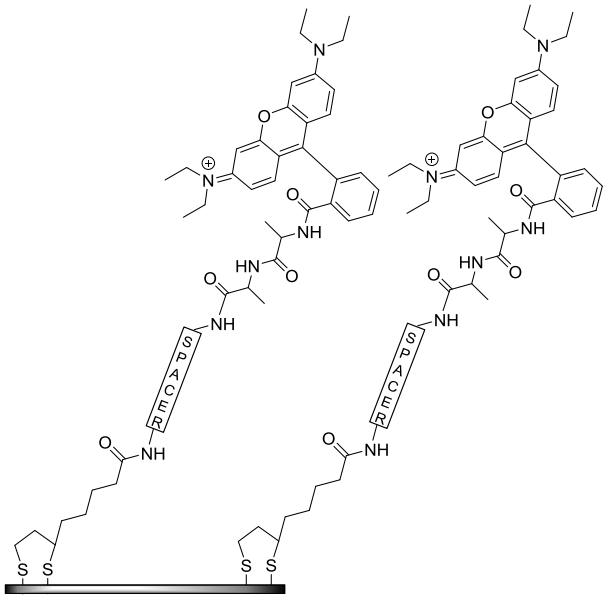

Figure 4.7
Preliminary surfaces prepared on klarite surface using stepwise SPPS. Spacer unit represents $(CH_2)_4$ or $CH_2CH_2O(CH_2CH_2O)_6CH_2CH_2$.

Figure 4.7 shows the surface functionalisation of gold with the familiar dialanine-containing sequence, using the methodology discussed in 3.0. Once prepared, deprotection of the terminal Fmoc moiety was achieved through immersion of the cover slips in a solution of piperidine and *N,N*-dimethylformamide before Rhodamine B was coupled on to the terminal amine (section 7.3.3). In an effort to visualise the enzymatic digestion process, and quantify the Rhodamine B signal observed, Raman maps corresponding to the area underneath the 1618 cm^{-1} peak were collected. Raman mapping is a powerful imaging tool and can be used on a

wide range of substrates; the 1618 cm^{-1} peak was chosen because it is clear and well defined, thus making it ideal for this technique.

Once the surfaces shown in figure 4.7 were prepared, 25 × 25 μm maps were obtained. Each sample was run in triplicate; pixel counting was utilised to determine the number of pixels for each sample which presented an intensity value greater than 1000 arbitrary units (a.u.).

Table 4.1
Pixel counting results from Raman mapping of Klarite SERS substrates

Spacer Unit	Elastase (mg mL^{-1})	Mean Number of Pixels >1000 a.u.	Std. Dev.
Control	Control	3.5	0.71
$(CH_2)_4$	0	79	96.9
$CH_2CH_2O(CH_2CH_2O)_6CH_2CH_2$	0	348	197.5
$(CH_2)_4$	1	422.8	308.2
$CH_2CH_2O(CH_2CH_2O)_6CH_2CH_2$	1	116.5	41.7

Samples containing the $CH_2CH_2O(CH_2CH_2O)_6CH_2CH_2$ spacer unit show a clear decrease in number of pixels greater than 1000 a.u. upon elastase treatment; however, the system containing the $(CH_2)_4$ spacer shows the opposite trend. This may be as a result of non-specific protein adsorption on the klarite surface, as an increase in proteinaceous matter would account for the increase in intensity.

Analysis of the elastase solution by HPLC after incubation showed a peak corresponding to the retention time of Rhodamine B, providing further confirmation that digestion of the sequence had occurred for all samples.

4.3.5 Optimisation of a SERS Biosensor for Elastase

Although a decrease in overall intensity was observed for the $CH_2CH_2O(CH_2CH_2O)_6CH_2CH_2$ containing system, there was concern that elastase

was unable to fully digest the sequence. Elastase is specific for small hydrophobic amino acids; as the terminal Rhodamine B moiety is much larger than Fmoc it is possible that the dye unit may be hindered from entering the enzyme's active site. In an effort to overcome this surfaces were prepared as per figure 4.8.

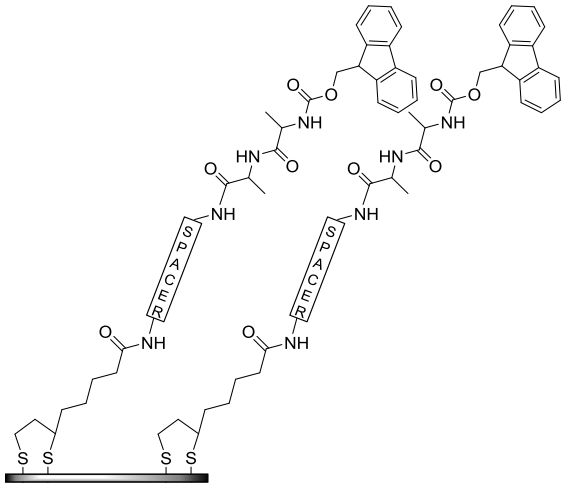

Figure 4.8
Surfaces prepared on klarite surface using stepwise SPPS. Spacer unit represents $(CH_2)_4$ or $CH_2CH_2O(CH_2CH_2O)_6CH_2CH_2$.

Once prepared, half of the substrates were treated with elastase (1 mg mL^{-1}) while the others were treated with the equivalent volume of phosphate buffer. After incubation, the samples were washed, dried and then treated with Rhodamine B. It was postulated that this approach would enable elastase to digest the peptide sequence to the same extent as observed in 3.0, and the digested surfaces would be observed as having greater signal intensity due to the subsequent treatment with Rhodamine B.

Table 4.2
Pixel counting results from Raman mapping of Klarite SERS substrates

Spacer Unit	**Elastase (mg mL^{-1})**	**Mean Number of Pixels >1000 a.u.**	**Std. Dev.**
Control	Control	3.5	0.75
$(CH_2)_4$	0	1812	1201.8
$CH_2CH_2O(CH_2CH_2O)_6CH_2CH_2$	0	1704.5	565.5
$(CH_2)_4$	1	2613.8	1044
$CH_2CH_2O(CH_2CH_2O)_6CH_2CH_2$	1	4568.3	1387.6

In this system, we see an increase in intensity for both spacer systems; however, the overall intensity values and standard deviations are much higher. This may be as a result of residual Rhodamine B on the Klarite surfaces before analysis, as every sample was immersed in a dye solution. Optimisation of this iteration would require the subsequent washing steps to be analysed in order to minimise overall intensity increases.

The final system investigated whether the addition of a secondary PEGylated spacer located after the elastase cleavable segment (figure 4.9) lead to enhanced differences *versus* the system outlined in 4.3.4.

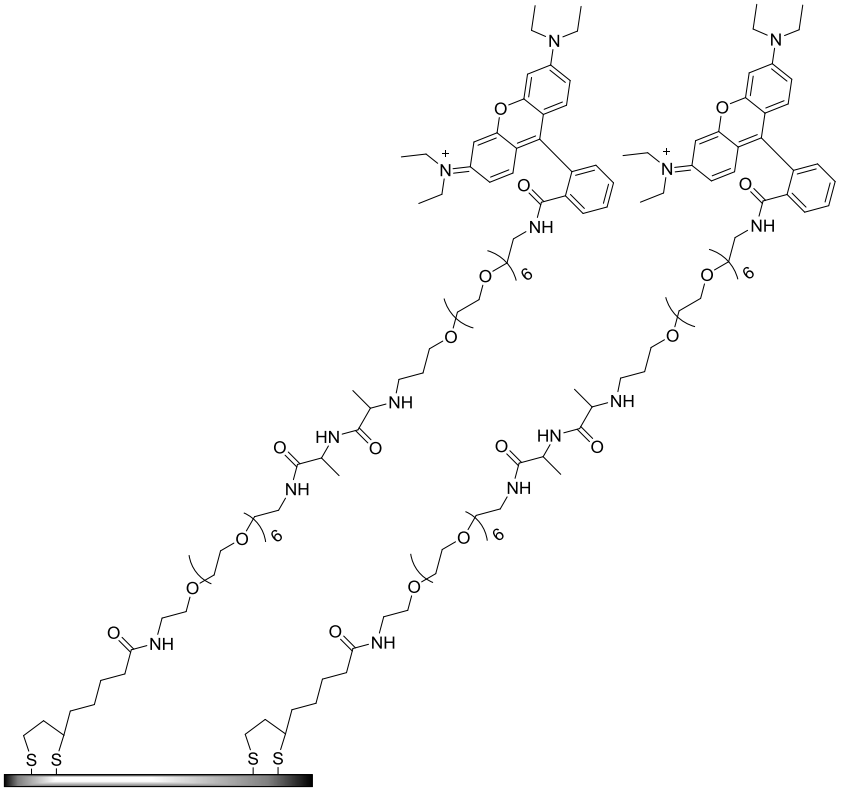

Figure 4.9

Surfaces prepared on Klarite surface using stepwise SPPS.

Table 4.3

Pixel counting results from Raman mapping of Klarite SERS substrates

Spacer Unit	**Elastase (mg mL^{-1})**	**Mean Number of Pixels >1000 a.u.**	**Std. Dev.**
Control	Control	3.5	0.75
$CH_2CH_2O(CH_2CH_2O)_6CH_2CH_2$	0	569.8	429.2
$CH_2CH_2O(CH_2CH_2O)_6CH_2CH_2$	1	152	116.1

Analysis of the pixel intensity for this system shows the greatest difference between the enzymatically treated sample *versus* the non-treated substrate of all the systems analysed. It is believed that this is due to a combination of factors; the PEGylated chain preventing non-specific adsorption of elastase onto the Klarite

surface which appears to skew the results obtained for the samples containing the $(CH_2)_4$ unit, the secondary spacer unit after the enzyme cleavable section allows elastase better access to the dialanine sequence to enable digestion and finally treatment with Rhodamine B is not the final synthetic step enabling the subsequent wash steps to reduce the quantity remaining unbound on the Klarite surface.

4.4 Conclusions

This chapter details the translation of the stepwise SPPS methodology from planar gold coated cover-slips onto a Klarite, a commercially available SERS substrate with a nanostructured surface comprised of inverted pyramidal pits. LDI-ToF MS was undertaken on the samples as a confirmatory test to ensure synthesis was successful on an alternative surface type. Proof-of-concept work and subsequent optimisation steps towards the first example of a combined SERS and Klarite system for enzyme detection are detailed.

Further optimisation steps in the future may include the use of mixed monolayer systems e.g. utilising alcohol terminated SAMS such as PEG thiols which would reduce the number of dye molecules on the Klarite surface. Once this system is fully optimised, translation onto alternative SERS substrates e.g. Au/Ag nanohole arrays such as those developed by Masson *et al*.[9] or Au/Al nanorod arrays developed by Berlouis *et al*.[10] will be possible. This in turn may lead to increased elastase sensitivity as a consequence of their enhanced SERS sensitivity *versus* Klarite.

CHAPTER FIVE – DESIGN AND PREPARATION OF A COLORIMETRIC ELASTASE SENSOR

5.1 Abstract

Preparation of the first colorimetic elastase detection system utilising gold nanoparticles is described. The remainder of the chapter is subdivided into smaller sections, each focussing on a distinct approach to the development of a colorimetric sensor. Topics include step-wise peptide synthesis directly upon gold nanoparticles alongside more classical solution and solid phase peptide synthesis. The work was targeted towards the development potentially more robust system, through incorporation of a disulfide rather than a thiol moiety. Several target molecules were successfully however, further optimisation of the system is required in order to enable enzymatic responsiveness.

5.2 Introduction

Nanoparticles prepared from coinage metals such as silver and gold possess dielectric functions which allow these metals to support a surface plasmon in the visible wavelength range i.e. the resulting nanoparticles are coloured.[1] Consequently, these metals are of great interest in sensing and diagnostics as their optical response can be easily investigated.

The class of enzymes known as the proteases act by hydrolysing peptide bonds and play a key role in many pathological processes. Deregulation of protease expression has been shown to play a role in diseases including rheumatoid arthritis, bacterial and viral infections, cancer and Alzheimer's disease.[2] A system whereby subtle changes, such as the expression of specific proteases, can be

monitored may provide a means of detecting disease. As such, sensitive and robust sensors for the detection of these enzymes are required.

Application of the methodologies discussed in 3.0 & 4.0, for the peptide functionalisation of gold surfaces, to colloidal substrates will provide a well characterised and understood starting point for the development of colorimetric enzyme detection systems.

5.2.1 Background

The impact of nanomaterials has been particularly significant in the field of diagnostics, where a number of nanoparticle-based assays have been introduced for biomolecule detection. To date, applications of nanoparticles have largely focused on oligonucleotide functionalised gold nanoparticles.[3] However, recent years have seen a number of studies utilising the colorimetric properties of gold nanoparticles for enzyme sensing purposes; including notable work by Stevens, Katayama and Scrimin on the detection of thermolysin and α_1-antichymotrypsin prostate specific antigen, kinase and thrombin respectively.[4-6]

Further details regarding the use of gold nanoparticles for colorimetric enzyme detection can be found in section 2.3.2.1, and interested readers are directed to the recent review by Stevens *et al*. for a comprehensive overview of this area.[7]

5.3 Project Aim

The aim of this research was to develop a colorimetric sensor system which could be used for the real-time detection of the serine protease, elastase. A proof-of-concept system is described whereby gold nanoparticles were functionalised with a peptide sequence to give the first example of a colorimetric system for elastase detection; similar in approach to that used in studies by Stevens.[4] Once proven, this work aimed to refine the peptide sequence in order to enhance the system's sensitivity and robustness. A further intention of this work was to build upon the

work detailed in chapters 3.0 and 4.0 to develop a method for stepwise solid-phase peptide synthesis on the nanoparticle surface. This would allow facile nanoparticle modification negating the arduous purification steps often encountered in organic synthesis.

5.4 Results and Discussion

This results and discussion section is split into five sub-sections which will be discussed in sequence.. The section begins with proof of concept work, followed by stepwise SPPS on gold nanoparticles, solution phase and solid phase synthesis of an elastase cleavable peptide sequence respectively and finally elastase detection. By separating the sections in this way, the reader is guided through the progression from proof-of-concept to optimisation attempts and suggestions for future work.

5.4.1 Proof of Concept Work

Stevens *et al.* demonstrated that nanoparticle-peptide conjugates containing the tripeptide sequence Fmoc-GFC-NH_2 (figure 5.1, structure **5.1**) could be utilised to monitor the real-time proteolytic action of thermolysin (*B. Thermoproteolyticus rokko)*.[4]

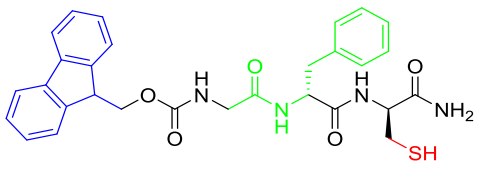

5.1

Figure 5.1
Structure of Fmoc-GFC-NH_2.

The system is elegant in its simplicity; functionalisation of a single population of nanoparticles with Fmoc-GFC-NH_2 created a tri-component sensor which the authors claim has enhanced thermolysin sensitivity compared with those previously reported i.e. the system is able to detect thermolysin at levels of 90 zg

mL^{-1}. As illustrated in figure 5.1, this system consists of three sections; the thiol-containing side chain of the cysteine residue provides the anchor to the surface of the nanoparticle (shown in red), a protease cleavable sequence specific to thermolysin (shown in green) and finally Fmoc (shown in blue) will drive assembly of the system through π-stacking interactions. Once conjugated to the nanoparticle surface, Fmoc-GFC-NH_2 induces aggregation of the nanoparticles due to the aforementioned π-stacking interactions and results in a colour change of the nanoparticles from ruby-red to blue. Upon introduction of thermolysin, enzymatic cleavage (hydrolysis) would occur i.e. Fmoc-G↓FC-NH_2 causing re-dispersion of the nanoparticles, and the accompanying colour change (figure 5.2).

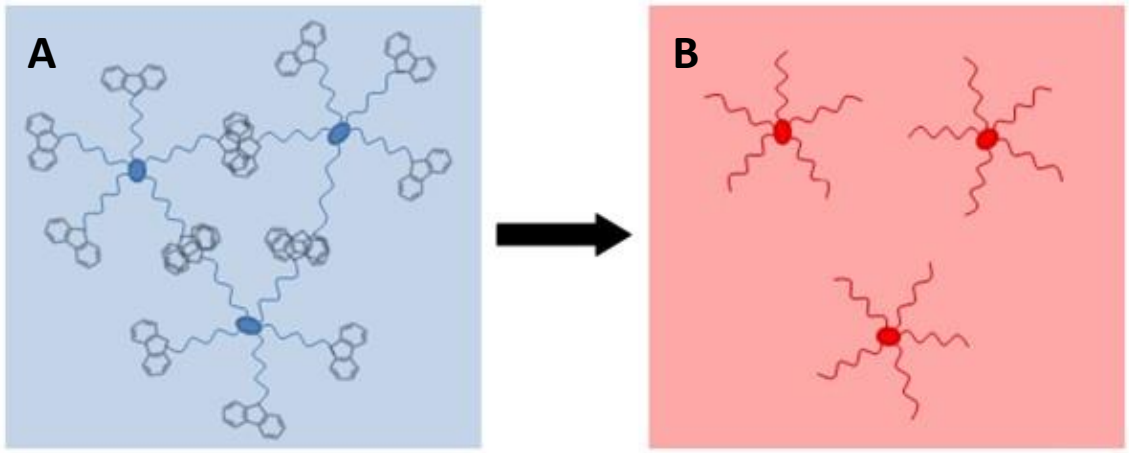

Figure 5.2
Schematic of the Stevens *et al*. sensor system; (A) gold nanoparticle-peptide conjugates assemble into aggregate structures as a result of π-stacking and thus appear blue, (B) thermolysin added to hydrolyse the peptide bond between glycine and phenylalanine residues, resulting in dispersion and a distinctive colour change to ruby-red.

The most noteworthy feature of this sensor system is that adaptation of the protease cleavable sequence may enable researchers to detect other enzymes i.e. by selecting a sequence specific to the enzyme of interest. Stevens *et al*. presented data for the detection of α_1-antichymotrypsin prostate specific antigen (nACT-PSA)

using an alternative peptide sequence without the need for further system modifications.

In order to confirm that such a tri-component system could be used to detect elastase, the tripeptide Fmoc-AAC-NH_2 (figure 5.3, structure **5.2**) was synthesised.

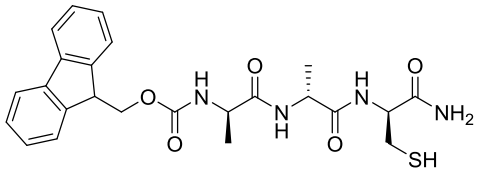

5.2

Figure 5.3
Structure of Fmoc-AAC-NH_2.

10 nm gold nanoparticles were stabilised through complexation with dipotassium bis(*p*-sulfonatophenyl)phenylphosphine dihydrate which prevents aggregation in aqueous buffers and enables the nanoparticles to withstand repeated NaCl precipitation.[7-8] The nanoparticles were then incubated overnight with an *N,N*-dimethylformamide solution of Fmoc-AAC-NH_2 and excess peptide was removed by centrifugation. The nanoparticles were then resuspended in phosphate buffer containing BSA and NaCl (section 7.4.6). Analysis by UV-Vis spectrophotometry before and after peptide-nanoparticle conjugation indicated that the SPR of the Fmoc-AAC-NH_2 modified nanoparticles had been red-shifted 12 nm and the peak had broadened (figure 5.4). All testing was run in duplicate and the spectra presented were plotted using the mean value calculated.

It should be noted that the degree of nanoparticle aggregation observed for the Fmoc-AAC-NH_2 functionalised nanoparticles was not as pronounced as for the Fmoc-GFC-NH_2 modified population; λ_{max} of the SPR detected at 533 nm *versus* 565 nm reported in the literature. This may be due to a number of factors; firstly, the difference in peptide sequence used i.e. AAC *versus* GFC. The aromatic side chain of the phenylalanine residue may enhance the extent of aggregation experienced by

the functionalised nanoparticles; phenylalanine is known to contribute towards π-stacking interactions in molecular self-assembly applications.[9] The peptide sequence selected for the detection of nACT-PSA also contains phenylalanine and thus would support this observation. Secondly, no information is given in the paper or supporting information regarding the aggregation state of the nanoparticles prior to functionalisation with either the thermolysin or the nACT-PSA. It is possible that the nanoparticles were already partially aggregated prior to introduction of the peptide sequence. Finally, and perhaps least likely, the molecular structure for Fmoc-GFC-NH_2 was drawn incorrectly in the journal article, as a result of an omitted methylene group on the cysteine side chain. As no experimental details or characterisation data were provided for either of the peptide sequences prepared, it may be that the peptides were mistakenly prepared using 2-amino-2-mercaptoacetic acid rather than cysteine.

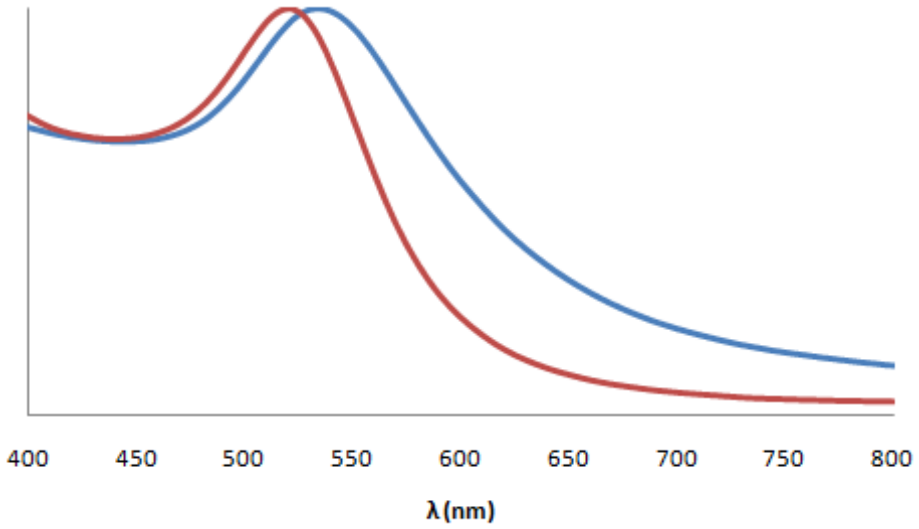

Figure 5.4
Normalised UV-Vis spectra of gold nanoparticles before (red line) and after (blue line) conjugation with Fmoc-AAC-NH_2.

Despite this difference in extent of aggregation upon introduction of an Fmoc-terminated peptide, results echoed that of Stevens *et al.*,[4] when modification of gold nanoparticles with a control sequence lacking the Fmoc moiety (L-cysteine methyl

ester hydrochloride) was attempted, and aggregation was not induced. Furthermore, it was confirmed that the addition of Fmoc-terminated amino acids with no thiol functionality had no effect upon the dispersion of colloidal gold nanoparticles (figure 5.5).

Please note, unless otherwise stated the y-axes of all UV-Vis spectra relate to normalised absorption, thus it is the position of λ_{max} which is of interest.

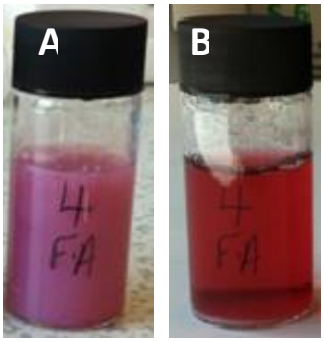

Figure 5.5
Colloidal gold nanoparticles (4 nM concentration) after incubation with Fmoc-A-OH. (A) t = 0 hours, opacity caused by vortexing sample and (B) t = 24 hours. No aggregation of the nanoparticles is observed either visually by eye or by UV-Vis spectrophotometry *versus* control sample containing no Fmoc-A-OH.

The work in this chapter was undertaken using gold nanoparticles purchased from a commercial supplier which were then further stabilised through complexation with dipotassium bis(*p*-sulfonatophenyl)phenylphosphine dihydrate. Attempts were made to recreate this work using nanoparticles which had been prepared in-house *via* the citrate reduction of sodium tetrachloroaurate (III) dihydrate (section 7.4.3). Despite several attempts, the non-commercial gold colloid was unstable under the salt conditions used during the peptide conjugation process, resulting in irreversible aggregation. Had the colloid been able to tolerate the conjugation conditions a truly ideal system could have been developed; given that researchers would know exactly what was present in the reaction mixture which is impossible when using proprietary commercial formulations.

Figure 5.6 shows the UV-Vis spectra of Fmoc-AAC-NH_2 modified gold nanoparticles before and after treatment with 1 mg mL^{-1} elastase, which shows the SPR blue-shifting from a broad peak at 533 nm prior to elastase addition to a narrower signal 525 nm after treatment. The λ_{max} of the SPR after elastase treatment is not dissimilar to that of Stevens *et al*. who report the final SPR position as 532 nm after an incubation period of six hours, although clearly the change in SPR pre and post enzymatic treatment is less pronounced for the elastase system.[4]

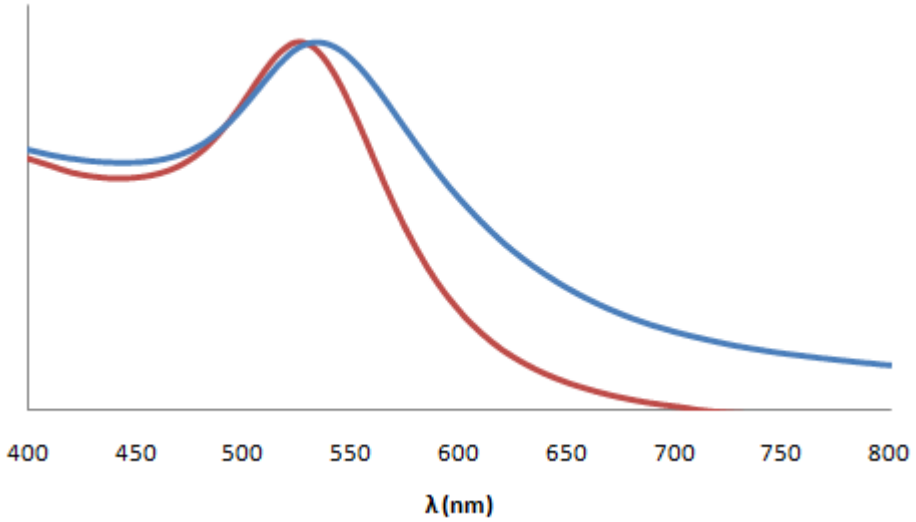

Figure 5.6
Normalised UV-Vis spectra of Fmoc-AAC-NH_2 modified gold nanoparticles before (blue line) and after treatment with 1 mg mL^{-1} elastase (red line).

Figure 5.7
(A) Control sample of Fmoc-AAC-NH_2 modified nanoparticles incubated with deionised water. (B) Colour change observed for Fmoc-AAC-NH_2 modified gold nanoparticles after 60 minute incubation with 1 mg mL^{-1} elastase.

Visual examination of the elastase treated conjugates after 60 minutes showed a noticeable colour change from the control sample, as evidenced in figure 5.7. Although not as dramatic as that observed for the thermolysin system, this change in colour indicated that even a small shift in SPR (in this case 8 nm) is visible to the naked eye. This was confirmed using a small test group (n = 8) all of whom stated that the sample treated with elastase was more red in colour than the control which was described as tending towards purple/blue-ish red.

Time course analysis of the Fmoc-AAC-NH_2 nanoparticle conjugates indicated a rapid blue shift of SPR upon introduction of 1 mg mL^{-1} elastase into the system (figure 5.8). After 2 minutes, the SPR had been shifted to almost the minimum value (by 7 nm to 526 nm) observed over the 60 minute incubation period. It is possible that had the system been allowed to incubated for a longer period i.e. 6 hours as per Stevens *et al*., that further blue shifting would be observed, however, given the overlapping nature of the spectra observed this appears unlikely.

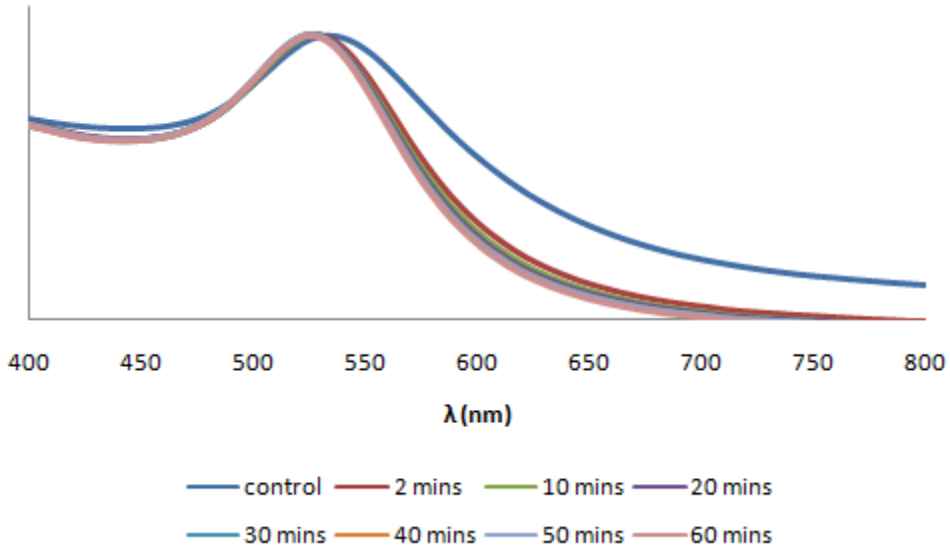

Figure 5.8
Normalised UV-Vis spectra of Fmoc-AAC-NH_2 modified gold nanoparticles, over a 60 minute period, upon introduction of 1 mg mL^{-1} elastase to the sensor system.

The spectra generated upon treatment of the conjugates with 1 μg mL^{-1} elastase (figure 5.9) is similar to that for the 1 mg mL^{-1}time course, albeit the peaks are somewhat broader than those observed for the higher enzyme concentration. Once again, a rapid blue shift can be seen upon introduction of elastase to the system which slows over time to give a final SPR position of 527 nm after 60 minutes.

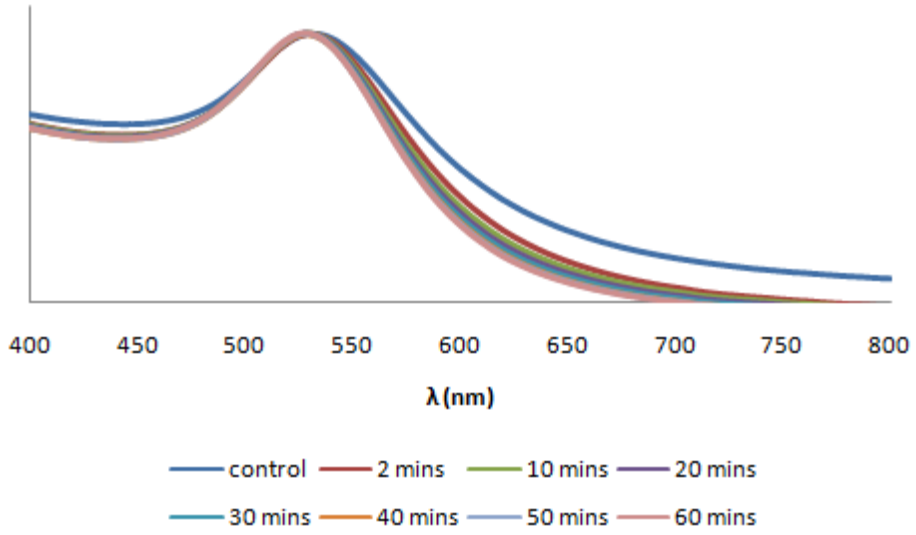

Figure 5.9
Normalised UV-Vis spectra of Fmoc-AAC-NH_2 modified gold, over a 60 minute period, upon introduction of 1 μg mL^{-1} elastase to the sensor system.

The final enzyme concentration tested was 250 ng mL^{-1} elastase as shown in figure 5.10. In this example the blue shifting is slower than is observed for the higher enzyme concentrations, and the final position of the SPR is shown to be 528 nm.

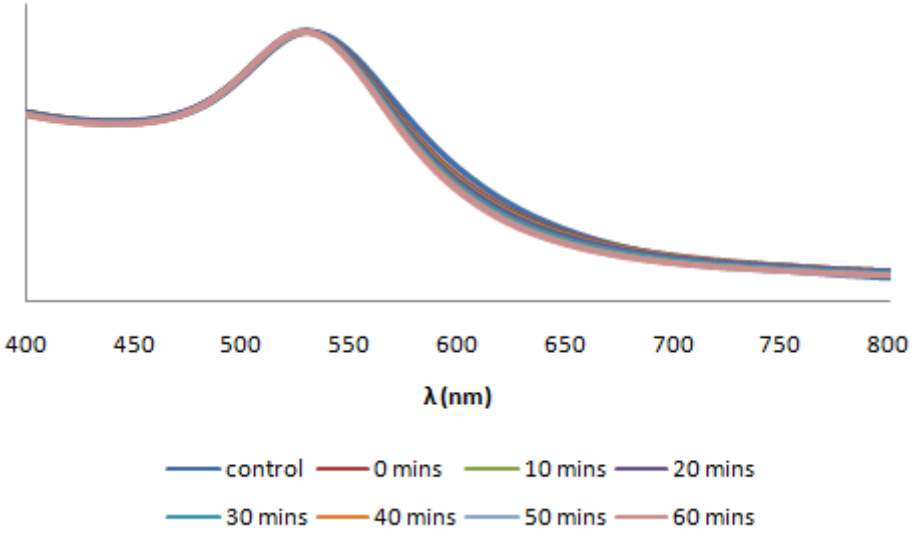

Figure 5.10
Normalised UV-Vis spectra of Fmoc-AAC-NH_2 modified gold nanoparticles, over a 60 minute period, upon introduction of 250 ng mL^{-1} elastase to the sensor system.

Spectra were analysed to establish the extent to which treatment with elastase caused re-dispersion of the nanoparticles. By calculation of the area underneath each of the spectrum over a predetermined region of the axis, it was possible to determine a value for A/D.

$$\frac{A}{D} = \frac{\left(\int_{700}^{550} f(UV - vis\ spectra)\right)}{\left(\int_{540}^{490} f(UV - vis\ spectra)\right)}$$

Equation 5.1

Using the parameters determined by Stevens *et al.*;[4] region A refers to the aggregated plasmon resonance occurring between 550 – 700 nm, while region D indicates the region of the UV-Vis spectrum which is representative of the SPR of gold nanoparticles in their disperse state i.e. 490 – 540 nm. As the value for A/D decreases over time, this is evidence that the system is moving towards a more disperse state. Analysis of the A/D values of the three elastase concentrations tested (figure 5.11) indicates that the systems treated with 1 mg mL^{-1} and 1 μg mL^{-1} elastase display almost identical dispersion behaviour despite differing by three orders of magnitude. From the data provided in figure 5.11 and from optical inspection of the nanoparticle systems (figure 5.7), it can be concluded that such a system can detect elastase at a microgram level.

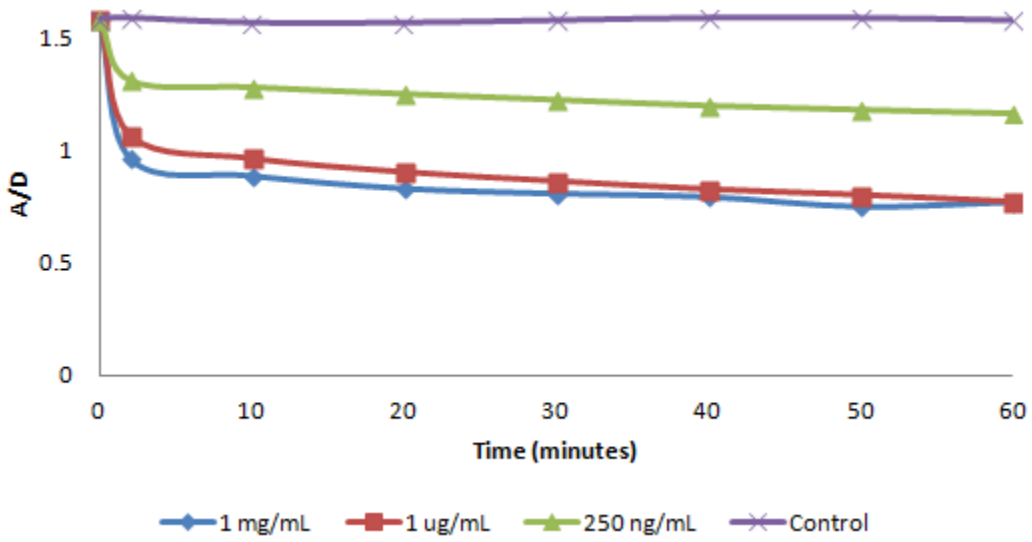

Figure 5.11
Rate of change in ratio of A/D over time for elastase treated samples.

Consultation with the literature suggests that the system developed is the first elastase detection system found on gold nanoparticles. However, the stability of alkane thiols, such as cysteine terminated peptides, on gold surfaces can be compromised when the surface is exposed to elevated temperatures or treated with biological buffer additives. The disulfide functionality of (±)-α-lipoic acid overcomes these issues by acting as a robust anchor,[10] as demonstrated in chapters 3.0 & 4.0. The remainder of this chapter will focus on the utility of this molecule in the development of a more robust colorimetric elastase sensor.

5.4.2 Stepwise Solid-Phase Peptide Synthesis on Gold Nanoparticles

Following the successful stepwise synthesis of peptide sequences on planar and nanostructured gold surfaces (refer to chapters 3.0 and 4.0 respectively), work was undertaken to determine whether this step-wise methodology could be extended to gold nanoparticles. Scanning electron microscopy (SEM) images were then obtained for uncomplexed gold nanoparticles and those complexed with dipotassium bis(*p*-sulfonatophenyl)phenylphosphine dihydrate to aid stability, figure 5.12.

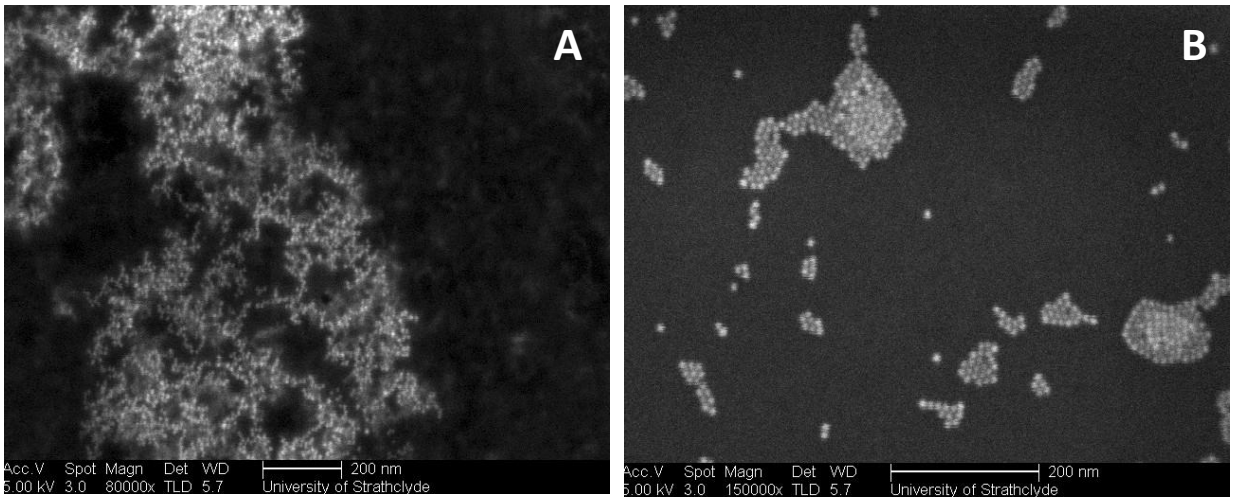

Figure 5.12
SEM images of (A) gold nanoparticles and (B) complexed with dipotassium bis(*p*-sulfonatophenyl)phenylphosphine dihydrate.

From the SEM images, it is clear that complexation with the dipotassium salt results in the formation of distinct nanoparticle assemblies which are not observed for uncomplexed nanoparticles; as the λ_{max} of both samples were 522 nm, and ruby-red in colour, this cannot be due to aggregation. SEM sample preparation involves allowing a solution to air dry overnight on a silicon wafer, and so this difference may be an artefact caused by drying the sample out, rather than a feature present in a solution of said sample. Particle sizing of the nanoparticles was also undertaken, and although the samples were at the measurement threshold, the size was confirmed to be 9 ± 3 nm.

The first attempt to functionalise the gold nanoparticles utilised a modified version of the method used by Stevens *et al.*[4] Solutions of (±)-α-lipoic acid, NaCl and sodium phosphate were prepared and added to stabilised gold nanoparticles. An immediate colour change from ruby-red to purple/blue was observed, indicating aggregation had taken place. Attempts to resuspend the nanoparticles in an aqueous solution of dipotassium bis(*p*-sulfonatophenyl)phenylphosphine

dihydrate were unsuccessful, indicating that aggregation was irreversible, likely a result of the high salt concentration (100 mM).

A further attempt was made at solid phase synthesis using the following formula to calculate the number of moles of (±)-α-lipoic acid required to functionalise a nanoparticle:[10]

$$Required\ number\ of\ moles\ = An\ \times Cn\ \times D \times V$$

Where An = surface area of nanoparticle
Cn = concentration of nanoparticle solution
Sc = surface coverage of small molecule on each particle
V = volume of nanoparticle solution

Assuming nanoparticles are spherical, this can also be written as:

$$Required\ number\ of\ moles = 4\pi r^2 \times Cn\ \times Sc \times V$$

Where r = radius of nanoparticle

Equation 5.2

This method was originally designed to calculate the number of moles of oligonucleotide required to coat a gold nanoparticle. However, as (±)-α-lipoic acid is a commonly used linker for oligonucleotide-nanoparticle conjugates, an accepted density value for disulfide modified oligonucleotide conjugates,[11] D = 12.6 $\pm$ 0.8 pmol cm^{-2} was used. A solution containing the required number of moles of (±)-α-lipoic acid was prepared and allowed to react overnight with stabilised gold nanoparticles. SEM images were obtained for these (±)-α-lipoic acid functionalised nanoparticles, figure 5.13, which showed no visually detectable difference in particle size when compared to stabilised nanoparticles.

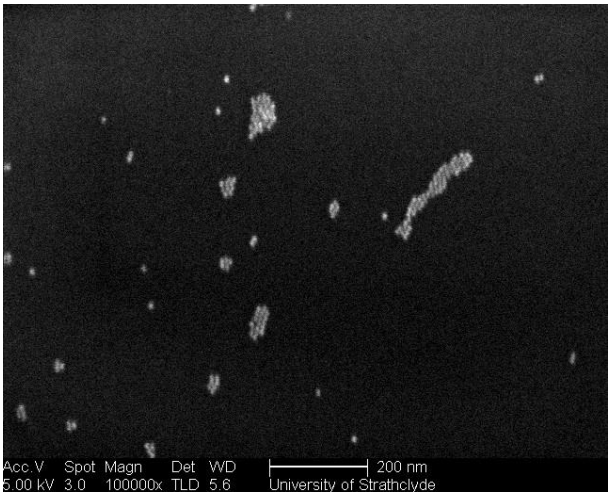

Figure 5.13
SEM image of nanoparticles complexed with dipotassium bis(*p*-sulfonatophenyl)phenylphosphine dihydrate and then functionalised with (±)-α-lipoic acid.

Particle sizing measurements made using a CPS Disc Centrifuge instrument indicated that samples functionalised with (±)-α-lipoic acid had a 0.8 nm increase in diameter *versus* stabilised gold nanoparticles, figure 5.14. This increase is less than would be expected for a molecule modified with (±)-α-lipoic acid, which has a length of 1.2 nm, as an increase in the order of 2.4 nm would be predicted. However, the CPS instrument calculates particle size as a function of absolute density, and the attachment of (±)-α-lipoic acid would account for this difference.

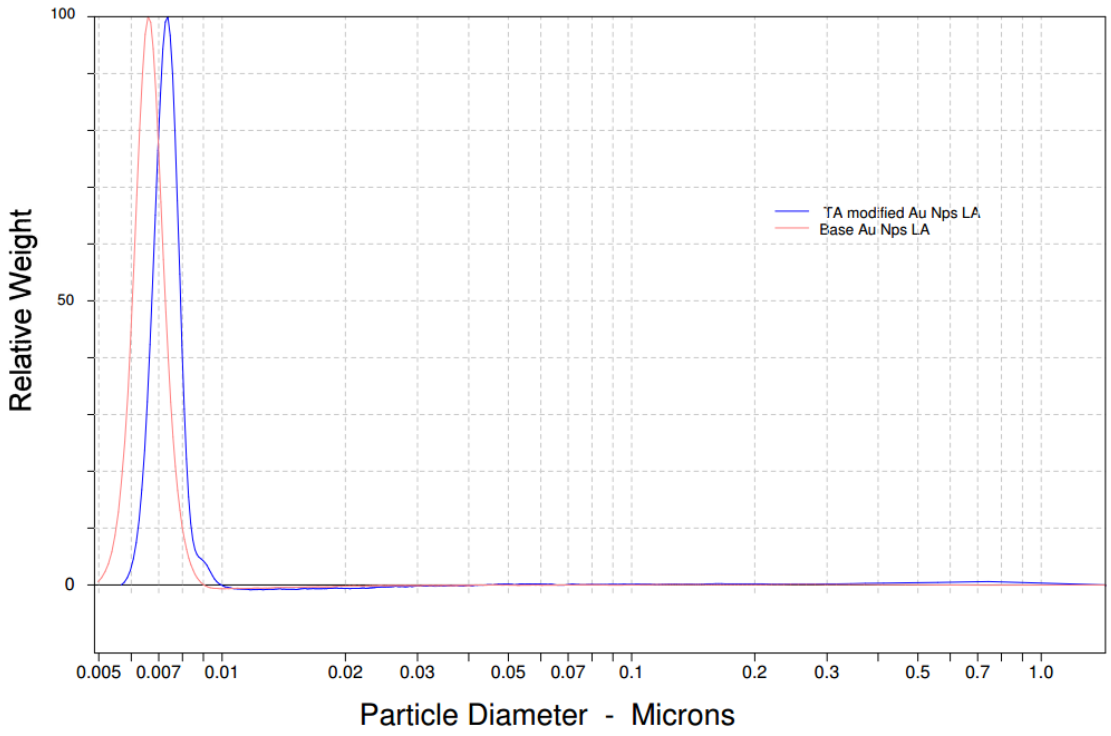

Figure 5.14
Comparison of CPS Disc Centrifuge measurements for bare (red) and (±)-α-lipoic acid modified (blue) nanoparticles. Image provided by Hiran Vegad, Analytik Ltd.

Attempts to activate the (±)-α-lipoic acid by NHS ester formation directly upon the nanoparticle surface resulted in huge losses due to irreversible aggregation, and the decision was made to terminate the experiment. As a result, this method requires optimisation before the synthesis of the peptide of interest can be performed in a stepwise manner on gold nanoparticles. This may involve adding excess reagent to the nanoparticle solution to negate the need for washing steps, or perhaps immobilising nanoparticle upon functionalised resin, as demonstrated by Jacobson *et al.*[12] It is possible that utilising the optimised poly(ethylene) glycol (PEG) system discussed in 4.0 may overcome these aggregation difficulties, as the PEG chains would confer additional stability to the nanoparticles.[13]

5.4.3 Solution-Phase Synthesis of an Elastase Cleavable Peptide Sequence

As a result of the challenges encountered attempting stepwise SPPS upon gold nanoparticles, an alternative methodology was deemed necessary. Solution-phase peptide synthesis was utilised to prepare an elastase specific peptide sequence which could be tethered directly to the nanoparticle surface. Scheme 5.1 shows a retrosynthetic route to target molecule **5.3**; this molecule could be prepared using standard Fmoc-peptide coupling techniques from free amine **5.4** which in turn could be prepared from (±)-α-lipoic acid, structure **5.5**.

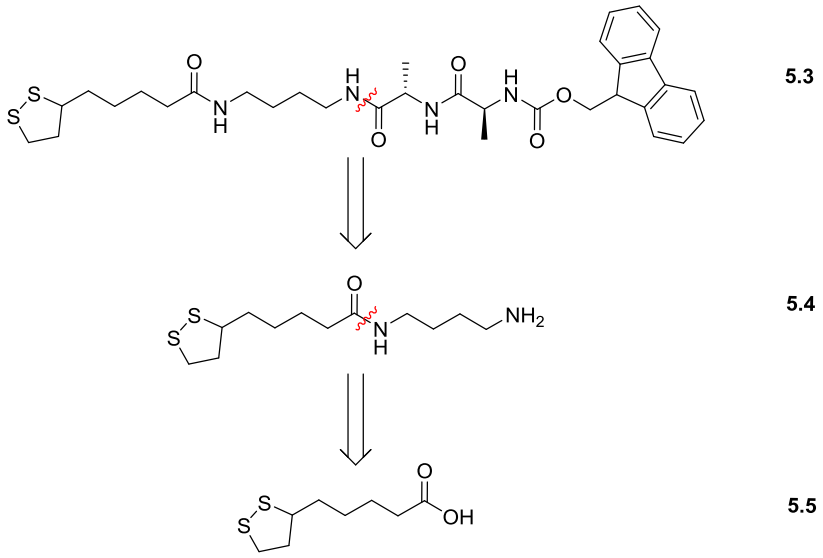

Scheme 5.1
Retrosynthetic route for the preparation of target molecule **5.3** using (±)-α-lipoic acid **5.5** as a precursor.

Following the disconnection approach outlined above, scheme 5.2 shows the initial synthetic strategy employed to achieve the target structure **5.3**. Utilising the approach developed by Graham *et al.*,[11] (±)-α-lipoic acid (scheme 5.2, structure **5.5**) was treated with EDC·HCl and *N*-hydroxysuccinimide to afford a readily characterised ester (scheme 5.2, structure **5.6**) which was stable over a period of months. Despite this stability, **5.6** reacted readily with primary amines, and was

coupled with *N*-Fmoc-1,4-butanediamine·HBr, to give **5.7** using the mild experimental conditions detailed by Koufaki *et al*.[14-15]

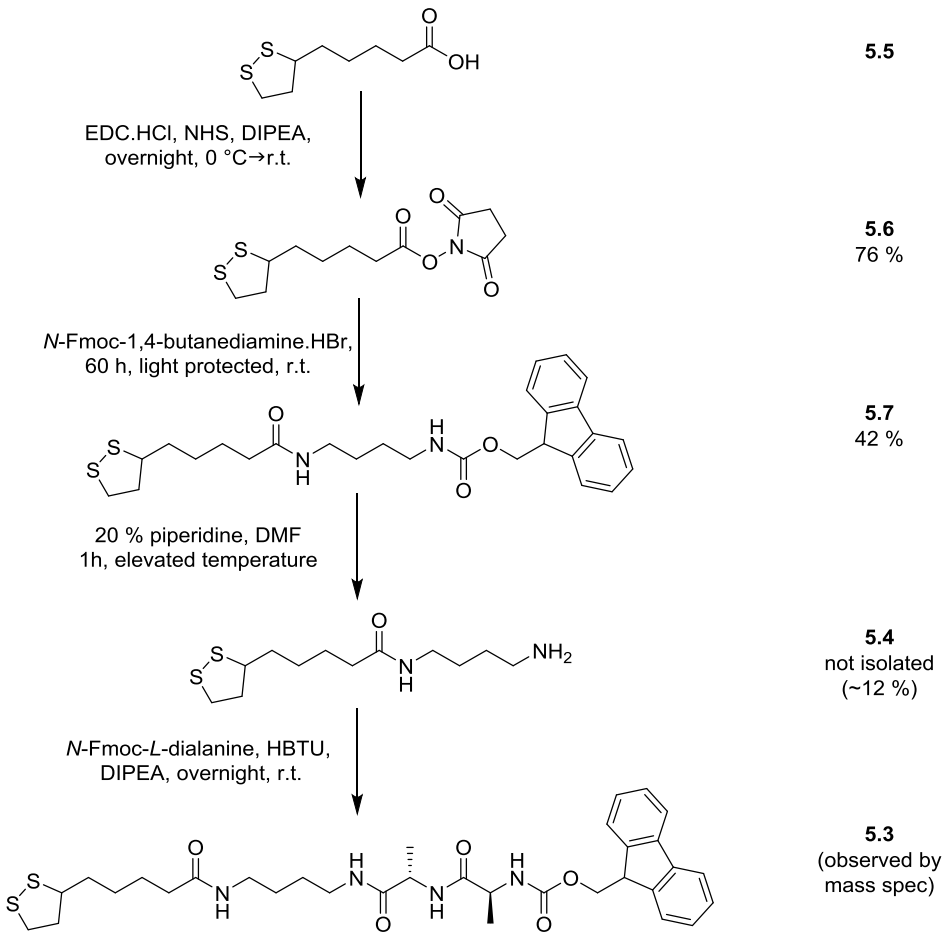

Scheme 5.2
Initial strategy for solution-phase synthesis and resulting experimental yields.

Upon deprotection of the terminal Fmoc group of **5.7**, the free amine (scheme 5.2, structure **5.4**) could not be isolated. This can be explained by the poor solubility of **5.4** in organic solvents of various polarities; purification by flash column chromatography, recrystallisation, reverse phase chromatography and preparative HPLC were all attempted, however, **5.4** could only be observed within a mixture of products by ^{1}H NMR.

A small quantity of crude material was coupled with Fmoc-AA-OH; however, the material obtained was insufficient for full characterisation, although the target molecule (scheme 5.2, structure **5.3**) was observed by ESI-MS.

In order to circumvent the difficulties encountered during the removal of the terminal fluorenyl group to afford free amine **5.4**, alternative routes to **5.3** were proposed. Scheme 5.3 shows the reaction conditions employed when *N*-Fmoc-1,4-butanediamine·HBr was replaced with the analogous 1,4-diaminobutane.

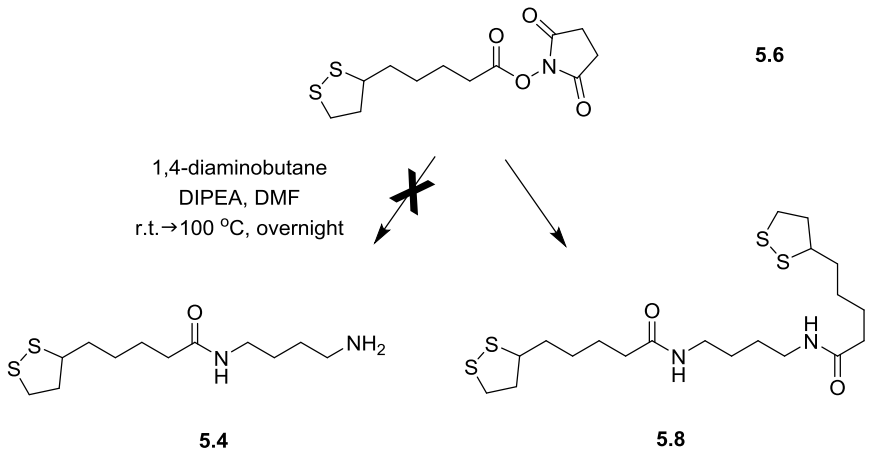

Scheme 5.3
Synthetic strategy for the preparation of **5.4** using 1,4-diaminobutane.

It was anticipated that the approach detailed in scheme 5.3 would mitigate the purification difficulties encountered during the preparation of structure **5.3** (scheme 5.2), as deprotection of a terminal fluorenyl group would not be required. The resulting reaction mixture would contain **5.4** and 1,4-diaminobutane only; as 1,4-diaminobutane is soluble in aqueous solutions the unreacted material could be removed *via* washing steps to yield pure **5.4**.

The reaction was designed with an excess of 1,4-diaminobutane (3 eq. *versus* 1 eq. **5.6**) in order to minimise the formation of side product **5.8**. However, upon NMR analysis of the reaction product **5.8** was observed as the major product. Similar to the previous synthesis route (scheme 5.2), the crude material prepared *via* scheme

5.3 was poorly soluble; attempts were made to isolate amine **5.4** using flash column chromatography, however, only doubly disulfide functionalised **5.8** was observed. It is possible that **5.4** was prepared, even though it could not be observed by NMR or mass spectrometry due to its inability to dissolve in conventional solvents.

The final synthetic strategy attempted for the preparation of **5.4** entailed the use of 4-amino-1-butanol, followed by the subsequent conversion of the secondary alcohol to a primary amine.

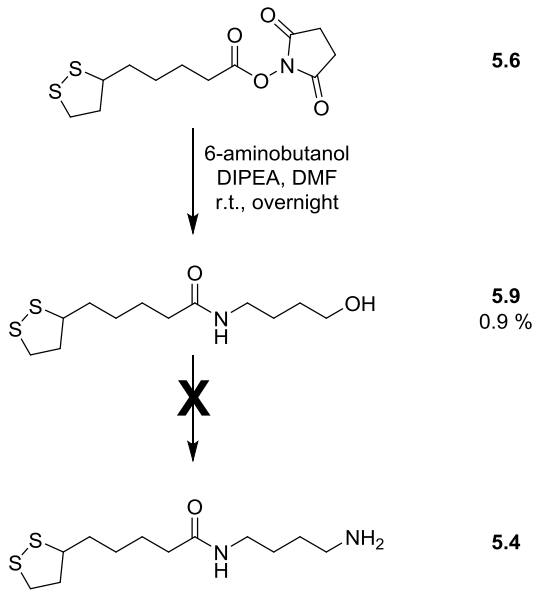

Scheme 5.4
Synthetic strategy for the preparation of **5.4** using 4-amino-1-butanol.

The rationale behind this route was that once coupled to ester 5.6 the terminal hydroxyl group of 4-amino-1-butanol could be converted into an amino group, thus forming **5.4**. Several papers describe a modified Mitsunobu reaction to enable the "one pot conversion of primary alcohols to amines" using sodium azide and triphenylphosphine.[16-17] However, despite successfully synthesising hydroxyl terminated **5.9** (scheme 5.4), insufficient material was generated to enable further

modification to **5.4**. As per schemes 5.2 and 5.3, this was believed to be as a result of poor solubility on the part of structure **5.4**.

5.4.4 Solid-Phase Peptide Synthesis of an Elastase Cleavable Peptide Sequence

As a result of the solubility difficulties encountered during solution-phase synthesis (section 5.3.4), it was determined that a different approach was necessary in order to generate an elastase specific peptide sequence. Fmoc-AAK-NH_2 (figure 5.15, structure **5.10**) was determined to be a close structural match to a fragment of target molecule **5.3**, and could be prepared *via* solid-phase peptide synthesis.

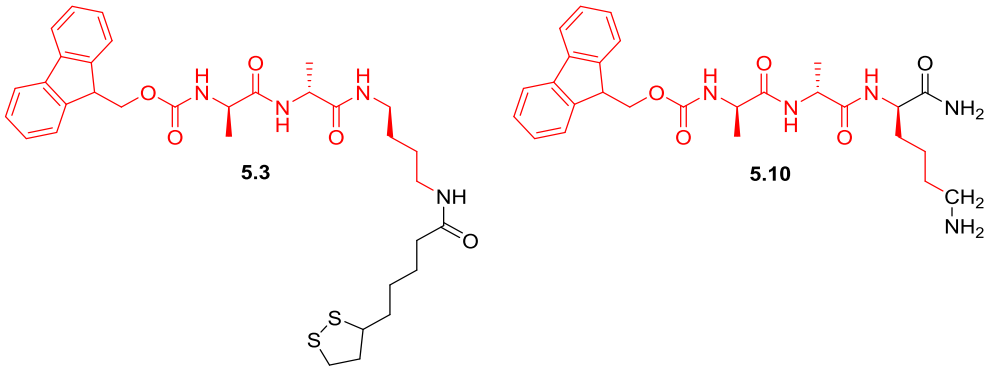

Figure 5.15
Structural similarities between **5.3** and Fmoc-AAK-NH_2 (**5.10**) highlighted in red.

Upon coupling **5.10** with NHS-ester **5.6,** structure **5.11** was obtained which bears similarity to desired structure **5.3** (figure 5.16)**. 5.11** has an additional methylene unit which may lead to additional chain flexibility, while the presence of a primary amide may contribute to further structural organisation through hydrogen bonding.

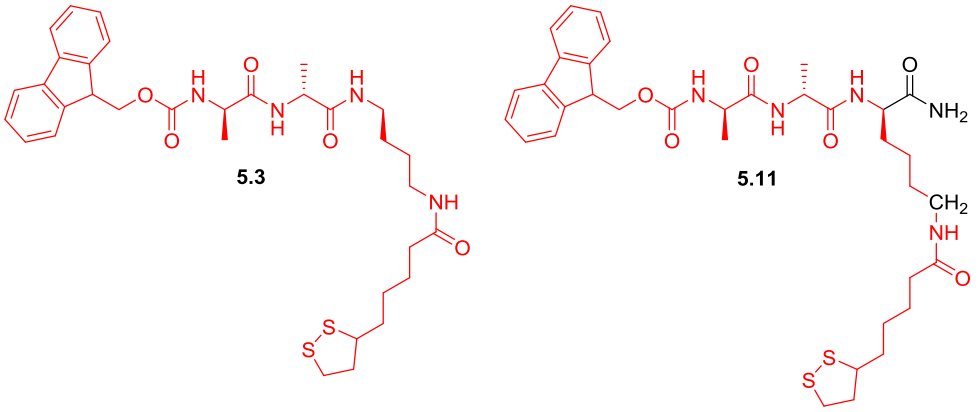

Figure 5.16
Structural similarities between **5.3** and **5.11** highlighted in red.

Applications which do not permit the inclusion of a lysine residue into the sequence may be able to utilise the Hofmann rearrangement.[18] This reaction causes the conversion of a terminal amide into a primary amine with the loss of a carbon atom. Scheme 5.5 demonstrates the use of a Hofmann rearrangement for an analogue of **5.10**. Fmoc-AA-GABA-NH_2 **5.12** was prepared using standard solid-phase peptide synthesis and stirred overnight in a basic solution of benzyltrimethylammonium tribromide. Structural rearrangement occurred to afford **5.14** (scheme 5.5) as part of an inseparable mixture of compounds due to multiple sites of bromination. Thus, for the purposes of this work, the use of Fmoc-AAK-NH_2 **5.10** was preferred due to ease of preparation.

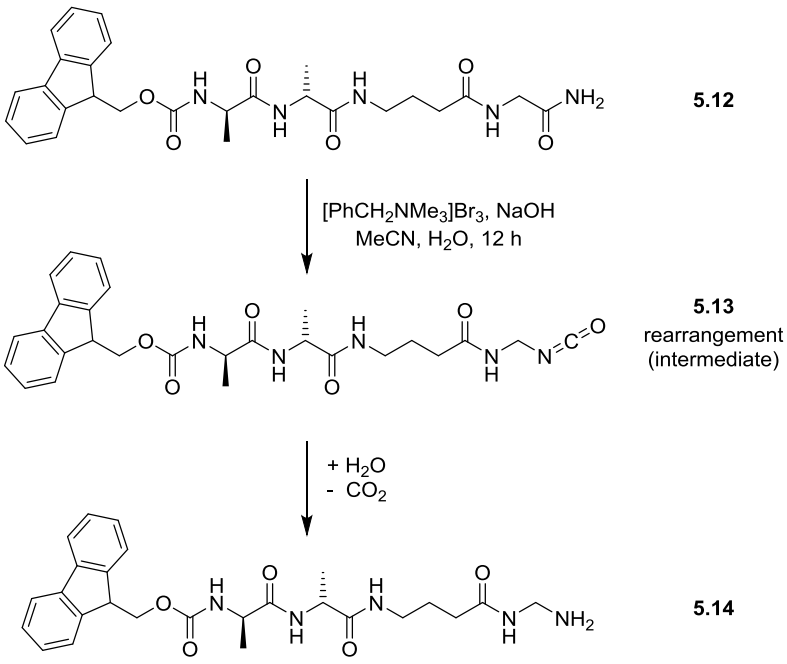

Scheme 5.5
Hofmann rearrangement of Fmoc-AA-GABA-NH_2, **5.12**.

5.4.5 Elastase Detection

Peptide-nanoparticle conjugates were prepared through incubation of the stabilised gold nanoparticles in an organic solution of **5.11** (see section 7.4.5 for experimental details).

Upon UV-Vis analysis of the resulting conjugates it was noted that the SPR λ_{max} was observed at higher wavelength than for the equivalent cysteine tethered sequences, 538 nm compared with 533 nm for Fmoc-AAC-NH_2 functionalised nanoparticles. Upon treatment with both 1 mg mL^{-1} and 5 mg mL^{-1} elastase, no dispersion of nanoparticles was observed (figure 5.17).

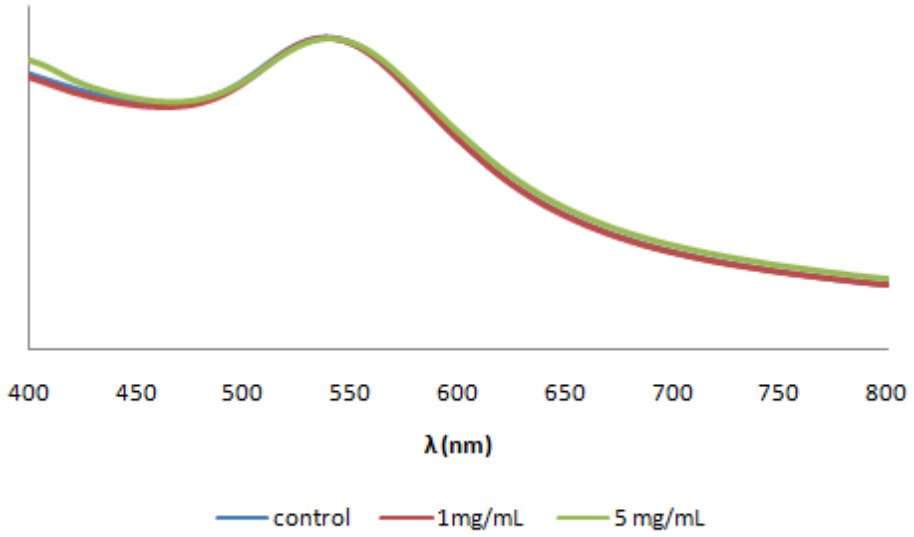

Figure 5.17
Normalised UV-Vis spectra of gold nanoparticles functionalised with structure **5.11** in the absence of elastase (control) and after treatment with 1 mg mL^{-1} and 5 mg mL^{-1}.

As the sensor system utilising (±)-α-lipoic acid as an anchor to the nanoparticle surface did not show the desired response upon introduction of elastase, the isomer isolipoic acid was prepared. It was anticipated that the symmetrical structure of isolipoic acid would enhance the sensor sensitivity as the attached peptide sequence was more likely to be projected perpendicularly outwards from the nanoparticle surface *versus* the corresponding derivatives of lipoic acid which would inherently present the elastase cleavable sequence at an acute angle.

Following a modified version of the route published by Tucker *et al.*[19] scheme 5.6 shows the stages involved in the preparation of isolipoic acid, **5.20**. 6-Bromo-hex-1-ene **5.15** was reacted with diethyl malonate to afford diethyl 2-(hex-5-enyl)malonate **5.16**. Malonate **5.16** was subsequently reduced to the corresponding diol **5.17** by lithium aluminium hydride and purified by filtration through Celite. Conversion of the diol **5.17** to dimesylate **5.18** was achieved by dropwise addition of methanesulfonyl chloride and was subsequently purified *via*

column chromatography. Oxidation of **5.18** to afford carboxylic acid **5.19** was achieved using osmium tetroxide, and the crude material was used as such for the next step. Tucker *et al*. detail the use of a combination of sulfur and sodium sulfide hydrate in order to generate isolipoic acid **5.20**. However, the decision was made to alter this final step as preparation *via* potassium thioacetate is the more conventional route for the preparation of thiols.[20] Furthermore, sodium sulfide hydrate is toxic and the use of sulfur may lead to multiple sulfur units within the five-membered ring e.g. a trisulfide compound may be generated.

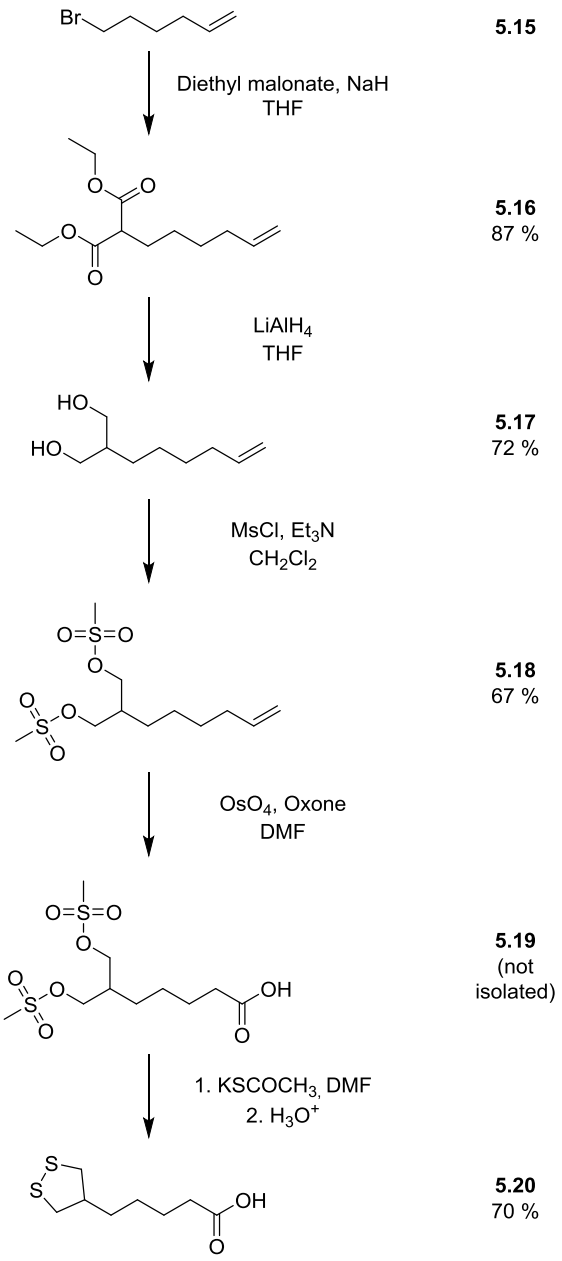

Scheme 5.6
Synthetic strategy for the preparation of isolipoic acid, **5.20**.

Isolipoic acid **5.20** reacts in a similar manner to (±)-α-lipoic acid **5.5,** and thus could be activated by forming an NHS ester (structure **5.21** – section 7.4.7). Once formed, this active ester was reacted with Fmoc-AAK-NH_2 to give the isolipoic isomer **5.22** (figure 5.18) of previously synthesised structure **5.11**.

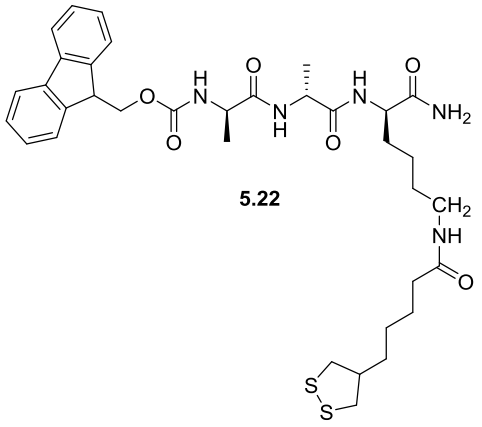

Figure 5.18
Isolipoic isomer derived peptide **5.22**.

As illustrated in figure 5.19, incorporation of isolipoic acid into the system had no effect on the ability of the functionalised nanoparticles to disperse. It may be that in order to use such anchoring systems to good effect on nanoparticle surfaces, that incorporation of polyethylene glycol (PEG) is required.

To date, the use of Fmoc-AAC-NH_2 (presented in section 5.3.1) is the only elastase detection system found on gold; however, the successful synthesis of molecules such as **5.22** (which contains an AA unit and a disulfide) may provide a system that can be further investigated with a slight modification to this molecule (e.g. PEG) or to the digestion conditions.

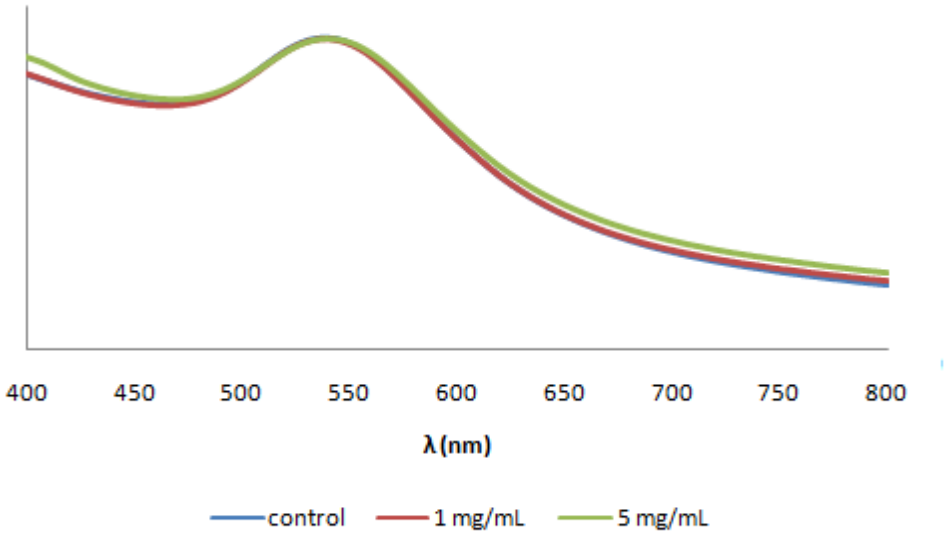

Figure 5.19
Normalised UV-Vis spectra of gold nanoparticles functionalised with structure **5.22** in the absence of elastase (control) and after treatment with 1 mg mL^{-1} and 5 mg mL^{-1}.

5.5 Conclusions

This chapter details the development of the first elastase detection system found on gold nanoparticles, utilising the rationale used by Stevens *et al.* for thermolysin detection. Furthermore, this chapter builds on the methodological work discussed in 3.0 and 4.0.

The remainder of the work presented in the chapter focuses on the development of a potentially more robust system, through incorporation of a disulfide rather than the single thiol of cysteine. It was envisioned that such a modification would provide more thermally and chemically robust peptide-nanoparticle conjugates. To date, several target molecules have been successfully synthesised that contain an AA unit and a disulfide; however, none of these molecules provide an elastase responsive system. Modifications to the structure of these molecules or to the

conditions that they are used in during elastase treatment may provide the basis of future investigations.

CHAPTER SIX - CONCLUSIONS

6.1 Conclusions

This thesis details the journey towards the development of a colorimetric elastase sensor utilising peptide functionalised gold nanoparticles. This involved the development of a series of elastase responsive gold surfaces. Each surface type displayed an increasing degree of complexity from planar gold surfaces to nanostructured and then ultimately to colloidal gold nanoparticles. These sequential increases in complexity allowed full characterisation of the surfaces, and consequently indicate the surface interactions which will be present in the final particulate sensor. In the future systems such as these may serve a role in disease detection.

The literature reviewed in 2.0 introduces the reader to the huge range of enzyme responsive nanomaterials (ERNMs) which have been developed over the last decade. For the purposes of brevity it was necessary to restrict the scope of this review to systems whereby an enzyme-sensitive substrate is immobilised on a nanoparticle, or similar nanoscale structure, in order to cause a reporting event. In spite of this, the number of combinations of enzymes, nanostructure components and means by which to detect an enzyme invoked change are vast and constantly being updated. Indeed one would be foolish to imagine that such a diverse and vibrant field could be covered in a single review.

Initial work upon peptide functionalisation of gold began in 3.0 on planar gold surfaces. A combination of surface analysis techniques including ToF-SIMS, XPS, LDI-ToF MS and WCA were utilised to fully characterise the system and ensure the methodologies developed produced consistent, homogenous surfaces in a predictable manner. This chapter also detailed the optimisation of the technique

through comparison of linker systems, in order to minimise the phenomenon of non-specific protein adsorption.

The methodology developed in 3.0 was translated from planar surfaces to nanostructured surfaces by utilising gold coated Klarite SERS substrates. In addition to confirming that the methodology worked successfully on alternative surface types, this chapter detailed the development of the first Klarite based enzyme detection system. Steps were taken towards optimisation, and future work suggested.

The final experimental chapter sees the development of the first colorimetric elastase sensor using gold nanoparticles, building on published work by Stevens *et al.*.[1] Sensitivity limits were explored and the synthetic route towards a potentially more stable system investigated.

6.2 Future Work

The work detailed herein focuses solely on gold surfaces and nanoparticles; however, as discussed in section 2.3.2.1, silver nanoparticles offer superior SERS enhancement and catalytic properties. The initial work by Graham *et al*. on (±)-α-lipoic acid involved the development of silver nanoparticles conjugates which were more stable than the corresponding gold species.[2] Due to the potential applications such conjugates may have, it would be useful to determine whether the method developed for stepwise SPPS (Chapter 3.0) was translatable to planar silver surfaces. If this methodology proved unsuitable, it would be worthwhile to determine whether minor adjustments e.g. the introduction of benzotriazole functionality in place of disulfide, proved successful in the development of a robust method for peptide functionalisation of silver.

In a similar vein, it would be of interest to determine whether alternative array structures could be utilised to further optimise the sensitivity of the SERS

biosensor developed in Chapter 4.0. Additional work to determine the elastase sensitivity threshold of the current system could be carried out with relative ease.

By employing careful design, it is possible that stepwise SPPS could be used to prepare sequences containing multiple Raman reporters between enzyme specific peptide sequences. Upon introduction of an enzyme, the sequence would be cleaved at a particular residue liberating one or more Raman reporter. Upon subsequent analysis by SERS and HPLC of the enzymatic digest, researchers would be able to determine at which residue an enzyme had cleaved, and therefore identify the enzyme.

The utilisation of larger gold nanoparticles in Chapter 5.0 would potentially lead to greater differences in the λ_{max} values observed for both functionalised and non-functionalised nanoparticles. This could provide a simple means of optimisation for the Fmoc-AAC-NH_2 system whereby the colour change upon introduction of elastase is more pronounced optically.

Further optimisation to the nanoparticle sensor systems described in this thesis may involve the introduction of the optimised PEG spacer system investigated in Chapter 4.0. It is possible that by decreasing the density of structures **5.11** or **5.22** on the nanoparticle surface, elastase will be better able to digest the sequence and blue shifting of the λ_{max} will be observed.

As discussed by Stevens *et al.*, by modifying the sequence tethered to the nanoparticle, it is possible to tailor the sensor system to any hydrolytic enzyme of interest.[1] This could be particularly useful in the detection of papain-like proteases (PLpro) which Mescecar *et al.* have recently discovered plays an important role in the development of middle east respiratory syndrome (MERS), a virus related to severe acute respiratory syndrome (SARS).[3] As the first confirmed instance of MERS was confirmed in the United States in May 2014, a sensor system able to detect such an enzyme would be a valuable asset in medical diagnosis.[4]

If the sensor systems described in Chapter 5.0 are to be utilised for diagnostic testing in a medical environment, then it is critical to determine the limitation of sensitivity when serum samples are used. It is likely that the present iteration will not be sufficiently robust to tolerate the extent of non-specific protein adsorption on the nanoparticle surface. Utilisation of the PEGylated systems described in Chapter 4.0 will be an ideal starting point for this work.

Encapsulation of functionalised nanoparticles within a hydrogel matrix could provide an ideal means for transportation of a sensing device, particularly for air transportation where volumes of liquid may be prohibited or restricted. Additionally, encapsulation within a gel system may prevent spillage of colloidal material. Preliminary work undertaken during the course of this project (data not shown) confirms encapsulation within a gel has no effect upon the aggregation state of nanoparticles over a period of several weeks. In the case of the Fmoc-AAC-NH_2 system developed in Chapter 5.0, encapsulation within an Fmoc-AA-OH hydrogel would be ideal, as elastase would be easily able to digest the gel system.

Finally, work to substitute the fluorenyl moiety to an alternative structural component would be interesting. Although Fmoc was used as a spectrophotometric marker in 3.0 and replaced with Rhodamine B in 4.0, it would be interesting to determine whether changing the assembly driven actuator would have a measurable effect on sensitivity limits in a peptide-nanoparticle context. Potential alternatives may include naphthalene or phenylalanine derivaties which would still contribute towards the π-π interactions required for the formation of nanoparticle assemblies.

CHAPTER SEVEN – MATERIALS AND METHODS

7.1 General Methods

All chemicals and reagents, unless stated otherwise, were purchased from Sigma Aldrich Company Ltd. (Gillingham, U.K.) and used as received.

Proton (^{1}H) and carbon (^{13}C) NMR were recorded on a Bruker AV400 spectrometer, unless stated otherwise. The chemical shifts are quoted in parts per million (ppm) by taking tetramethylsilane as a reference ($\delta = 0$) but calibrated on the residual non-deuterated solvent signal. The coupling constants (J) are given in Hz. In cases where superimposition of the signals of two or more isomers occurred, the signals have been reported as multiplets.

Mass spectrometry was undertaken using a Finnigan LCQ duo ESI instrument. Samples were prepared in methanol.

Infra-red spectra were recorded on a Perkin Elmer Spectrum One FT IR Spectrometer.

Elemental analysis (CHN) was performed on a Perkin Elmer 2400 Series II CHNS/O analyser.

Melting points were measured using Griffin melting point apparatus and are uncorrected.

HPLC (manufactured by Dionex, CA) consisted of a P.680 HPLC pump joined to an ASI-100 automated sample injector with a Dionex UVD17OU UV-Vis detector. The column was an EC 250/4.6 Nucleosil 100-5 C18 column, with an internal diameter of 4.6 mm and a column length of 250 mm containing particles of 5 μm in diameter.

Flash column chromatography was performed using silica gel 60 (200-400 mesh). Thin layer chromatography carried out on aluminium backed F_{254} silica gel plates (Merck), and visualised under UV light (256 nm).

Solid phase peptide synthesis was performed on a Protein Technologies Tribute UV peptide synthesiser with UV monitoring.

Incubation of samples was undertaken using a Stuart S160D incubator.

Samples were centrifuged using an Eppendorf 5415R centrifuge.

The IUPAC names of some compounds were obtained using ChemDraw Ultra version 12.0.

7.2 Peptide Functionalisation of Planar Gold Surfaces (Chapter 3.0)

7.2.1 Peptide Synthesis on Gold-coated Cover Slips

Gold-coated glass cover slips (12 mm diameter, 5 nm Ti base layer and 15 nm Au thickness) (Kelvin Nanotechnology Ltd., Glasgow, U.K.) were cleaned prior to use by immersion in piranha solution, a 3:7 v:v mixture of 30 % hydrogen peroxide solution:concentrated sulphuric acid for 1 hour, followed by rinsing in copious amounts of deionised water and drying in an oven at 100 ℃ overnight. **WARNING: piranha solution reacts violently with organic compounds and should be handled with extreme caution**. Once dried, the surfaces were cleaned using oxygen plasma (Diener Electronic, Germany).

Stepwise peptide synthesis was undertaken with reference to Flitsch *et al*.[1] Carboxylic acid functionality was introduced to the surfaces by immersion overnight in an ethanolic solution of (±)-α-lipoic acid (10 mM). The cover slips were then washed in ethanol and dried in a nitrogen flow before activating with a solution of EDC·HCl (*N*-(3-dimethylaminopropyl)-*N*′-ethylcarbodiimide·HCl, 200

mM) and NHS (*N*-hydroxysuccinimde, 50 mM) in anhydrous *N,N*-dimethylformamide. After 2 hours, the cover slips were washed with dimethylsulfoxide (anhydrous), ethanol and dried with compressed air. A solution of *N*-Fmoc-1,4-butanediamine·HBr (100 mM) was prepared in *N,N*-dimethylformamide (anhydrous), and 1.1 eq. DIPEA added, into which the cover slips were immersed and allowed to react overnight. The cover slips were then washed and dried as before.

Deprotection of the terminal Fmoc moiety was achieved through immersion of the cover slips in a solution of 20:80 v:v piperidine:*N,N*-dimethylformamide (anhydrous) for 2 hours. Following further washing and drying, Fmoc-amino acid coupling was undertaken by immersing the cover slips overnight, at 37 ℃, in a *N,N*-dimethylformamide solution of Fmoc-A-OH (2 mM) (Bachem Ltd., St. Helens, U.K.), HBTU (2 mM) and DIPEA (2.6 mM). This process was then repeated in order to couple on a further Fmoc-A, resulting in a terminal Fmoc-A-A sequence.

For stepwise peptide synthesis utilising Boc-amino-PEG_6-amine (Polypure AS, Oslo, Norway) the above method was also followed; however, the terminal Boc group was removed by immersion in 50:50 v:v trifluoroacetic acid:dichloromethane for 2 hours before Fmoc-amino acid coupling was undertaken.

7.2.2 Enzyme Treatment of Gold-coated Cover Slips

Cover slips were incubated overnight, at 37 °C, in 2 mL of elastase (*Porcine Pancreas*, 1 mg mL^{-1}, 4.4 U/mg P; where 1 unit converts 1 μmole of *N*-succinyl-trialynyl *p*-nitroanilide per minute at 25 °C, 91 % protein) (Worthington Biochemical Corporation, New Jersey, U.S.A.) solution followed by washing with distilled water, dimethylsulfoxide and ethanol.

7.2.3 Time-of-Flight Secondary-Ion Mass Spectrometry (ToF-SIMS)

Instrumentation operated by Dr. David J. Scurr (Laboratory of Biophysics and Surface Analysis, School of Pharmacy, The University of Nottingham).

Secondary-ion mass spectrometric analysis was carried out using a ToF-SIMS IV time-of-flight instrument (ION-TOF, GmbH, Münster, Germany) equipped with a bismuth liquid metal ion gun and a single-stage reflectron analyzer. Typical operating conditions utilized a Bi_3^+ primary ion energy of 25 kV, a pulsed target current of approximately 1.0 pA, and post-acceleration of 10 kV. Imaging was performed by rastering the primary ion beam, using a raster area of 500 × 500 μm^2 for 256 × 256 pixels. All doses were kept well below the static limit, with a maximum dose of 1×10^{12} ions/cm^2 for both polarities combined. Acquisition of full raw data sets allowed for the retrospective construction of spectra from the imaged areas. Spectra were normalized to the total ion intensity for comparison between samples.

7.2.4 X-ray Photoelectron Spectroscopy (XPS)

Instrumentation operated by Emily F. Smith (X-ray Photoelectron Spectroscopy Facility, School of Chemistry, The University of Nottingham).

XPS was carried out on a Kratos Axis Ultra DLD instrument in Fixed Analyser Transmission (FAT) mode (Kratos Analytical Ltd., Manchester, U.K.) using a monochromated aluminium source, run at 210 W. A take off angle of 90 ° was used, and all samples were analysed with charge neutralizing electrons. The survey spectra were collected using a pass energy of 80 eV, and the C1s core level spectra were collected at a pass energy of 20 eV. The spectra were charge corrected to position the C-C within the C1s core level at a binding energy of 285.0 eV. Symmetrical sum Gaussian/Lorenzian 30 % peak shapes were used for all components and shifts presented relative to the C-C component at 285.0 eV.

7.2.5 Direct Laser Desorption/Ionisation Time-of-Flight Mass Spectrometry (LDI-ToF MS)

Mass analysis was performed using a Shimadzu Axima-CFR instrument (Kratos Analytical Ltd., Manchester, U.K.). A 337 nm nitrogen laser was used as the

desorption-ionization source, and all spectra were acquired with 20 kV accelerating voltage using reflectron positive ion mode. The extraction delay time was 100 ns, and 1000 laser shots were applied for each spectrum. All spectra were obtained by moving the laser beam to several different spots within a sample.

7.2.6 Contact Angle Geniometry (CAG)

Contact angle goniometry measurements were obtained using a Krűss contact angle DSA30B goniometer using a sessile drop methodology. Advancing contact angles were measured for both "left" and "right" contact angles, using 4-5 μL of Millipore purified water, 20 – 30 seconds after drop-surface contact.

7.2.7 Surface Coverage Analysis[2]

Fmoc deprotection and enzymatic hydrolysis yields were analyzed by HPLC. Surfaces were rinsed in 4 mL of a 50:50 v:v mixture of acetonitrile:water. The rinsing solution was kept and added to the Fmoc/piperidine or enzyme solution that the surface was in, and 1 mL of this solution was placed into a HPLC autosampler vial. A total of 100 μL was injected into the HPLC column at the start of each run and a buffer gradient run through the column; buffer A was 99.9 % water and 0.1 % trifluoroacetic acid, and buffer B was 99.9 % acetonitrile and 0.1 % trifluoroacetic acid. The mobile phase ramped from 20 – 80 % acetonitrile over 35 minutes at a flow rate of 1 mL min^{-1}. Fmoc-terminated moieties were detected at a wavelength of 300 nm.

7.2.8 Thiol Displacement

Method based on published work by Viswanadham *et al.*[3] and Graham *et al.*[4] Peptide functionalised gold-coated glass cover slips were immersed in a 2 mL solution of dithiothreitol (DTT, final concentration 12 mM) in 0.3 M PBS. After 18 hours at room temperature, with intermittent shaking, the cover slips were removed and the resulting solution analysed. 50 μL was injected into the HPLC column and a buffer gradient run through the column; buffer A was 99.9 % water

and 0.1 % trifluoroacetic acid, and buffer B was 99.9 % acetonitrile and 0.1 % trifluoroacetic acid. The mobile phase ramped from 20 – 80 % acetonitrile over 35 minutes at a flow rate of 1 mL min^{-1}.

7.3 Peptide Functionalisation of Nanostructured Gold Surfaces (Chapter 4.0)

7.3.1 Peptide Synthesis on Klarite, Nanohole and Nanorod Array Substrates

Klarite substrates (Gold-coated nanostructured silicon. 10 × 6 × 0.7 mm in dimension with a 4 × 4 mm active area) (Renishaw Diagnostics, Glasgow, U.K.) were cleaned prior to use by immersion in piranha solution, a 3:7 v:v mixture of 30 % hydrogen peroxide solution:concentrated sulphuric acid for 1 hour, followed by rinsing in copious amounts of deionised water and drying in an oven at 100 ℃ overnight. **WARNING: piranha solution reacts violently with organic compounds and should be handled with extreme caution**. Once dried, the surfaces were cleaned using oxygen plasma (Diener Electronic, Germany).

Nanohole and nanorod array substrates were cleaned prior to use by washing with copious ethanol and drying with compressed nitrogen.

Stepwise peptide synthesis and enzymatic treatment were achieved on all substrates following the protocols outlined in sections 7.2.1 and 7.2.2 respectively.

7.3.2 Direct Laser Desorption/Ionisation Time-of-Flight Mass Spectrometry (LDI-ToF MS)

Mass analysis performed as per section 7.2.5. Care was taken to target the laser towards the flat handling regions of the Klarite substrate, thus ensuring the differing surface heights of the nanostructured region had no effect upon the signals observed.

7.3.3 Addition of Raman Reporter Molecules

7.3.3.1 Addition of Raman Reporter After Stepwise Peptide Synthesis

Upon completion of the stepwise peptide synthesis detailed in 7.2.1, deprotection of the terminal Fmoc moiety was achieved through immersion of the cover slips in a solution of 20:80 v:v piperidine:*N,N*-dimethylformamide (anhydrous) for 2 hours. Following further washing and drying, coupling of the Raman reporter molecule was undertaken by immersing the SERS substrates overnight, at 37 ℃, in a *N,N*-dimethylformamide solution of Rhodamine B (2 mM), HBTU (2 mM) and DIPEA (2.6 mM).

7.3.3.2 Addition of Spacer Units

For stepwise peptide synthesis utilising Boc-amino-PEG_6-diglycolic acid (Polypure AS, Oslo, Norway) the stepwise synthesis method detailed in 7.2.1 was followed; however, the terminal Boc group was removed by immersion in 50:50 v:v trifluoroacetic acid:dichloromethane for 2 hours before coupling of the Raman reporter of interest was undertaken.

7.3.4 Preparation of Klarite Surfaces with Mixed Monolayers

Mixed monolayer surfaces were prepared to give an overall surface concentration of 10 mM.

Surfaces were prepared as in 7.2.1; functionality was introduced by immersion overnight in an ethanolic solution of (±)-α-lipoic acid (5 mM) and PEG_6-thiol (5 mM) (Polypure AS, Oslo, Norway) for 1:1 surfaces. 1:5 surfaces were prepared using (±)-α-lipoic acid (1.67 mM) and PEG_6-thiol (8.33 mM). Subsequent stepwise synthesis on these surfaces was carried out as detailed previously.

7.3.5 Raman Mapping

Raman mapping was carried out using confocal WITec Alpha300 R instrumentation (WITec, Ulm, Germany) and a 633 nm excitation laser (Research Electro-Optics,

Colorado, U.S.A; full power = 13 mW). This instrumental set-up allowed mapping of approximately 25 × 25 μm areas. The laser power values were measured using a handheld LaserCheck power meter (Coherent, California, U.S.A).

The approximate unfocussed power of the 633 nm excitation laser was 1 mW (7.7 % of total power). The parameters were set as follows: 0.005 s integration time, 100 × objective (Olympus MPlan, NA = 0.9). Two maps were taken from duplicate separate, identically prepared substrates at each etch time. WITec project 2.02 software was used for further data processing.

7.4 Design and Preparation of a Colorimetric Elastase Sensor (Chapter 5.0)

7.4.1 Solid Phase Peptide Synthesis for Proof of Concept Work

Preparation of (9*H*-fluoren-9-yl)methyl(1-((1-((1-amino-3-mercapto-1-oxopropan-2-yl)amino)-1-oxopropan-2-yl)amino)-1-oxopropan-2-yl)carbamate (5.2)

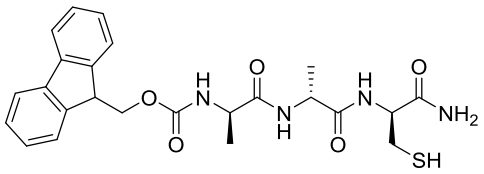

5.2

Rink amide 4-methylbenzhydrylamine resin (0.5 g, 1 mmol/g loading, 1 eq.) was swollen in *N,N*–dimethylformamide (10 mL) for 20 minutes before the resin was treated with 20:80 v:v piperidine:*N,N*-dimethylformamide for 30 minutes. Once deprotection was complete, the resin was washed thoroughly with *N,N*-dimethylformamide prior to addition of Fmoc-C(Trt)-OH (0.439 g, 0.75 mmol, 3 eq.), HBTU (0.285 g, 0.75 mmol, 3 eq.) and DIPEA (0.262 mL, 1.5 mmol, 6 eq.). The reaction vessels were then shaken for 2.5 hours before the resin was filtered and washed with *N,N* –dimethylformamide.

Loading of the resin with Fmoc-C(Trt)-OH was measured by taking 5 mg of resin and immersing in a 0.5 mL solution of 20:80 v:v piperidine:*N,N*-dimethylformamide for 3 minutes. *N,N*–dimethylformamide was added to dilute the solution to 50 mL. Absorbance of the Fmoc-piperidine adduct was measured at 301 nm, and loading calculated using the following equation:

$$\frac{A_{301} \times Volume\ (mL)}{7800 \times Weight\ (g)} = Loading\ (mmol/g)$$

$$\frac{0.498 \times 50}{7800 \times 0.005} = 0.638\ (mmol/g)$$

500 mg of the pre-loaded resin was weighed into a reaction vessel and loaded into the synthesiser. The reaction scale for 500 mg of resin was calculated as follows:

$$0.638\ mmol/g \times 0.5\ g = 0.32\ mmol$$

Fmoc-A-OH (0.233 g, 0.75 mmol, 2.3 eq.) was weighed into cartridges which each contained HCTU (0.310 g, 1.6 mmol, 5 eq.). The cartridges were then loaded into the synthesiser. The programmes used to perform the synthesis were as follows; swelling of the resin with dichloromethane, UV-Vis extended deprotection of the terminal Fmoc with 20:80 v:v piperidine:*N,N*-dimethylformamide and standard amino acid coupling. Once synthesis was complete, the reaction vessel was removed from the synthesiser. The sequence was cleaved from the resin and the trityl protecting group removed from the cysteine residue by immersion of the resin in a stirred solution of 95:5 trifluoroacetic acid:water for 3 hours.

Upon completion of cleavage, the cleavage mixture was filtered into chilled diethyl ether (20 mL). Once the peptide had precipitated in the ether the mixture was centrifuged for 1 hour at 5500 r.p.m to form a pellet, the supernatant was discarded and the process was repeated. The resulting peptide was concentrated *in vacuo* to give 222 mg of crude product; purification by RP-HPLC gave 15 mg pure product.

^{1}H NMR (400 MHz; d_3-MeCN) δ = 1.42 (3H, s, CH_3), 1.48 (3H, s, CH_3), 2.78-2.89 (2H, m, CH_2), 4.30-4.67 (6H, m. 4 × CH and 1 × CH_2), 6.51 (2H, bs, NH_2), 7.29 (2H, dd, J = 1.4, 7.3 Hz, ArH), 7.39-7.50 (4H, m, ArH), 7.74 (2H, m, J = 1.2, 7.4 Hz, ArH); (found found M + Na^+ 507.02; $C_{24}H_{28}N_4O_5S$ + Na^+ requires 507.18).

7.4.2 Stabilisation of Colloidal Gold Nanoparticles[9]

Colloidal gold nanoparticles (10 nm, 100 mL) (BBI Solutions, Cardiff, U.K.) were stirred with dipotassium bis(*p*-sulfonatophenyl)phenylphosphine dihydrate (15 mg) for 18 hours at room temperature. NaCl (5.8 g) was added to the solution in order to cause a colour change from burgundy red to violet blue. The reaction mixture was then centrifuged for 1.5 hours at 2750 r.p.m. and the supernatant removed. The pellet was resuspended in an aqueous solution of dipotassium bis(*p*-sulfonatophenyl)phenylphosphine dihydrate (25 mg in 100 mL) and vortexed.

MeOH (50 mL) was added to the solution in order to cause a colour change from burgundy red to violet blue. The reaction mixture was again centrifuged for 1.5 hours at 2750 r.p.m. and the supernatant removed. The pellet was resuspended in an aqueous solution of dipotassium bis(*p*-sulfonatophenyl)phenylphosphine dihydrate (25 mg in 100 mL) and vortexed. Sample stored at 4 ^{o}C.

7.4.3 Synthesis of Colloidal Gold Nanoparticles

A three necked flask was cleaned thoroughly using Aqua Regia. After 3 hours, the flask was rinsed with water (deionised, 4 × 500 mL).

Water (deionised, 500 mL) was added to the flask, followed by sodium tetrachloroaurate (III) dihydrate (50 mg) pre-dissolved in water (deionised, 10 mL). The solution was stirred using a glass rod and brought to the boil using a Bunsen burner. The necks of the flask were covered with aluminium foil. Once boiling, citric acid trisodium salt (anhydrous, 75 mg) in water (deionised, 10 mL) was added. The solution was maintained at boiling point for 15 minutes and

thereafter, with continued stirring, the solution was allowed to cool to room temperature. Once at room temperature the colloidal nanoparticle solution was concentrated by centrifugation at 6000 r.p.m for 1.5 hours.

7.4.4 Stepwise SPPS on Gold Nanoparticles

7.4.4.1 Stepwise SPPS following modified version of Stevens et al.[10]

0.65 mM solution of (±)-α-lipoic acid was prepared in *N,N*-dimethylformamide; addition of 0.5 mL to 5 mL of gold nanoparticles stabilised as per 7.4.2 to give a final concentration of 50 μM for 6.5 mL.

Sodium phosphate buffer (pH 8, 130 mM) was prepared; addition of 0.5 mL gold nanoparticles functionalised by (±)-α-lipoic acid to give a final concentration of 10 mM for 6.5 mL.

Sodium chloride (1.3 M) was prepared; addition of 0.5 mL to gold nanoparticles functionalised by (±)-α-lipoic acid and containing sodium phosphate to give a final concentration of 10 mM for 6.5 mL. Addition of salt induced irreversible aggregation.

7.4.4.1 Stepwise SPPS following modified version of Current Protocols in Nucleic Acids[11]

$$Required\ number\ of\ moles\ of\ lipoic\ acid = 4\pi r^2 \times Cn \times Sc \times V$$

$$= 4\pi(5\ nm)^2 \times 2.48\ nm \times (6.02 \times 10^{23}\ mol^{-1}) \times 12.6\ \text{ρmol cm}^{-2} \times 0.005$$

Thus, 0.295 nmoles of lipoic acid were required. A solution containing 0.762 mg lipoic acid in 12.5 mL *N,N*-dimethylformamide was prepared and 1 μL added to 5 mL of gold nanoparticles stabilised as per 7.4.2. Nanoparticles functionalised with lipoic remained stable at room temperature for a period of weeks.

Attempts to activate the lipoic acid using *N*-hydroxysuccinimide were consistently unsuccessful and lead to irreversible aggregation.

7.4.5 Preparation of Peptide-Nanoparticle Conjugates[10]

Nanoparticles stabilised in section 7.4.2 were incubated at room temperature overnight with 50 μM of peptide (structures **5.2**, **5.11** or **5.22** as required) in *N*,*N*-dimethylformamide with 10 mM sodium phosphate (pH 8) and 100 mM NaCl, to yield peptide nanoparticle conjugates. Excess peptide was removed by centrifugation and removal of supernatant prior to resuspension of the nanoparticles to initial volume with phosphate buffer (pH 8), 0.05 % w:v Bovine Serum Albumin.

7.4.6 Enzymatic Hydrolysis of Peptide-Nanoparticle Conjugates[10]

Hydrolysis reactions were carried out in disposable 10 mm pathlength polystyrene cuvettes. All reactions were undertaken in duplicate at 37 °C. Elastase was added to the peptide-nanoparticle conjugates in the required concentration, and spectral measurements were taken at appropriate time intervals. UV-Vis spectra were recorded on a Jasco V660 spectrophotometer over the range 200-800 nm with 1 nm resolution and background correction.

7.4.7 Synthesis of an Elastase Specific Peptide Sequence

Preparation of 2,5-dioxopyrrolidin-1-yl 5-(1,2-dithiolan-3-yl)pentanoate (5.6)[5], **Scheme 5.2**

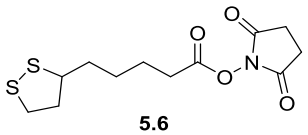

5.6

EDC·HCl (1.84 g, 9.6 mmol, 1.2 eq.) was dissolved in dichloromethane (anhydrous, 40 mL), and DIPEA (anhydrous, 1.7 mL, 9.6 mmol, 1.2 eq.) added. The reaction mixture was then stirred for 10 minutes. To this, *N*-hydroxysuccinimide (1.29 g, 11.2 mmol, 1.4 eq.) was added and the reaction mixture placed in an ice bath. (±)-α-lipoic acid **5.5** (1.64 g, 8.0 mmol, 1 eq.) pre-dissolved in dichloromethane (anhydrous, 10 mL) was then added drop-wise over 20 minutes. The resulting

mixture was stirred overnight at room temperature. The solution was washed with HCl (5 % v:v, 50 mL × 2) and distilled water (50 mL) before drying the combined organic layer over sodium sulfate and refrigerating for 2 hours. Sodium sulfate was removed by filtration and the sample concentrated *in vacuo* to yield a yellow solid. The sample was purified by flash column chromatography, using dichloromethane with 5 % methanol, to give 1.73 g of sweet smelling product in a 75.7 % yield.

^{1}H NMR (400 MHz; DMSO) δ = 3.58-3.63 (1H, m, C*H*H), 3.31 (1H, s, C*H*), 3.11-3.18 (2H, m, CH_2), 2.81 (4H, s, succinimidyl CH_2), 2.68 (2H, t, *J* = 6.53 Hz, CH_2), 2.37-2.45 (1H, m, C*H*H), 1.83-1.92 (1H, m, C*H*H), 1.46-1.69 (6H, m, CH_2); ^{13}C NMR (100 MHz; DMSO) δ = 170.1 (C), 168.8 (C), 55.9 (CH_2), 39.3 (CH), 38.1 (CH_2), 33.9 (CH_2), 30.6 (CH_2), 30.0 (CH_2), 27.6 (CH_2), 25.4 (CH_2), 24.0 (CH_2); (found C 47.32 %, H 5.65 %, N 4.60 % and S 20.79 %; $C_{12}H_{17}NO_4S_2$ requires C 47.5 %, H 5.65 %, N 4.62 %, S 21.14 %); (found M^+ 302.92; $C_{12}H_{17}NO_4S_2^+$ requires 303.06).

Preparation of (9*H*-fluoren-9-yl)methyl (4-(5-(1,2-dithiolan-3-yl)pentanamido)-butyl)carbamate (5.7)[6-7]**, Scheme 5.2**

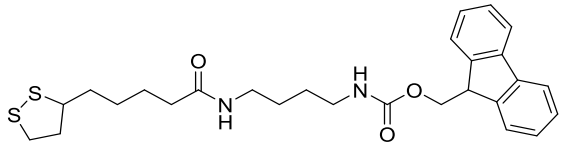

5.7

N-Fmoc-1,4-butanediamine·HBr (0.65 g, 1.65 mmol, 1 eq.) was dissolved in dichloromethane (anhydrous, 20 mL) with *N,N*-dimethylformamide (anhydrous, 1 mL) to aid dissolution. DIPEA (0.345 mL, 1.97 mmol, 1.2 eq.) was added and the reaction mixture stirred for 5 minutes. 2,5-dioxopyrrolidin-1-yl 5-(1,2-dithiolan-3-yl)pentanoate **5.6** (0.5 g, 1.65 mmol, 1 eq.) was added and the mixture was stirred in the dark overnight. Distilled water (20 mL) was added and the reaction mixture was again stirred overnight. The sample was extracted with dichloromethane (3 × 10 mL) and washed repeatedly with water and brine. The extracted organics were

dried over sodium sulfate, concentrated *in vacuo* and triturated overnight with diethyl ether to afford 1.85 g purified product, with a 42.4 % yield.

^{1}H NMR (400 MHz; DMSO) δ = 7.60 (2H, d, *J* = 7.5 Hz, Ar*H*), 7.59 (2H, d, 7.4 Hz, Ar*H*), 7.39 (2H, dd, *J* = 7.4, 7.4 Hz, Ar*H*), 7.30 (2H, dd, *J* = 7.5, 7.4 Hz, Ar*H*), 5.62 (1H, bs, N*H*), 4.92 (1H, bs, N*H*), 4.40 (2H, d, *J* = 6.8 Hz, CH_2), 4.21 (1H, t, *J* = 6.8 Hz, C*H*), 3.52-3.59 (1H, m, C*H*), 3.00-3.28 (6H, m, CH_2), 2.39-2.47 (1H, m, C*H*H), 2.16 (2H, t, *J* = 7.4 Hz, CH_2), 1.84-1.93 (1H, m, C*H*H), 1.38-1.75 (10H, m, CH_2); (found C 64.69 %, H 6.87 %, N 5.99 %, S 12.79 %; $C_{27}H_{34}N_2O_3S_2$ requires C 65.03 %, H 6.87 %, N 5.62 %, S 12.86 %); (found M + Na^+ 521.20; $C_{27}H_{34}N_2O_3S_2$ + Na^+ requires 521.69).

Preparation of *N*-(4-aminobutyl)-5-(1,2-dithiolan-3-yl)pentanamide (5.4), Scheme 5.2

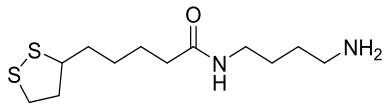

5.4

(9*H*-fluoren-9-yl)methyl (4-(5-(1,2-dithiolan-3-yl)pentanamido)butyl)carbamate **5.7** (1.85 g, 3.71 mmol, 1 eq.) was dissolved in *N,N*-dimethylformamide (anhydrous, 8 mL). Piperidine (2 mL, 20 mmol, 5 eq.) was added to the resulting yellow solution and stirred for 1 hour with continuous heating to 70 °C. The sample was concentrated *in vacuo,* before it was taken up in distilled water (80 mL), acidified to pH 3 with HCl (conc.) and extracted with diethyl ether (3 × 80 mL). Throughout the extraction process, a white precipitate was present that would not go into solution and was filtered and dried before continuing. The aqueous extract was then basified (pH 11) using NaOH (5 M) and extracted further with dichloromethane (80 mL). The combined organic layer was then dried over sodium sulfate before concentrating *in vacuo*. ^{1}H NMR spectroscopy indicated a mixture of products within the organic extracts which were the same as the precipitate material; poor solubility prevented chromatographic purification. The concentrated extracts and precipitate were combined and upon attempted recrystallisation with ethanol, the

resulting opaque suspension was filtered to afford 14.8 mg of crude material, with ^{1}H NMR spectroscopy indicating the same mixture as before. The crude material was used as such for the next synthetic step.

Preparation of (9*H*-fluoren-9-yl)methyl (1-((1-((4-(5-(1,2-dithiolan-3-yl)pentanamido)butyl)amino)-1-oxopropan-2-yl)amino)-1-oxopropan-2-yl)carbamate (5.3), Scheme 5.2

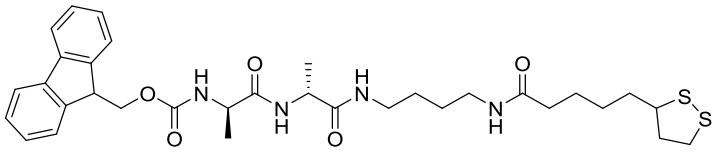

5.3

N-Fmoc-L-dialanine (22 mg, 0.05 mmol, 1 eq.) was dissolved in *N,N*-dimethylformamide (anhydrous, 100 µL). To this, HBTU (22 mg, 0.06 mmol, 1.1 eq.) and DIPEA (22 µL, 0.13 mmol, 2.5 eq.) were added and the reaction mixture allowed to stir for 1 h. A solution of *N*-(4-aminobutyl)-5-(1,2-dithiolan-3-yl)pentanamide **5.4** (14.8 mg, 0.05 mmol, 1 eq.) in *N,N*-dimethylformamide (anhydrous, 100 µL) was added and the mixture was stirred overnight. The solution was washed with HCl (5 % v:v, 1 mL × 2) and distilled water (1 mL) before the sample was concentrated *in vacuo*. The sample was purified by flash column chromatography, using dichloromethane with 5 % methanol, to give 1.6 mg of product in a 5 % yield.

Found M + Na^+ 662.80; $C_{33}H_{44}N_4O_5S_2$ + Na^+ requires 663.28.

Preparation of *N*-(4-aminobutyl)-5-(1,2-dithiolan-3-yl)pentanamide (5.4), Scheme 5.3

2,5-dioxopyrrolidin-1-yl 5-(1,2-dithiolan-3-yl)pentanoate **5.6** (1 g, 4.84 mmol, 1 eq.) was dissolved in *N,N*-dimethylformamide (anhydrous, 10 mL) and DIPEA (2.19 mL, 12.1 mmol, 2.5 eq.) added. The system was then stirred for 1 hour, at room temperature. To this, 1,4-diaminobutane (1.46 mL, 14.52 mmol, 3 eq.)

predissolved in *N,N*-dimethylformamide (anhydrous, 30 mL) was added. The resulting mixture was stirred overnight, at 100 °C.

The sample was concentrated *in vacuo* yielding a yellow slurry-like material. The sample was successfully taken up in dichloromethane (20 mL) and washed with sodium bicarbonate (saturated solution, 20 mL), citric acid (saturated solution, 20 mL) and brine (20 mL). The combined organic layer was dried over magnesium sulfate. After removal of the magnesium sulfate, the sample was concentrated *in vacuo* once more, yielding an oily residue. The product was then purified by flash column chromatography, using dichloromethane with 5 % methanol, to give 617 mg of material. Analysis confirmed the reaction was unsuccessful, due to formation of *N,N'*-(butane-1,4-diyl)bis(5-(1,2-dithiolan-3-yl)pentanamide), **5.8**.

^{1}H NMR (400 MHz; DMSO, major component) δ =1.41-1.62 (20H, m, CH_2), 2.09-2.22 (4H, m, CH_2), 3.05-3.31 (10H, 2 × CH and 4 × CH_2).

Preparation of 5-(1,2-dithiolan-3-yl)-N-(4-hydroxybutyl)pentanamide (5.9), Scheme 5.4

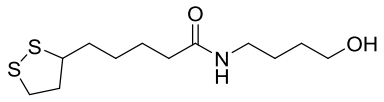

5.9

2,5-dioxopyrrolidin-1-yl 5-(1,2-dithiolan-3-yl)pentanoate **5.6** (1 g, 4.84 mmol, 1 eq.) was dissolved in *N,N*-dimethylformamide (anhydrous, 10 mL) and DIPEA (2.19 mL, 12.1 mmol, 2.5 eq.) added. The system was then stirred for 1 hour, at room temperature. To this, 6-aminobutan-1-ol (0.567 g, 4.84 mmol, 1 eq.) predissolved in *N,N*-dimethylformamide (anhydrous, 10 mL) was added. The resulting mixture was stirred overnight.

The sample was concentrated *in vacuo* and taken up in dichloromethane (20 mL) and washed with sodium bicarbonate (saturated solution, 20 mL), citric acid (saturated solution, 20 mL) and brine (20 mL). The combined organic layer was

dried over magnesium sulfate to yield a brown oil which solidified overnight. Attempts to purify using column chromatography were unsuccessful so trituration of the solid in hexane was performed overnight. The resulting solution contained a small quantity of suspended white solid which was recovered by filtration to give 11.54 mg of product, in 0.9 % yield.

Found M + Na^+ 300.41; $C_{12}H_{23}NO_2S_2$ + Na^+ requires 300.43.

Preparation of (9H-fluoren-9-yl)methyl (1-((1-((1,6-diamino-1-oxohexan-2-yl)amino)-1-oxopropan-2-yl)amino)-1-oxopropan-2-yl)carbamate (5.10)

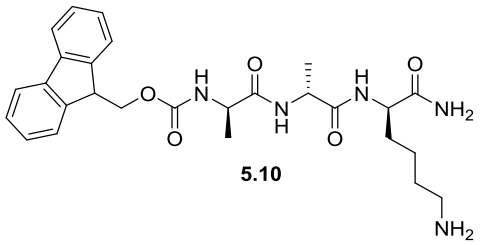

5.10

Rink amide 4-methylbenzhydrylamine resin (0.5 g, 1 mmol/g loading, 1 eq.) was swollen in *N,N*–dimethylformamide (10 mL) for 20 minutes before the resin was treated with 20:80 v:v piperidine:*N,N*-dimethylformamide for 30 minutes. Once deprotection was complete, the resin was washed thoroughly with *N,N*-dimethylformamide prior to addition of Fmoc-K(Boc)-OH (0.351 g, 0.75 mmol, 3 eq.), HBTU (0.285 g, 0.75 mmol, 3 eq.) and DIPEA (0.262 mL, 1.5 mmol, 6 eq.). The reaction vessels were then shaken for 2.5 hours before the resin was filtered and washed with *N,N* –dimethylformamide.

Loading of the resin with Fmoc-K(Boc)-OH was measured by taking 5 mg of resin and immersing in a 0.5 mL solution of 20:80 v:v piperidine:*N,N*-dimethylformamide for 3 minutes. *N,N*–dimethylformamide was added to dilute the solution to 50 mL. Absorbance of the Fmoc-piperidine adduct was measured at 301 nm, and loading calculated as per 7.4.1.

The pre-loaded resin was weighed into a reaction vessel and loaded into the synthesiser. Fmoc-A-OH (0.233 g, 0.75 mmol, 2.5 eq.) was weighed into cartridges which each contained HCTU (0.310 g, 1.6 mmol, 5 eq.). The cartridges were then loaded into the synthesiser. The programmes used to perform the synthesis were as follows; swelling of the resin with dichloromethane, UV-Vis extended deprotection of the terminal Fmoc with 20:80 v:v piperidine:*N,N*-dimethylformamide and standard amino acid coupling. Once synthesis was complete, the reaction vessel was removed from the synthesiser. The sequence was cleaved from the resin and the trityl protecting group removed from the cysteine residue by immersion of the resin in a stirred solution of 95:5 trifluoroacetic acid:water for 3 hours.

Upon completion of cleavage, the cleavage mixture was filtered into chilled diethyl ether (20 mL). Once the peptide had precipitated in the ether the mixture was centrifuged for 1 hour at 5500 r.p.m to form a pellet, the supernatant was discarded and the process was repeated. The resulting peptide was concentrated *in vacuo* to give 150 mg of product; HPLC analysis determined 90 % purity.

Found M + Na^+ 532.68; $C_{27}H_{35}N_5O_5$ + Na^+ requires 532.27.

Preparation of (9H-fluoren-9-yl)methyl (1-((1-((6-(5-(1,2-dithiolan-3-yl)pentanamido)-1-amino-1-oxohexan-2-yl)amino)-1-oxopropan-2-yl)amino)-1-oxopropan-2-yl)carbamate (5.11)

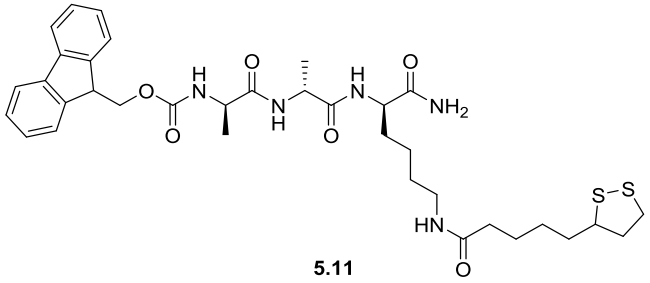

5.11

5.10 (100 mg, 0.161mmol, 1 eq.) was dissolved in dichloromethane (anhydrous, 3 mL) before DIPEA (62 µL, 0.354 mmol, 2.2 eq.) was added and the reaction mixture

stirred for 5 minutes. **5.6** (49 mg, 0.161 mmol, 1 eq.) was added and the mixture was stirred in the dark overnight.

Distilled water (3 mL) was added and the reaction mixture was again stirred overnight. The sample was extracted with dichloromethane (3 × 2 mL) and washed repeatedly with water and brine. The extracted organics were dried over sodium sulfate, concentrated *in vacuo* and triturated overnight with diethyl ether to afford 26 mg purified product, with a 23 % yield.

Found M + Na^+ 720.27; $C_{35}H_{47}N_5O_6S_2$ + Na^+ requires 720.29.

Preparation of (9*H*-fluoren-9-yl)methyl (1-((1-((4-((2-amino-2-oxoethyl)amino)-4-oxobutyl)amino)-1-oxopropan-2-yl)amino)-1-oxopropan-2-yl)carbamate (5.12), Scheme 5.5

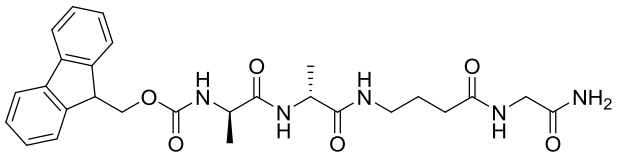

5.12

Rink amide 4-methylbenzhydrylamine resin (0.5 g, 1 mmol/g loading, 1 eq.) was swollen in *N,N*–dimethylformamide (10 mL) for 20 minutes before the resin was treated with 20:80 v:v piperidine:*N,N*-dimethylformamide for 30 minutes. Once deprotection was complete, the resin was washed thoroughly with *N,N*-dimethylformamide prior to addition of Fmoc-G-OH (0.222 g, 0.75 mmol, 3 eq.), HBTU (0.285 g, 0.75 mmol, 3 eq.) and DIPEA (0.262 mL, 1.5 mmol, 6 eq.). The reaction vessels were then shaken for 2.5 hours before the resin was filtered and washed with *N,N* –dimethylformamide.

Loading of the resin with Fmoc-G-OH was measured by taking 5 mg of resin and immersing in a 0.5 mL solution of 20:80 v:v piperidine:*N,N*-dimethylformamide for 3 minutes. *N,N*–dimethylformamide was added to dilute the solution to 50 mL.

Absorbance of the Fmoc-piperidine adduct was measured at 301 nm, and loading calculated as per 7.4.1.

500 mg of the pre-loaded resin was weighed into a reaction vessel and loaded into the synthesiser. Fmoc-A-OH (0.233 g, 0.75 mmol, 2.5 eq.) and Fmoc-GABA-OH (0.244 g, 0.75 mmol, 2.5 eq.) were weighed into cartridges which each contained HCTU (0.310 g, 1.6 mmol, 5 eq.). The cartridges were then loaded into the synthesiser. The programmes used to perform the synthesis were as follows; swelling of the resin with dichloromethane, UV-Vis extended deprotection of the terminal Fmoc with 20:80 v:v piperidine:*N,N*-dimethylformamide and standard amino acid coupling. Once synthesis was complete, the reaction vessel was removed from the synthesiser. The sequence was cleaved from the resin and the trityl protecting group removed from the cysteine residue by immersion of the resin in a stirred solution of 95:5 trifluoroacetic acid:water for 3 hours.

Upon completion of cleavage, the cleavage mixture was filtered into chilled diethyl ether (20 mL). Once the peptide had precipitated in the ether the mixture was centrifuged for 1 hour at 5500 r.p.m to form a pellet, the supernatant was discarded and the process was repeated. The resulting peptide was concentrated *in vacuo* to give 325 mg of product; HPLC analysis determined 100 % purity.

^{1}H NMR (400 MHz; $CDCl_3$) δ = 7.77 (2H, d, *J* = 7.6 Hz, Ar*H*), 7.54 (2H, d, *J* = 7.5 Hz, Ar*H*), 7.42 (2H, dd, *J* = 7.5, 7.4 Hz, Ar*H*), 7.33 (2H, dd, *J* = 7.6, 7.4 Hz, Ar*H*), 4.45-4.50 (2H, m, CH_2), 4.36 (1H, q, *J* = 7.1 Hz, C*H*), 4.19 (1H, t, *J* = 6.4 Hz, C*H*), 4.08-4.14 (1H, m, C*H*), 3.98 (2H, d, *J* = 4.7 Hz, CH_2), 3.25-3.39 (2H, m, CH_2), 2.28-2.40 (2H, m, CH_2), 1.87-2.06 (2H, m, CH_2), 1.39 (3H, s, CH_3), 1.37 (2H, s, CH_3); ^{13}C NMR (100 MHz; DMSO) δ = 174.5 (C), 159.4 (C), 159.0 (C), 157.0 (C), 143.3 (C), 141.3 (C), 127.9 (CH), 127.1 (CH), 124.7 (CH), 120.1 (CH), 116.1 (C), 67.5 (CH_2), 51.5 (CH), 49.9 (CH), 46.9 (CH), 42.7 (CH_2), 38.4 (CH_2),38.0 (CH_2),32.0 (CH_2),17.5 (CH_3), 16.8 (CH_3); (found M + Na^+ 546.27; $C_{27}H_{33}N_5O_6$ + Na^+ requires 546.23).

Preparation of (9*H*-fluoren-9-yl)methyl (1-((1-((4-((aminomethyl)amino)-4-oxobutyl)amino)-1-oxopropan-2-yl)amino)-1-oxopropan-2-yl)carbamate (5.14), Scheme 5.5

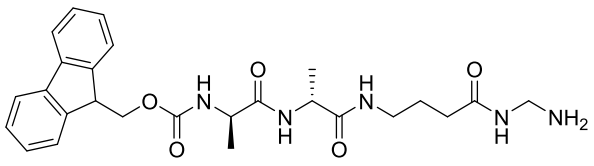

5.14

5.12 (0.149 mmol, 0.078 g, 1eq.) and benzyltrimethylammonium tribromide (1.49 mmol, 0.580 g, 10 eq.) were added to a solution of NaOH (8.94 mmol, 0.358 g, 60 eq.) in 1.5:1 v:v acetonitrile:water (12.75 mL) and the mixture was stirred for 12 h. During the period of stirring, benzyltrimethylammonium tribromide (orange red) soon dissolved in the alkaline solution and the mixture turned to light yellow. The resulting two phase solution was saturated with NaCI and extracted with ethyl acetate (4 × 10 ml). The collected organic layers were dried with magnesium sulfate and concentrated *in vacuo*. The resulting mixture could not be separated by chromatography; a single broad spot was observed by thin layer chromatography using various solvent systems. Mass spectral analysis indicated that the reaction mixture contained bromination products of **5.14**.

Found Br-M + Na^+ 596.32 and 598.24; Br_2-M + Na^+ 674.06, 676.06 and 678.05.

Preparation of Diethyl 2-(Hex-5-enyl)malonate (5.16)[8], Scheme 5.6

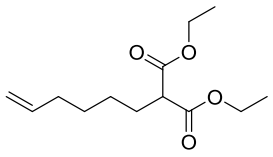

5.16

Sodium hydride was rinsed to remove traces of mineral oil and a suspension (2.80 g, 70 mmol, 1 eq.) in tetrahydrofuran (anhydrous, 170 mL) was prepared. Diethyl malonate (10.62 mL, 70 mmol, 1 eq.) was added, dropwise, to the stirred sodium hydride suspension at 0 °C. The resulting mixture was stirred at 0 °C for 15

minutes and at room temperature for 30 minutes before cooling again to 0 °C. 6-bromo-1-hexene **5.15** (8.50 mL, 63.6 mmol, 0.9 eq.) in tetrahydrofuran (anhydrous, 80 mL) was added and the reaction mixture heated at reflux for 18 hours. Once cooled to room temperature, water (25 mL) was added to quench the reaction. The reaction mixture was washed with ethyl acetate (100 mL) and water (200 mL); the aqueous layer was extracted with ethyl acetate (2 × 100 mL). The combined organic extracts were washed with brine and dried over magnesium sulfate before concentrating *in vacuo* to afford 13.4 g of purified product, with 87 % yield.

^{1}H NMR (400 MHz; $CDCl_3$) δ = 5.77 (1H, tdd, *J* = 16.9, 10.1, 6.7 Hz, CH_2=C*H*), 4.89-4.99 (2H, m, CH_2=CH), 4.18 (4H, q, *J* =7.1 Hz, OC$H_2$$CH_3$), 3.30 (1H, t, *J* =7.6 Hz, CH_2C*H*), 2.00-2.06 (2H, m, CH_2), 1.85-1.91 (2H, m, CH_2), 1.30-1.42 (4H, m, CH_2), 1.28 (6H, t, *J* =7.1 Hz, OCH_2CH_3); ^{13}C NMR (100 MHz; $CDCl_3$) δ = 169.5 (C), 138.5 (CH), 114.5 (CH_2), 61.2 (CH_2), 51,9 (CH), 33.3 (CH_2), 28.5 (CH_2), 28.4 (CH_2), 26.7 (CH_2), 14.0 (CH_3); (found M^+ 242.94; $C_{13}H_{22}O_4^+$ requires 242.152).

Preparation of 2-(Hex-5-enyl)propane-1,3-diol (5.17)[8], Scheme 5.6

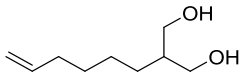

5.17

5.16 (12.8 g**,** 52.80 mmol, 1 eq.) was dissolved in tetrahydrofuran (anhydrous, 80 mL) and added to a stirred suspension of lithium aluminium hydride (4.0 g, 106 mmol, 2 eq.) in tetrahydrofuran (anhydrous, 220 mL), at 0 °C. The resulting mixture was stirred at 0 °C for 30 minutes and then at room temperature for 3 hours before diluting with tetrahydrofuran (anhydrous, 150 mL) and cooling once again to 0 °C. Aliquots of water (3.8 mL), sodium hydroxide (aqueous, 5.7 mL, 2 M) and water (3.8 mL) were added to the reaction vessel and the resulting solution stirred vigorously overnight. The resulting mixture was filtered through Celite and washed with ethyl acetate before concentrating *in vacuo* to give 5.80 g of the title compound in a 72 % yield.

^{1}H NMR (400 MHz; $CDCl_3$) δ = 5.81 (1H, tdd, *J* = 17.0, 10.2, 6.7 Hz, CH_2=C*H*), 4.91-5.01 (2H, m, CH_2=CH), 3.61-3.82 (4H, m, CH_2OH), 2.49 (2H, bs, CH_2O*H*), 2.02-2.07 (2H, m, CH_2), 1.73-1.78 (1H, m, C*H*), 1.26-1.48 (6H, m, CH_2); ^{13}C NMR (100 MHz; $CDCl_3$) δ =138.3 (CH), 113.9 (CH_2), 65.9 (CH_2), 41.4 (CH), 33.0 (CH_2), 28.5 (CH_2), 27.0 (CH_2), 26.1 (CH_2); (found M – H^+ 156.93; $C_9H_{18}O_2$ - H^+ requires 157.124).

Preparation of 2-(Hex-5-en-1-yl)propane-1,3-diyl dimethanesulfonate (5.18)[8], Scheme 5.6

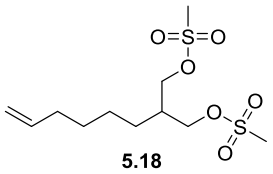

5.18

Methanesulfonyl chloride (6.23 mL, 80 mmol, 4 eq.) was added dropwise to a stirred solution of **5.17** (3.19 g, 20.13 mmol, 1 eq.) and triethylamine (14.0 mL. 100 mmol, 5 eq.) in dichloromethane (200 mL) at 0 °C. The reaction mixture was stirred for 30 minutes at 0 °C and then a further 3 hours at room temperature. Water (200 mL) was added, and the aqueous layer was extracted with dichloromethane (2 × 100 mL). The combined organic extracts were washed with brine and dried over magnesium sulfate before concentrating *in vacuo.* Column chromatography was used to purify the reaction mixture and afforded 8.433 g of purified product, with 67 % yield.

^{1}H NMR (400 MHz; $CDCl_3$) δ = 5.72-5.83 (1H, m, CH_2=C*H*), 4.93-5.02 (2H, m, CH_2=CH), 4.16-4.29 (4H, m, CHCH_2O), 3.03 (6H, s, CH_3), 2.13-2.19 (1H, m, CH_2C*H*), 2.03-2.08 (2H, m, CH_2), 1.35-1.43 (6H, m, CH_2); ^{13}C NMR (100 MHz; $CDCl_3$) δ = 138.3 (CH), 114.8 (CH_2), 68.2 (CH_2), 38.1 (CH), 37.3 (CH_3), 33.3 (CH_2), 28.6 (CH_2), 26.8 (CH_2), 25.9 (CH_2); (found M + Na^+ 337.00; $C_{11}H_{22}O_6S_2$ + Na^+ requires 337.076).

Preparation of 7-((methylsulfonyl)oxy)-6-(((methylsulfonyl)oxy)methyl)heptanoic acid (5.19) [8]**, Scheme 5.6**

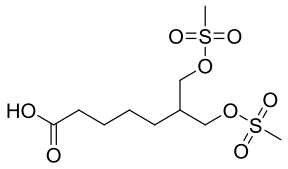

5.19

Osmium tetroxide (1.24 mL of a 2.5% w/w solution in tertiary butanol, 0.10 mmol, 0.01 eq.) was added to a solution of **5.18** (3.10 g, 9.86 mmol, 1 eq.) in *N,N*-dimethylformamide (65 mL), and was stirred for 5 min. Oxone (24.2 g, 39.4 mmol, 4 eq.) was then added, over 30 minutes, and the resulting mixture was stirred vigorously for a further 5 hours. Sodium sulfite (19.1 g) was added, and the resulting mixture was stirred for a further 2 hours. Water (200 mL), aqueous hydrochloric acid solution (2 M; 50 mL), and 1:1 v:v ethyl acetate:ether (200 mL) were added and the layers separated. The organic extracts were washed with brine (150 mL), dried over magnesium sulfate and concentrated *in vacuo* to give 1.5 g of white solid. The crude product was used as such for the next step.

^{1}H NMR (500 MHz; $CDCl_3$) δ = 4.19-4.30 (4H, m, C*H*$_2$), 3.05 (6H, s, C*H*$_3$), 2.39 (2H, t, *J* = 7.2 Hz, C*H*$_2$), 2.18-2.23 (1H, m, CH_2CH), 1.65-1.68 (2H, m, C*H*$_2$), 1.25-1.27 (4H, m, C*H*$_2$); ^{13}C NMR (100 MHz; $CDCl_3$) δ = 178.7 (C), 68.1 (CH_2), 38.0 (CH), 37.3 (CH_3), 33.4 (CH_2), 26.7 (CH_2), 25.8 (CH_2), 24.4 (CH_2); (found M + Na^+ 355.01; $C_{10}H_{20}O_8S_2$ + Na^+ requires 355.05).

Preparation of Isolipoic Acid (5.20), Scheme 5.6

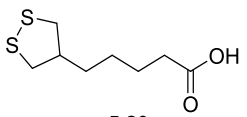

5.20

A solution of potassium thioacetate (1.3 g, 11.3 mmol, 2.5 eq) in dry N,N-DIMETHYLFORMAMIDE (10 mL) was added to a solution of **5.19** (1.5 g, 4.5 mmol,

1.0 eq) in dry N,N-DIMETHYLFORMAMIDE (10 mL) under argon and stirred overnight. NaOH (2M, 20 mL) was added to the reaction mixture and stirred for 2 hours. The mixture was acidified by dropwise addition of HCl (conc.) until the solution was pH 4 and stirred overnight. Ethyl acetate (40 mL) was added and the organics were washed repeatedly with water and brine. The extracted organics were dried over sodium sulfate, concentrated in vacuo and stirred with hexane for 2 hours to give a yellow oil phase below the hexane layer. The hexane was decanted and this step was repeated twice, followed by concentrating the yellow oil *in vacuo*. This afforded 0.650 g of a yellow waxy solid, in 70 % yield.

^{1}H NMR (400 MHz; $CDCl_3$) δ = 3.67 (1H, s, O*H*), 3.25 (2H, dd, *J* = 11.0, 6.6 Hz, *CH*$_2$), 2.81 (2H, dd, *J* = 11.0, 6.6 Hz, *CH*$_2$), 2.52 (1H, sept, *J* = 6.6 Hz, C*H*), 2.32-2.39 (2H, m, *CH*$_2$), 1.63-1.68 (2H, m, *CH*$_2$), 1.51-1.57 (2H, m, *CH*$_2$), 1.46-1.50 (2H, m, *CH*$_2$); ^{13}C NMR (100 MHz; DMSO) δ = 174.3 (C), 47.1 (CH), 43.2 (CH_2), 33.4 (CH_2), 32.5 (CH_2), 27.3 (CH_2), 24.5 (CH_2); (found M – H^+ 204.86; $C_8H_{14}O_2S_2$ - H^+ requires 205.037).

Preparation of 2,5-dioxopyrrolidin-1-yl 5-(1,2-dithiolan-4-yl)pentanoate (5.21)

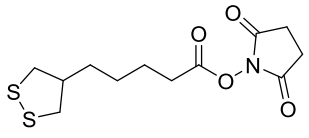

5.21

EDC·HCl (0.705 g, 3.68 mmol, 1.2 eq.) was dissolved in dichloromethane (anhydrous, 15 mL), and DIPEA (anhydrous, 0.652 mL, 3.68 mmol, 1.2 eq.) added. The reaction mixture was then stirred for 10 minutes. To this, *N*-hydroxysuccinimide (0.495 g, 4.30 mmol, 1.4 eq.) was added and the reaction mixture placed in an ice bath. **5.20** (0.63 g, 3.07 mmol, 1 eq.) pre-dissolved in dichloromethane (anhydrous, 10 mL) was then added drop-wise over 20 minutes. The resulting mixture was stirred overnight at room temperature. The solution was washed with HCl (5 % v:v, 20 mL × 2) and distilled water (20 mL) before drying the combined organic layer over sodium sulfate and refrigerating for 2

hours. The sodium sulfate was removed and the sample concentrated *in vacuo* to yield a yellow solid. Attempts were made to purify the material by flash column chromatography, using dichloromethane with 5 % methanol, to give 0.195 g of a dark yellow solid. Residual starting material was detected by NMR and the decision was made to use the crude ester for the next synthetic step.

Preparation of (9H-fluoren-9-yl)methyl (1-((1-((6-(5-(1,2-dithiolan-4-yl)pentanamido)-1-amino-1-oxohexan-2-yl)amino)-1-oxopropan-2-yl)amino)-1-oxopropan-2-yl)carbamate (5.22)

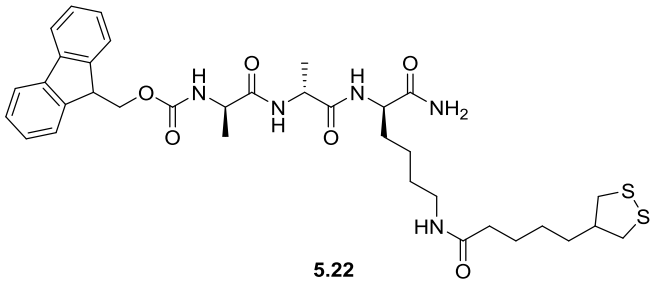

5.22

5.10 (100 mg, 0.161mmol, 1 eq.) was dissolved in dichloromethane (anhydrous, 3 mL) before DIPEA (62 µL, 0.354 mmol, 2.2 eq.) was added and the reaction mixture stirred for 5 minutes. **5.21** (50 mg, 0.161 mmol, 1 eq.) was added and the mixture was stirred in the dark overnight.

Distilled water (3 mL) was added and the reaction mixture was again stirred overnight. The sample was extracted with dichloromethane (3 × 2 mL) and washed repeatedly with water and brine. The extracted organics were dried over sodium sulfate, concentrated *in vacuo* and triturated overnight with diethyl ether to afford 5 mg purified product, with a 4 % yield.

Found M + Na^+ 720.31; $C_{35}H_{47}N_5O_6S_2$ + Na^+ requires 720.29.

CHAPTER EIGHT – REFERENCES

8.1 Chapter 0ne References

1. Southan, C., *Drug Discov. Today*, 2001, **6**, 681-688.

2. Lopez-Otin, C.; Bond, J. S., *J. Biol Chem*., 2008, **283**, 30433–30437.

3. Royal Society of Chemistry, *Chemistry for Tomorrow's World – A Roadmap for the Chemical Sciences*, Royal Society of Chemistry, Cambridge, 2010.

4. Daniel, M.; Astruc, D., *Chem. Rev.,* 2004, **104**, 293.

8.2 Chapter Two References

1. Pantarotto, D.; Browne, W. R.; Feringa, B. L., *Chem. Commun*., 2008, 1533-1535.

2. Ansari, S. A.; Husain, Q., *Biotechnol. Adv.*, 2012, **30**, 512–523

3. Caponi, P. F.; Ulijn, R. V., Chapter 9: Enzyme-Responsive Drug Delivery Systems, Smart Materials for Drug Delivery, eds. Alvarez-Lorenzo, C; Concheiro, A., 2013, Royal Society of Chemistry – Smart Materials Series, RSC Publishing, Cambridge.

4. Zelzer, M.; Todd, S. J.; Hirst, A. R.; McDonald, T. O.; Ulijn, R. V., *Biomater. Sci*., 2013, **1**, 11-39.

5. Lee, H. J.; Wark, A. W.; Goodrich, T. T.; Fang, S.; Corn, R. M., *Langmuir*, 2005, **21**, 4050-4057.

6. Bernardos, A.; Mondragon, L.; Aznar, E.; Marcos, M. D.; Martinez-Manez, R.; Sancenon, F.; Soto, J.; Barat, M.; Perez-Paya, E.; Guillem, C.; Amoros, P., *ACS Nano*, 2010, **4**, 6353–6368.

7. Laromaine, A.; Koh, L.; Murugesan, M.; Ulijn, R. V.; Stevens, M. M., *J. Am. Chem. Soc.,* , 2007, **129**, 4156.

8. Algar, W. R.; Malanoski, A. P.; Susumu, K.; Stewart, M. H.; Hildebrandt, N.; Medintz, I. L., *Anal. Chem*., 2012, **20**, 10136-10146.

9. Rodriguez-Lorenzo, L.; de la Rica, R.; Alvarez-Puebla, R. A.; Liz-Marzan, L. M.; Stevens, M. M.; *Nat. Mater*., 2012, **11**, 604-607.

10. Gupta, S.; Andresen, H.; Ghadiali, J.; Stevens, M. M., *Small*, 2010, **6**, 1509-1513.

11. Ghadiali, J.; Cohen, B. E.; Stevens, M. M., *ACS Nano*, 2010, **4**, 4915-4919.

12. Gallo, J.; Kamaly, N.; Lavdas, I.; Stevens, E.; Nguyen, Q.-D.; Wylezinska-Arridge, M.; Aboagye, E. O.; Long, N. J., *Angew. Chem. Int. Ed.*, 2014, **53**, 1-6.

13. Wang, X.; Xia, Y.; Liu, Y.; Qi, W.; Sun, Q.; Zhao, Q.; Tang, B., *Chem. Eur. J*., 2012, **18**, 7189-7195.

14. Caponi, P. F.; Winnik, F.M.; Ulijn, R. V., *Soft Matter*, 2012, **8**, 5127-5130.

15. Xue, W. X.; Zhang, G. X.; Zhang, D. Q., *Analyst*, 2011, **136**, 3136–3141.

16. Zhang, G.; Yang, M.; Cai, D.; Zheng, K.; Zhang, X.; Wu, L.; Wu, Z., *ACS Appl. Mater. Interfaces*, 2014, **6**, 8042-8047.

17. Park, C.; Kim, H.; Kim, S.; Kim, C., *J. Am. Chem. Soc.*, 2009, **131**, 16614–16615.

18. Amir, R. J.; Zhong, S.; Pochan, D. J.; Hawker, C. J., *J. Am. Chem. Soc.,* 2009, **131**, 13949–13951.

19. Page, M. J.; Di Cera, E., *Cell. Mol. Life Sci.*, 2008, **65**, 1220-1236.

20. Southan, C., *Drug Discov. Today*, 2001, **6**, 681-688.

21. de la Rica, R.; Aili, D.; Stevens, M. M., *Advanced Drug Delivery Reviews*, 2012, **64**, 967-978.

22. Song, G.; Chem, C.; Ren, J.; Qu, X., *ACS Nano*, 2009, **3**, 1183-1189.

23. von Maltzahn, G.; Min, D. -H.; Zhang, Y.; Park, J. –H.; Harris, T. J.; Sailor, M.; Bhatia, S. N., *Adv. Mater*., 2007, **19**, 3579-3583.

24. Liu , Y.; Terrell, J. L.; Tsao, C.-Y.; Wu, H.-C.; Javvaji, V.; Kim, E.; Cheng, Y.; Wang, Y.; Ulijn, R. V.; Raghavan, S. R; Rubloff, G. W.; Bentley, W. E.; Payne, G. F., *Adv. Funct. Mater.*, 2012, **22**, 3004-3012.

25. MacNaught, A. D.; Wilkinson, A. R., 1997, Compendium of Chemical Terminology: IUPAC Recommendations (2nd ed.), Blackwell Science Publications, Oxford.

26. Daniel, M; Astruc, D., *Chem. Rev.*, 2004, **104**, 293.

27. Ghosh, S. K.; Pal, T., *Chem. Rev*., 2004, **107**, 4797.

28. Solomon, S. D.; Bahadory, M.; Jeyarajasingam, A. V.; Rutkowsky, S. A., Boritz, C., *J. Chem. Educ*., 2007, **84**, 322.

29. Elghanian, R.; Storhoff, J. J.; Mucic, R. C.; Letsinger, R. L.; Mirkin, C. A., *Science*, 1997, **277**, 1078.

30. Alivisatos, A. P., *Scientific American*, 2001, **285**, 66.

31. Guarise, C.; Pasquato, L.; De Filippis, V.; Scrimin, P., *Proc Natl Acad Sci USA*, 2006, **103**, 3978-3982.

32. Kanaras, A. G.; Wang, Z.; Brust, M.; Cosstick, R.; Bates, A. D., *Small*, 2007, **3**, 590-594.

33. Wang, Z. X.; Levy, R.; Fernig, D. G.; Brust, M., *J. Am. Chem. Soc.,* 2006, **128**, 2214–2215.

34. Choi, Y.; Ho, N. H.; Tung, C. H., *Angew. Chem., Int. Ed.,* 2007, **46**, 707–709.

35. Hutter, E.; Maysinger, D., *Trends Pharmacol Sci*., 2013, **34**, 497-507.

36. Lee, S.; Cha, E.-J.; Park, K.; Lee, S.-Y.; Hong, J.-K.; Sun, I.-C.; Kim, S. Y.; Choi, K.; Kwon, I. C.; Kim, K.; Ahn, C.-H., *Angew. Chem. Int. Ed.*, 2008, **47**, 2804-2807.

37. Bharathi, S.; Nogami, M., *Analyst*, 2001, **126**, 1919-1922.

38. Dougan, J. A.; Karlsson, C.; Smith, W. E.; Graham, D., *Nucleic Acids Res.*, 2007, **35**, 3668.

39. Ingram, A.; Byers, L.; Faulds, K.; Moore, B. M.; Graham, D.; *J. Am. Chem. Soc*., 2008, **130**, 11846-11847.

40. Moore, B. D.; Stevenson, L.; Watt, A.; Flitsch, S.; Turner, N. J.; Cassidy, C.; Graham, D., *Nature Biotechnol*., 2004, **22**, 1133-1138.

41. Larmour, I. A.; Faulds, K.; Graham, D., *Chem. Sci*., 2010, **1**, 151-160.

42. Wei, H.; Chen, C.; Han, B.; Wang, E., *Anal. Chem*., 2008, **80**, 7051-7055.

43. Rai, M.; Yadav, A.; Gade, A., *Biotechnology Advances*, 2009, **27**, 76-83.

44. Kim, J. Y.; Voznyy, O.; Zhitomirsky, D.; Sargent, E. H., *Adv. Mater.*, 2013, **25**, 4986-5010.

45. Welser, K.; Adsley, R.; Moore, B. M.; Chan, W. C.; Aylott, J. W., *Analyst*, 2011, **136**, 29-41.

46. del Rosario, L. S.; Demirdirek, B,; Harmon, A.; Orban, D.; Uhrich, K. E., *Macromol. Biosci.*, 2010, **10**, 415.

47. Stokes, R. J.; Macaskill, A.; Dougan, J. A.; Hargreaves, P. G.; Stanford, H. M.; Smith, W. E.; Faulds, K.; Graham, D., *Chem. Commun*., 2007, 2811-2813.

8.3 Chapter Three References

1. Mendes, P. M., *Chem. Soc. Rev.*, 2008, **37**, 2512.

2. Zhang, S. G.; Yan, L.; Altman, M.; Lassle, M.; Nugent, H.; Frankel, F.; Lauffenburger, D. A.; Whitesides, G. M.; Rich, A., *Biomaterials*, 1999, **20**, 1213.

3. Mart, R. J.; Osborne, R. D; Stevens, M. M.; Ulijn, R. V., *Soft Matter*, 2006, **2**, 822.

4. Ulijn, R. V.; Smith, A. M., *Chem. Soc. Rev.*, 2008, **37**, 664.

5. Chow, D.; Nunalee, M. L.; Lim, D. W.; Simnick, A. J.; Chilkoti, A., *Materials Science and Engineering R-Reports*, 2008, **62**, 125.

6. Sun, T.; Wang, G.; Feng, L.; Liu, B.; Ma, Y.; Jiang, L.; Zhu, D., *Angew. Chem. Int. Ed.*, 2004, **43**, 357.

7. Palmer, L. C.; Stupp, S. I., *Acc. Chem. Res.*, 2008, **41**, 1674.

8. Yeo, W. S.; Yousaf, M. N.; Mrksich, M., *J. Am. Chem. Soc.,* , 2003, **125**, 14994.

9. Love, C. J.; Estroff, L. A.; Kriebel, J. K.; Nuzzo, R. G.; Whitesides, G. M., *Chem. Rev.*, 2004, **105**, 1103.

10. Yeo, W.-S.; Yousaf, M. N.; Mrksich, M., *J. Am. Chem. Soc.,* , 2003, **125**, 14994.

11. Daniel, M.; Astruc, D., *Chem. Rev.*, 2004, **104**, 293.

12. Laurent, N.; Haddoub, R.; Voglmeir, J.; Wong, S. C. C.; Gaskell, S. J.; Flitsch, S. L., *ChemBioChem*, 2008, **9**, 2592-2596.

13. Alivisatos, A. P.; Johnsson, K.P.; Peng, X.; Wilson, T. E.; Ioweth, C. J.; Bruchez, M. P.; Schultz, P. G., *Nature*, 1996, **382**, 607.

14. Mirkin, C. A.; Letsinger, R. L.; Mucic, R. C; Storhoff, J. J., *Nature*, 1996, **382**, 607

15. Doria, G.; Franco, R.; Baptista, P., *IET Nanobiotechnology*, 2007, **1**, 53-57.

16. Claridge, S. A.; Goh, S. L.; Frechet, J. M. J.; Williams, S. C.; Micheal, C. M.; Alivisatos, A. P., *Chem. Mater.*, 2005, **17**, 1628.

17. Wang, Z. X.; Lévy, R.; Fernig, D. G.; Brust, M., *Bioconjugate Chem.*, 2005, **16**, 497-500.

18. Laromaine, A.; Koh, L.; Murugesan, M.; Ulijn, R. V.; Stevens, M. M., *J. Am. Chem. Soc.,* , 2007, **129**, 4156.

19. Duchesne, L.; Wells, G.; Fernig, D. G.; Harris, S. A.; Lévy, R., *ChemBioChem*, 2008, **9**, 2127-2134.

20. Ryadnov, M. G.; Ceyhan, B.; Niemeyer, C. M; Woolfson, D. N., *J. Am. Chem. Soc.,* , 2003, **125**, 9388.

21. du Vigneaud, V.; Ressler, C.; Trippett, S., *J.Biol. Chem.*, 1953, **205**, 949.

22. Benoiton, N. L., *Chemistry of Peptide Synthesis*, Taylor and Francis, Boca Raton, **2006**, p125-154.

23. Merrifield, R. B., *J. Am. Chem. Soc.,* 1963, **85**, 2149.

24. Frank, R., *Tetrahedron*, 1992, **48**, 9217.

25. Ulijn, R. V.; Baragana, B.; Halling, P. J.; Flitsch, S. L., *J. Am. Chem. Soc.,* , 2002, **124**, 10988.

26. Meldal, M., *Tetrahedron Letters*, 1992, **33**, 3077.

27. Todd, S. J.; Scurr, D. J.; Gough, J. E.; Alexander, M. R.; Ulijn, R. V., *Langmuir*, 2009, **25**, 7533.

28. Lahiri, J.; Issacs, L.; Tien, J.; Whitesides, G. M., *Anal. Chem.*, 1999, **71**, 777.

29. Rawsterne, R. E.; Gough, J. E.; Rutten, F. J. M.; Pham, N. T.; Poon, W. C. K.; Flitsch, S. L.; Maltman, B.; Alexander, M. R.; Ulijn, R. V., *Surf. Interface Anal.,* 2006, **38**, 1505.

30. Mosse, W. K. J.; Koppens, M. L.; Gengenbach, T. R.; Scanlon, D. B.; Gras, S. L.; Ducker, W. A., *Langmuir*, 2009, **25**, 1488.

31. Dougan, J. A.; Karlsson, C.; Smith, W. E.; Graham, D., *Nucleic Acids Res.,* 2007, **35**, 3668.

32. Worthington, V., ed., *Worthington Enzyme Manual – Enzymes and Related Biochemicals*, Worthington Biochemical Corporation, Lakewood, **1993**, p170-174.

33. Hedstrom. L., *Chemical Reviews*, 2002, **102**, 4501-4523.

34. Worthington, V., ed., *Worthington Enzyme Manual – Enzymes and Related Biochemicals*, Worthington Biochemical Corporation, Lakewood, 1993.

35. Trengove, N. J.; Stacey, M. C.; Macauley, S.; Bennett, N,; Gibson, J. ; Burslem, F.; Murphy, G.; Schultz, G., *Wound Repair and Regeneration*, 1999, **7**, 442-452.

36. Kramer, S.; Xie, H.; Gaff, J.; Williamson, J. R.; Tkachenko, A. G.; Nouri, N.; Feldheim, D. A.; Feldheim, D. L., *J. Am. Chem. Soc.,* , 2004, **126**, 5388-5395.

37. Norde, W., *Advances in Colloid and Interface Science*, 1986, **25**, 267-340.

38. Wahlgreen, M.; Arnebrant, T., *TIBTech*, 1991, **9**, 201.

39. Lanza, R. P.; Langer, R.; Vacanti, J., *Principles of Tissue Engineering*, Academic Press, San Diego, **2000**, p243.

40. Wagner, M. S.; Castner, D. G., *Langmuir*, 2001, **17**, 4649.

41. Shotton, D. M.; Hartley, B. S., *Nature*, 1970, **225**, 802.

42. Wendeln, C.; Rinnen, S.; Schulz, C.; Kaufmann, T.; Arlinghaus, H. F.; Ravoo, B. J.; *Chem. Eur. J.*, 2012, **18**, 5880.

43. Zheng, M.; Davidson, F.; Huang, X.; *J. Am. Chem. Soc.,* , 2003, **125**, 7790.

44. Thierry, B.; Griesser, H. J., *J. Mater. Chem.*, 2012, **22**, 8810.

45. Prime, K. L.; Whitesides, G. M., *J. Am. Chem. Soc.,* 1993, **115**, 10714.

46. Mrksich, M.; Chen, C. S.; Xia, Y.; Dike, L. E.; Ingber, D. E.; Whitesides, G. M., *Proc. Natl. Acad. Sci. USA*, 1996, **93**, 10775.

47. Chapman, R. G.; Ostuni, E.; Liang, M. N.; Meluleni, G.; Kim, E.; Yan, L.; Pier, G.; Warren, H. S.; Whitesides, G. M., *Langmuir*, 2001, **17**, 1225-1233.

48. Su, J.; Mrksich, M., *Angew. Chem. Int. Ed.*, 2002, **41**, 4715.

49. Su, J.; Mrksich, M., *Langmuir*, 2003, **19**, 4867.

50. Marin, V. L.; Bayburt, T. H.; Sligar, S. G.; Mrksich, M., *Angew. Chem. Int. Ed.,* 2007, **46**, 8796.

51. Mrksich, M., *ACS Nano*, 2008, **2**, 7.

52. Ma, Z.; Qiang, L. –L.; Fan, Q. –L.; Wang, Y. –Y.; Pu, K. –Y.; Yin, R.; Huang, W.; *J. Mass Spectrom.*, 2007, **42**, 20-24.

53. Lamprou, D. A., *Contact Angle Measurement System*, Strathclyde Institute of Pharmacy and Biomedical Science, Glasgow, 2010.

54. Rawsterne, R. E.; Gough, J. E.; Rutten, F. J. M.; Pham, N. T.; Poon, W. C. K.; Flitsch, S. L.; Maltman, B.; Alexander, M. R.; Ulijn, R. V., *Surf. Interface Anal.*, 2006, **38**, 1505-1511.

55. Rawsterne, R. E.; Todd, S. J.; Gough, J. E.; Farrer, D.; Rutten, F.; Alexander, M. R.; Ulijn, R. V., *Acta. Biomaterialia*, 2007, **3**, 715-721.

56. Frutos, A. G.; Brockman, J. M.; Corn, R. M., *Langmuir*, 2000, **16**, 2192-2197.

57. Todd, S. J.; Scurr, D. J.; Gough, J. E.; Alexander, M. R.; Ulijn, R. V., *Langmuir*, 2009, **25**, 7533-7539.

58. McKenzie, F.; Steven, V.; Ingram, A.; Graham, D., *Chem. Commun*., 2009, 2872-2874.

59. Demers, L. M.; Mirkin, C. A.; Mucic, R. C.; Reynolds, R. A.; Letsinger, R. L.; Elghanian, R.; Viswanadham, G., *Anal. Chem*., 2000, **72**, 5535-5541.

8.4 Chapter Four References

1. Fleischmann, M.; Hendra, P. J.; McQuillan, A. J., *Chemical Physics Letters,* 1974, **26**, 163-166.

2. Jeanmaire, D. L.; Van Duyne, R. P., *Journal of Electroanalytical Chemistry and Interfacial Electrochemistry,* 1977, **84**, 1-20.

3. Albrecht, M. G.; Creighton, J. A., *J. Am. Chem. Soc.,* , 1977, **99**, 5215-5217.

4. Kneipp, K.; Kneipp, H.; Itzkan, I.; Dasari, R. R.; Feld, M. S., *Chemical Reviews* , 1999, **99**, 2957-2976.

5. Deschaines, T. O.; Wieboldt, D., *Practical Applications Of Surface-Enhanced Raman Scattering (SERS)*, Technical Note 51874, Thermo Fischer Scientific, Madison WI, 2010.

6. Perney, N. M. B.; Baumberg, J. J., *Optics Express,* 2006, **14**, 847-857.

7. Smith, A. M.; Collins, R. F.; Ulijn, R. V.; Blanch, E., *J. Raman Spectrosc.* 2009, ***40*****,** 1093–1095.

8. Geiman, I.; Leona, M.; Lombardi, J. R., *J. Forensic Sci*., 2009, **54**, 947-952.

9. Correia-Ledo, D,; Gibson, K. F.; Dhawan, A.; Couture, M.; Vo-Dinh, T.; Graham, D.; Masson, J. –F., J. Phys. Chem, 2012, 116, 6684-6892.

10. Berlouis, L.E.A.; McMillan, B.G.; Cruickshank, F.R.; Brevet, P.F., Electrochimica Acta, 53, 2007, 1157-1163.

8.5 Chapter Five References

1. Daniel, M.; Astruc, D., *Chemical Reviews*, 2004, **104**, 293.

2. Lopez-Otin, C.; Bond, J. S., *J. Biol Chem*., 2008, **283**, 30433–30437.

3. Doria, G.; Franco, R.; Baptista, P., *IET Nanobiotechnology*, 2007, **1**, 53-57.

4. Laromaine, A.; Koh, L.; Murugesan, M.; Ulijn, R. V.; Stevens, M. M *J. Am. Chem. Soc.,* 2007, **129**, 4156-4157.

5. Oishi, J.; Asami, Y.; Mori, T.; Kang, J. H.; Tanabe, M.; Niidome, T.; Katayama, Y., *ChemBioChem*, 2007, **8**, 875-879.

6. Guarise, C.; Pasquato, L.; De Filippis, V.; Scrimin, P., *Proceedings of the National Academy of Sciences of the United States of America*, 2006, **103**, 3978-3982.

7. Kramer, S.; Xie, H.; Gaff, J.; Williamson, J. R.; Tkachenko, A. G.; Nouri, N.; Feldheim, D. A.; Feldheim, D. L., *J. Am. Chem. Soc.,* , 2004, **126**, 5388-5395.

8. Loweth, C. J.; Caldwell, W. B.; Peng, X.; Alivisatos, A. P.; Schultz, P. G., *Angewandte Chemie – International Edition*, 1999, **38**, 1808-1812.

9. Jayawarna, V.; Smith, A.; Gough, J. E.; Ulijn, R. V., *Biochem. Soc. Trans*., 2007, **35**, 535-537.

10. Page, M. J.; Di Cera, E., *Cellular and Molecular Life Sciences*, 2008, **65**, 1220-1236.

11. Dougan, J. A.; Karlsson, C.; Smith, W. E.; Graham, D., *Nucleic Acids Res.*, 2007, **35**, 3668-3675.

12. Sung, K.-M.; Mosley, D. W.; Peelle, B. R.; Zhang, S.; Jacobson, J. M., *J. Am. Chem. Soc.,* , 2004, **126**, 5064-5065.

13. Manson, J.; Kumar, D.; Meenan, B. J.; Dixon, D., *Gold Bull,* 2011, **44**, 99-105.

24. Koufaki, M.; Detsi, A.; Theodorou, E.; Kizirdi, C.; Calogeropoulou, T.; Vassilopoulos, A.; Kourounakis, A. P.; Rekka, E.; Kourounakis, P. N.; Gaitanaki, C.; Papazafiri, P., *Bioorganic & Medicinal Chemistry*, 2004, **12**, 4835.

15. Koufaki, M.; Detsi, A.; Kizirdi, C., *Current Medicinal Chemistry*, 2009, **16**, 4728.

16. Reddy, G. V. S.; Rao, G. V.; Subramanyam, R. V. K.; Iyengar, D. S., *Synth. Commun*., 2000, **30**, 2233-2237.

17. Rokhum, L.; Bez, G., *J. Chem. Sci*., 2012, **124**, 687-691.

18. Colombo, L.; Di Giacomo, M.; Brusotti, G.; Sardone, N.; Angiolini, M.; Belvisi, L.; Maffioli, S.; Manzoni, L.; Scolastico, C., *Tetrahedron*, 1998, **54**, 5325-5336.

19. Joly, K. E.; Mirri, G.; Willener, Y.; Horswell, S. L.; Moody, C. J.; Tucker, J. H. R., *J. Org. Chem.*, 2010, **75**, 2395-2398.

20. Zheng, T. –C.; Burkart, M.; Richardson, D. E.; *Tetrahedron Letters*, 1999, **40**, 603-606.

8.6 Chapter Six References

1. Laromaine, A.; Koh, L.; Murugesan, M.; Ulijn, R. V.; Stevens, M. M., *J. Am. Chem. Soc.,* , 2007, **129**, 4156-4157.

2. Dougan, J. A.; Karlsson, C.; Smith, W. E.; Graham, D., *Nucleic Acids Res.*, 2007, **35**, 3668-3675.

3. Ratia, K.; Kilianski, A.; Baez-Santos, Y. B.; Baker, S. C.; Mesecar, A., *PLOS Pathogens*, 2014, **10**, e1004113.

4. Centre for Disease Control, http://www.cdc.gov/coronavirus/mers/US.html, accessed June 2014.

8.7 Chapter Seven References

1. Laurent, N.; Haddoub, R.; Voglmeir, J.; Wong, S. C. C.; Gaskell, S. J.; Flitsch, S. L., *ChemBioChem*, 2008, **9**, 2592-2596.

2. Todd, S. J.; Scurr, D. J.; Gough, J. E.; Alexander, M. R.; Ulijn, R. V., *Langmuir*, 2009, **25**, 7533-7539.

3. Demers, L. M.; Mirkin, C. A.; Mucic, R. C.; Reynolds, R. A.; Letsinger, R. L.; Elghanian, R.; Viswanadham, G., *Anal. Chem*., 2000, **72**, 5535-5541.

4. McKenzie, F.; Steven, V.; Ingram, A.; Graham, D., *Chem. Commun*., 2009, 2872-2874.

5. Dougan, J. A.; Karlsson, C.; Smith, W. E.; Graham, D., *Nucl. Acids Res*., 2007, **35**, 3668-3675.

6. Koufaki, M.; Detsi, A.; Theodorou, E.; Kizirdi, C.; Calogeropoulou, T.; Vassilopoulos, A.; Kourounakis, A. P.; Rekka, E.; Kourounakis, P. N.; Gaitanaki, C.; Papazafiri, P., *Bioorganic & Medicinal Chemistry*, 2004, **12**, 4835.

7. Koufaki, M.; Detsi, A.; Kizirdi, C., *Current Medicinal Chemistry*, 2009, **16**, 4728.

8. Joly, K. E.; Mirri, G.; Willener, Y.; Horswell, S. L.; Moody, C. J.; Tucker, J. H. R., *J. Org. Chem.*, 2010, **75**, 2395-2398.

9. Loweth, C. J.; Caldwell, W. B.; Peng, X.; Alivisatos, A. P.; Schultz, P. G., *Angew. Chem. Int. Ed.*, 1999, **38**, 1808-1812.

10. Laromaine, A.; Koh, L.; Murugesan, M.; Ulijn R. V.; Stevens, M. M., *J. Am. Chem. Soc.,* , 2007, **129**, 4156-4157.

11. Current Protocols in Nucleic Acid Chemistry, *Section 12.2.6 – Basic Protocol 2*, 2000.

CHAPTER NINE – APPENDIX

9.1 Mass Spectra of Synthesised Compounds

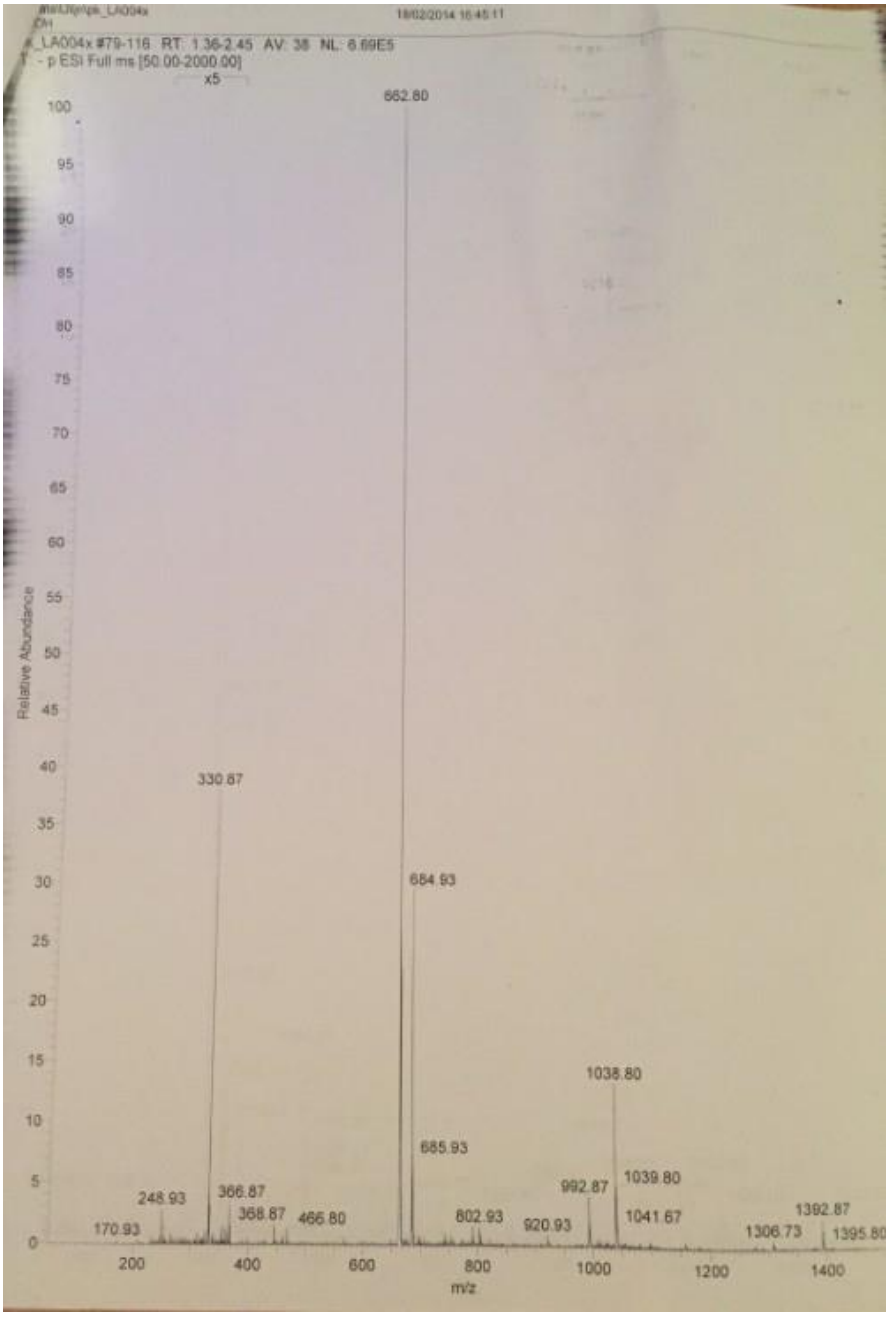

Figure 9.1
ESI-MS spectrum of structure 5.3. Synthetic procedure detailed in section 7.4.7.